1-1-2008

Experimental Study Of Short Hole Film-Cooling

Mohammed A. Gandhi
Ryerson University

EXPERIMENTAL STUDY OF SHORT HOLE FILM-COOLING

by

Mohammed A. Gandhi
B.Eng., Ryerson University, 2006

A thesis presented to
Ryerson University
in partial fulfillment of the
requirements for the degree of
Masters of Applied Science
in the Program of
Aerospace Engineering

Toronto, Ontario, Canada, 2008

Author's Declaration

I, Mohammed A. Gandhi, hereby declare that I am the sole author of this thesis titled, 'Experimental Study of Short Hole Film Cooling'.

I authorize Ryerson University to lend this thesis to other institutions or individuals for the purpose of scholarly research.

Signed: _____

I further authorize Ryerson University to reproduce this thesis by photocopying or by other means, in total or in part, at the request of other institutions or individuals for the purpose of scholarly research.

Signed: _____

"If we knew what it was we were doing, it would not be called research, would it?"

Albert Einstein

Abstract

Experimental Short Hole Film-Cooling
Master of Applied Science, 2008

by
Mohammed A. Gandhi
Aerospace Engineering, Ryerson University

An experimental study was conducted to investigate the film cooling effectiveness of a few configurations of short injection holes: single row, double row and both of the preceding cases with an upstream ramp placed at two different locations. In order to perform the above study, a wind-tunnel facility was assembled to facilitate in the successful culmination of the experiments. The focus of the study was to determine the cooling provided by the short injection holes at a variety of blowing ratios and whether adding an extra row of holes, upstream of the first row would make a difference. For the second part, a ramp was placed upstream of the single and double row configuration to help improve cooling. All of the experiments were performed in a low speed wind-tunnel with a mainstream velocity of 8 m/s and a turbulence intensity of 3.3%. Higher blowing ratios were ineffective in improving film-cooling effectiveness due to jet lift-off. Two rows of holes increased the cooling effectiveness by 200%, when compared to single row configurations at the same blowing ratio without ramps. Upstream ramps provided significant improvement in the near hole region of the injection holes.

Acknowledgements

The support provided by Dr. Bassam Jubran, my research supervisor, during the course of my studies has been pivotal to its outcome. This project would have been more of an insurmountable task if it were not for his words of encouragement, advise and most importantly, knowledge of the subject. I would like to thank him for his belief in me and the completion of the project; even when things were blight.

If Dr. Jubran and I, were the 'brains' of this project, it would be apt to call Mr. Peter Bradley its 'hands'. It was due to his unwavering eye for all things practical that most of the ideas in my head were transformed into tangible apparatus. With Peter by my side, I knew that 'Bob's My Uncle'. I truly appreciate his effort towards the completion of this research.

As long as I knew Dr. Hamid Ghaemi was in the building, I had a place to bounce my ideas and get valuable feedback on everything from structural to moral integrity. His disarming attitude allowed me to speak my mind without sounding obtuse. Thanks for sharing your knowledge and broadening my horizons.

I would like to thank Mr. Jerry Karpyncyk, Mr. Primoz Cresnik and Suketu Patel for helping with setting-up the wind-tunnel. Their contribution was instrumental in finishing the research.

I was fortunate to find a friend in Marc Ely, my lab mate. His umpteen trips to the hardware store are much appreciated. Lunch hour would have been a lot less exciting without our unconventional conversations.

Nader Abu El Samid has been extremely helpful with his invigorating ideas and I am thankful to him for sharing them with me. The write-up for this thesis would have been very difficult if it wasn't for the all-nighters we pulled together.

My uncles, Mr. Kutbuddin Rashid and Mr. Murtaza Gandhi have been extremely generous to me and I am indebted to them for not only their gifts, but also their encouragement.

I would like to express my gratitude to my parents, Tasneem and Asgar Gandhi, to whom I owe everything. They have provided unconditional love and support through all my endeavors and I believe that it is due to their prayers and blessings that I have been able to succeed. No amount of words would be able to sum up

the adoration and love I hold for them. I hope I can be half as good a son, as they have been parents.

My brothers Husein and Mustansir have been very supportive towards me and I would like to wish them all the best for their future.

My wife, Sophia, has been my source of inspiration. Her love, patience and endurance through the trying parts of my research exhorted me to strive on. I would like to acknowledge all the help and support I received from her - from fixing dinner to mending the lab apparatus.

Dedicated to my parents, Tasneem and Asgar Gandhi,
and the loving memory of my grandparents...

Contents

List of Tables

List of Figures

Abbreviations

RIT	**R**otor **I**nlet **T**emperature
FSTI	**F**ree **S**tream **T**urbulence **I**ntensity
CRVP	**C**ounter **R**otating **V**ortex **P**air
ATML	**A**ero **T**hermal **M**anagement **L**aboratory
CFM	**C**ubic **F**eet per **M**inute
RPM	**R**apid **P**rototyping **M**achine
CTA	**C**onstant **T**emperature **A**nemometer
A/D	**A**nalog to **D**igital

Nomenclature

$D.R.$	Density Ratio
E/D	Endwall Distance-to-Diameter Ratio (Plenum)
H/D	Height-to-Diameter Ratio (Plenum)
L/D	Length-to-Diameter Ratio
M	Blowing Ratio
P/D	Pitch-to-Diameter Ratio
R/D	Distance Between the Ramp and Row of Injection Holes Non-Dimensionalised by Diameter of Hole
Re_x	Reynold's Number
T_{aw}	Adiabatic Wall Temperature
T_c	Coolant Temperature
T_o	Uncooled Surface Temperature
T_∞	Mainstream Temperature
Tu	Turbulence Intensity
U_c	Coolant Velocity
U_∞	Mainstream Velocity

Greek

α	Angle of the Upstream Ramp
δ	Boundary Layer Thickness
δ^*	Boundary Layer Displacement Thickness
η	Adiabatic Efficiency
η_{av}	Laterally Averaged Adiabatic Efficiency
η_{cl}	Centerline Adiabatic Efficiency

η_o	Surface Effectiveness without Coolant Flow Used for Conduction Correction
η_{meas}	Measured Adiabatic Efficiency (without Conduction Correction)
θ	Momentum Thickness
ρ_c	Density of Coolant
ρ_∞	Density of Mainstream Fllow

Chapter 1

Introduction

1.1 The Working of a Typical Gas Turbine

Gas turbines have single-handedly changed the face of modern transportation. Gone are the days when an overnight train journey for a mere 500 km distance was considered efficient. With the advent of the airplane in 1903 by the Wright Brothers, and subsequently the jet engine, patented by Sir Frank Whittle in 1930, it is now possible to traverse the expanse of a continent in a matter of hours. For the purpose of aircraft propulsion: pressure of the ingested atmospheric air is increased significantly by a multi-stage compressor, each stage comprising of a row of rotating blades followed by a row of stationary or stator blades. This pressurized air is routed to the combustor, where fuel is added and the mixture ignited to increase the energy. This concoction of pressurized, high-temperature gas is passed through the turbine where enough energy is extracted to run the compressor and the remainder is used to propel the aircraft, by discharging accelerated flow through a nozzle. Similar to the compressor, the turbine consists of alternate rows of static blades and rotating blades. Apart from being used as power plants for aircraft propulsion; gas turbines are extensively used for electricity generation and other land-based industrial applications.

The thrust produced by an engine as well as its thermal efficiency is limited by the maximum inlet temperature of the gas entering the turbine blade, which in turn is the maximum temperature that can be endured by the rotor blades in the turbine. This essentially means: in order to increase the thermal efficiency and

This thesis follows the AIAA style of referencing.

power output of a turbine engine, the rotor inlet temperature (RIT) should be increased [3]. As speed requirements of modern aircraft increase, so do expectations from engineers to find innovative and efficient ways to improve upon engine power.

1.1.1 Need for Cooling Gas Turbines

The typical RIT ranges from 1800 °K - 2000 °K [4] in modern turbines, which is well beyond the melting temperature, 1300 °K, of a typical metallic turbine blade [5]. RIT has been consistently increasing by approximately 20 °C per year since the 1960s, driven by the demand of enhanced engine performance . Part of this temperature rise has been accommodated by improvements in materials and the rest has been realized through progressive enhancement of component cooling capabilities [6]. If engine designers are to keep up with this requirement imposed by the aviation industry, they will have to depend on the development of, either: high-temperature resistant material, such as thermal barrier coating, or sophisticated component cooling schemes like film cooling [3].

Although ceramics and other high-temperature materials are being investigated, serious limitations to their applicability due to the brittle fracture failure mode associated with non-metallic materials, still remains. Taking into consideration the risk of life and monetary loss, such a failure mode is unacceptable for an aircraft turbine engine. Thus in the short term, metallic turbine blades will be used in most, if not all, aircraft engines because of the ill-treatment that they can endure. In the long term, non-metallic turbine blades may be developed which might be able to withstand the current RIT without cooling [7]. Despite the progress made in blade metallurgy, efficient cooling mechanisms like film cooling and internal cooling of blades have to be employed, so that the turbine blades work efficiently, with as little maintenance as possible, over an extended period of time. Figure 1.1 shows a row of distressed turbine blades that was ravaged by the hot combustor gases and the stress of operation at extreme conditions; the purpose of cooling the blades is to prevent this kind of damage.

1.2 Gas Turbine Cooling

As the operating temperature in the turbine is far beyond the permissible metal temperature, the turbine blades are cooled by extracting relatively cooler air from

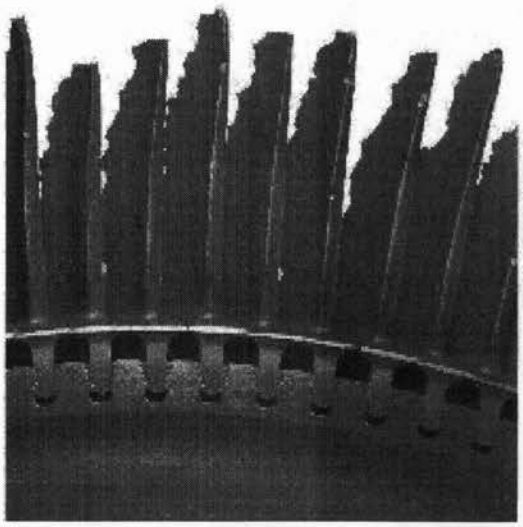

FIGURE 1.1: Damage to a turbine blade due to overheating [8]

the compressor and routing it to the turbine, bypassing the combustor. Gas turbine blades can be cooled internally as well as externally.

The simpler cooling methods involve purely internal flow of coolant within the turbine blade, also known as convective cooling. In this method, the heat transferred to the blade from the hot gases is absorbed through the blade wall by the relatively cooler air, flowing through the internal passages in the blade. The effectiveness of internal cooling may be improved with enhancements such as impingement, trip strips, and multi-pass arrangements. However, when the external gas temperature exceeds the maximum metal temperature by a significant amount, as it does in most modern aircraft engines, the above methods cannot adequately protect the blade from failure [6]. When internal cooling alone is inadequate, film cooling must be employed.

Film cooling is commonly used to prevent distress and failure of turbine blades in gas turbine engines – a consequence of excessive operating temperatures. With film cooling, cool air is bled from the compressor, ducted to the internal chambers of the turbine blades, and discharged through small discrete holes in the blade walls (Figure 1.2). This air provides a thin, cool, insulating blanket along the external surface of the turbine blade, insulating the blade from the detrimental high-temperature gas flow. The cooling effectiveness is dependent upon various parameters and design constraints. Film cooling remains the primary method of decreasing heat transfer to turbine blades.

The coolant to mainstream temperature ratio (T_c/T_∞) in a turbine is in the region of 0.5 to 0.85 [9], which means that the supposed 'coolant' can reach temperatures of up to 1300 °K [10]. Although, the coolant is very high in temperature itself; it is still relatively cooler than the temperature of the mainstream flow and thus sufficient to provide the appropriate amount of insulation and cooling to the turbine component.

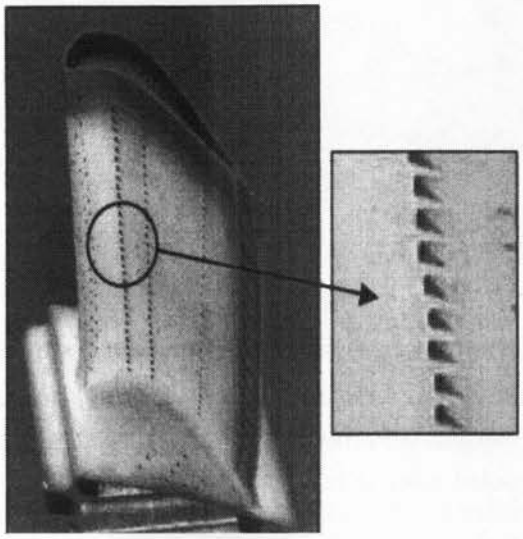

FIGURE 1.2: Modern film-cooled turbine blade [11]

1.3 Parameters Affecting Turbine Film-Cooling

Since the injected coolant, used for film cooling, is bled directly from the compressor, decreasing the flow through the combustion chamber, it represents a loss in the total power output, thus decreasing thermal efficiency. Therefore, the engine designers goal is to minimize the amount of coolant necessary to ensure adequate engine operation. As mentioned earlier, cooling effectiveness of film-cooling is dependent upon various parameters and constraints, which have to be optimized. Among these parameters, the blade and film-cooling hole geometries, the approach flow turbulence, the coolant temperature, velocity distribution and turbulence are some of the most crucial and pivotal conditions [12].

Presented below are some film-cooling parameters that are important to understand before venturing into detailed discussions of literature review and research

The competence of film cooling in effectively reducing heat transfer to the blade is quantified by a parameter know as adiabatic film cooling effectiveness, η, where a maximum value of 1 would mean complete insulation of the blade from the hot gas path and a minimum value of 0 would imply absolutely no protection from the temperature gradient of the hot gases (Equation 1.1).

$$\eta = \frac{T_\infty - T_{aw}}{T_\infty - T_c} \tag{1.1}$$

The blowing ratio, M, is the ratio of coolant to freestream mass flux (Equation 1.2).

$$M = \frac{\rho_c \cdot U_c}{\rho_\infty \cdot U_\infty} \tag{1.2}$$

The density ratio, DR, is the ratio of coolant to freestream density (Equation 1.3).

$$DR = \frac{\rho_c}{\rho_\infty} \tag{1.3}$$

The temperature ratio, TR, is the ratio of coolant to freestream temperature (Equation 1.4).

$$TR = \frac{T_c}{T_\infty} \tag{1.4}$$

In a typical gas turbine, the blowing ratio, M varies from 0.5 - 2.0; the DR is approximately 1.5 - 2.0; while the TR is in the vicinity of 0.5 - 0.85 [3].

The length-to-diameter ratio, L/D, is an important parameter of film-cooling injection holes and plays an important role in directing and settling the coolant flow before it is ejected on the blade or flat-plate.

1.4 Layout of the Thesis

The present thesis is divided into five chapters and a few appendices. Chapter 1 introduces the topic of film cooling and the important parameters associated with

it. In Chapter 2, a thorough literature survey is conducted of previous film-cooling research pertaining to short-holes, narrow plenum and additional innovative techniques used in improving cooling efficiency. This review is conducted to give the reader a sound background of the current research along with some perspective of the contributions made by this thesis. Chapter 3 describes the experimental apparatus and procedures that were followed to obtain the objective of measuring adiabatic film cooling effectiveness for an array of short hole configurations. This chapter would also be of immense help to fellow researchers and graduate students, who would like to establish their own film-cooling or wind-tunnel facility. Chapter 4 presents and discusses the various results obtained from conducting film-cooling research on short-holes coupled with a narrow plenum. Chapter 5 concludes the thesis by summarizing the current investigations: highlighting the pros and cons of the results, as well as, forwarding recommendations for future research on the subject.

Chapter 2

Literature Review

Temperature control inside the turbine is of utmost importance to avoid component distress and, the worse case scenario, failure. Convection or internal cooling of turbine components is a viable option but it is insufficient when the temperature inside the turbine exceeds 1400 °K (Figure 2.1). Higher turbine temperatures call for more sophisticated cooling techniques, like film-cooling, which ejects cooler air from the compressor on the surface of turbine components through discrete holes. This coolant infiltrates the boundary layer, forming a blanket over the turbine blade, shielding it from the hot combustor gases. The recent advancements in rotor inlet temperature (RIT), which is the temperature of the gas entering the turbine from the combustor, and engine efficiency are a direct result of implementing innovative cooling technology; however, there are aerodynamic losses that are accrued that affect the overall efficiency of the engine. These aerodynamic losses occur due to the viscous effect of irreversible mixing of the coolant and mainstream flow [13] . Researchers are trying to maximize cooling by using the least amount of coolant, in a bid to minimize these losses, by optimizing parameters related to film-cooling, like L/D ratio of injection holes, blowing ratio, density ratio, freestream turbulence, the spanwise spacing of adjacent holes, the spacing of two rows of holes, etc.

The majority of the open literature research is conducted on flat plates, emphasizing on surface measurements, such as adiabatic effectiveness and heat transfer, while other investigators have studied flow field related areas like freestream turbulence and vortex control. For the purpose of this literature review, studies concerning surface measurement will be discussed primarily as they are more relevant to the current research.

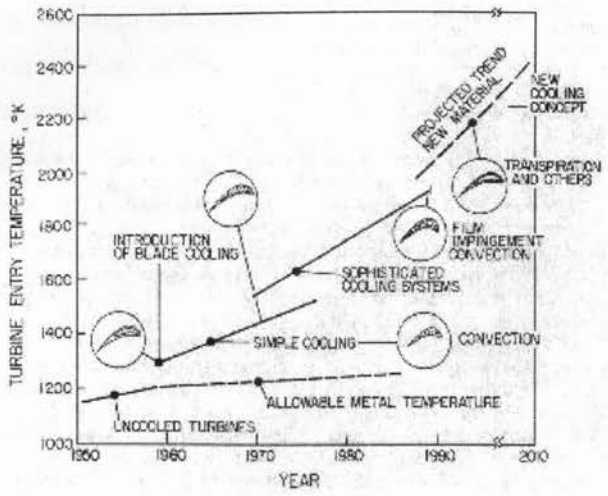

FIGURE 2.1: Advancements in cooling technology [3]

2.1 Review of Previous Research on Film-Cooling

Most of the studies on film-cooling have used injection holes with large length-to-diameter ratios, $L/D > 4$, that are not representative of actual turbine conditions; L/D ratios of unity are expected to be the norm in next generation engines [14]. In addition to that, a majority of these studies were fed with a large plenum that are unlike the narrow chambers that exist inside an actual turbine blade. Examples of research, investigating various aspects of film-cooling, that utilized injection holes having a large L/D ratio include: Ou and Rivir ($L/D = 11.69$) [15], Brown and Saluja ($L/D = 14.74$) [16] and Ligrani et al ($L/D = 8.4$) [17]. The fundamental problem with these studies is that their geometrical parameters are not representative of engine conditions, due to the exaggerated length of the film-cooling holes as well as the large plenums used as settling chambers, and are thus misleading. Figure 2.2 shows an actual turbine blade,which gives a sense of the space constraint that exists in an engine and amplifies the inconsistencies of the previous research, where significantly larger L/D ratios had been utilized.

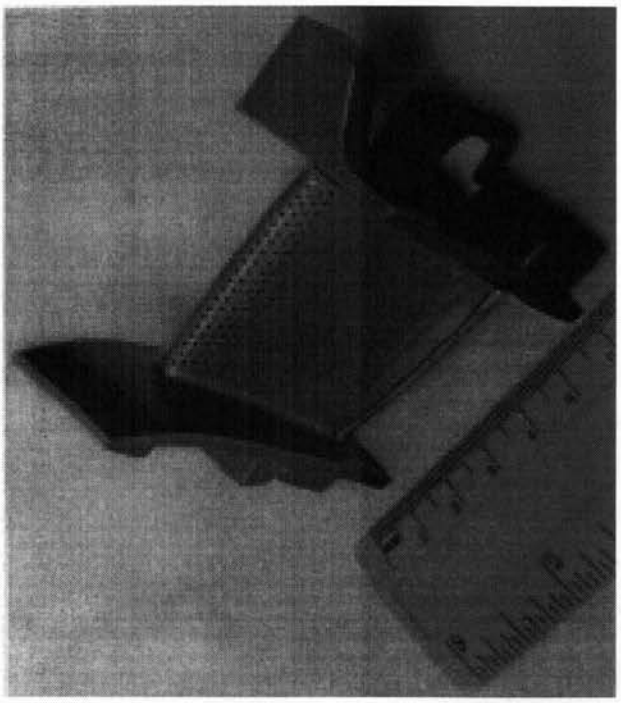

FIGURE 2.2: Picture of an actual turbine blade with a scale besides it for comparison [10]

2.2 Experimental Studies Conducted on Short Film-Cooling Holes

Sinha et al [18] analyzed the behavior of short holes ($L/D = 1.75$) with varying $D.R.$ with a large plenum. They concluded that longer holes attribute to higher adiabatic efficiencies; while the jet emanating from shorter holes is more susceptible to lift-off owing to the larger effective injection angle. Hydrodynamic studies were presented by Pietrzyk et al [19] for the flow characteristics of jets emanating from short holes ($L/D = 3.5$), with a $D.R. = 2.0$, found that there were no significant differences between flow patterns when compared to jets with a unit density ratio. Kohli and Bogard [20] conducted film-cooling and velocity field measurements for short holes ($L/D = 2.8$) inclined at an angle of 55°, which is considerably large compared to the more widely used 35° holes. Their results indicated that the large injection angle holes compared well with the 35° at low blowing ratios; but its performance degraded as the blowing ratio increased. Lutum and Johnson [21] tested

a variety of different L/D ratios, 1.75 – 18, to investigate the effects of length-to-diameter ratio on film-cooling effectiveness. Moderate change in film-cooling effectiveness was observed for L/D ratios greater than seven. The undeveloped flow characteristics and the greater effective injection angle were identified as the driving force for decreased effectiveness for hole lengths in the range of $1.75 \leq L/D \leq 5$, where the lowest effectiveness was measured for the shortest hole: $L/D = 1.75$. Results put forward by Bons et al [22] show significantly reduced effectiveness in the region directly downstream of the film-cooling holes ($L/D = 3.5$) when subjected to high FSTI ($Tu = 17\%$), while increasing cooling in the region adjacent to the coolant holes. Schmidt et al [23] and Sen et al [24] examined the effects of short holes ($L/D = 4$) on adiabatic effectiveness and heat transfer coefficients, respectively, on an identical flat plate experimental set-up. They provided comparison studies between cylindrical and shaped holes, highlighting the superior cooling achieved by the latter geometry.

All of the above studies employed a large reservoir type settling chamber as a plenum, where the coolant was fed perpendicular to the injection holes, unlike the narrow plenum used in the current study. Another common feature amongst all of the above studies was the injection angle of 35° utilized in their flat plate film-cooling set-up (with the exception of Kohli and Bogard [20]), inclined in the direction of the mainstream flow.

While all of the the above studies examined the effects of a single row of short holes inclined at an angle in the streamwise direction, there have also been studies to determine the effects of an array of holes or full-coverage film-cooling, using short holes. Harrington et al [25] utilized large density ratio and high FSTI, on ten rows of short ($L/D = 1$), normal coolant holes. Sasaki et al [26] also conducted a study on multiple rows of relatively short ($L/D = 4.12$) film-cooling holes.

2.3 Numerical Studies Conducted on Short Film-Cooling Holes

While the above section dealt with experimental studies; this part of the chapter will discuss the numerical studies conducted on short-hole film-cooling. Leylek and Zerkle [27] presented numerical results for short holes ($L/D = 1.75$ & 3.5) coupled with a plenum. They explained the jetting effect existing in short holes as

a direct consequence of counter-rotating vortices, which intensify in strength with higher blowing ratios, making the exiting coolant flow more turbulent. They also relate the presence of these vortices to the sudden change in direction that the flow undergoes when it enters the coolant hole from the plenum; thus, intrinsically linking the plenum design to the flow structure of the coolant. They also concluded that the flow structures existing in coolant holes with large L/D ratios are well developed and are as a result very different from those forming in short holes.

Numerical studies for short hole configurations were conducted by Laroche [28] ($L/D = 3.5$), who studied the effects of FSTI on cooling effectiveness, comparing it against experimental values. He deduced that higher levels of FSTI decrease film-cooling effectiveness.

Walters and Leylek [29] conducted computational studies, to validate the experimental work done by Sinha et al [18] ($L/D = 1.75$) and Pietrzyk et al [19] ($L/D = 3.5$). This research is very similar to the one conducted by Leylek and Zerkle [27]; but produced results that were in better agreement when compared to the experimental work.

2.4 Studies of Short Film-Cooling Holes Coupled with a Narrow Plenum

Burd et al [30] investigated the hydrodynamic difference between the injection patterns of long ($L/D = 7.0$) and short holes ($L/D = 2.3$) when subjected to different free stream turbulence intensity (FSTI). They concluded that injection holes with a shorter delivery length produce a jetting effect, where the flow had a tendency to mix with the mainstream flow but provided better spanwise coverage, while the flow ejecting from the longer holes was more settled offering more protection to the blade in the downstream region. The differences between the two hole lengths was less prominent at a higher FSTI of 12%. In a later study, Burd and Simon [12] included the effects of two designs of narrow plenums ($H/D = 2$); differing in their delivery pattern, co-flow and counter-flow, with long and short holes. They reported lower effectiveness values with a co-flow plenum due to jet detachment, while the the counter-flow plenum was attributed with keeping the jet attached. The counter-flow plenum also had the highest magnitude of effectiveness values

in the near-hole region and continued to be better placed even in the downstream region, when compared to a larger plenum.

Berhe and Patankar [31] introduced the narrow plenum ($H/D = 4$) and numerically investigated the effects of surface curvature on cooling effectiveness using relatively short holes ($L/D = 5$). They further extended their research [32] by conducting additional tests on varying L/D ratios from 1.75 – 6 and concluded that the hole length was a much less significant film-cooling parameter compared to surface curvature, blowing ratio and hole spacing; when tests were conducted on curved surfaces rather than a flat plate.

Walters and Leylek [33] performed another set of computational studies employing the same short hole ratios as their previous work [29], but added a plenum ($H/D = 4$) to the set-up. Their observations of short hole flow structures were similar to previous findings by Leylek and Zerkle [27].

2.4.1 The Case for a Counter-Flow Plenum

Researchers from Purdue University, have done extensive research in short hole film-cooling coupled with a narrow plenum. Hale et al [34] tested two lengths of angled holes ($L/D = 2.91$ & $L/D = 1.16$) and two normal injection holes ($L/D = 3$ & $L/D = 0.66$) with two narrow plenums (co-flow and counter-flow), having a $H/D = 1$. The longer injection holes resulted in higher spanwise spreading and better effectiveness values downstream compared to shorter holes, the only exception being at a low blowing ratio of M = 0.5, where the shorter normal holes fared better than their longer counterpart. The counter-flow plenum resulted in better centerline effectiveness and spanwise coverage for the short normal holes, while the long normal holes and short angle holes were impervious to the plenum flow direction. They also concluded that plenum and hole geometry can have significant effects on the flow-field, especially for short holes.

Peterson and Plesniak [35] analyzed the velocity fields of multiple-jets in cross-flow varying the same geometrical parameters as Hale et al [34]. They concluded that the counter-flow plenum worked better in tandem with short holes since it produced in-hole vortices that counteracted the counter-rotating vortex pair (CRVP). CRVP are kidney shaped vortices that exist downstream of the injection holes and are responsible for jet lift-off and mixing, thereby lowering cooling effectiveness (Figure 2.3). The in-hole vortices weakened the CRVP, producing lower

jet trajectory and increasing the spanwise spreading. In a later study by the same authors [14], additional findings were presented which show that a co-flow plenum strengthens the CRVP and thus reduces cooling. In an another study by Hale et al [36], that included both numerical simulations and experimental data, heat transfer measurements that corroborate the existence of CRVP and its adverse affect in increasing heat transfer and its relation to the flow direction in the plenum were presented.

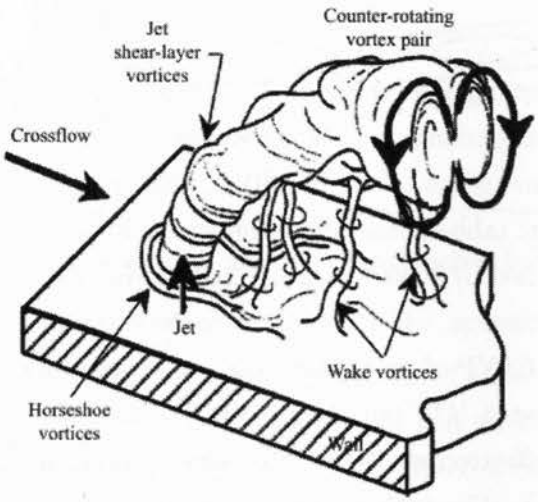

FIGURE 2.3: Structural features of jets in crossflow [14]

2.5 Recent Innovations in Film-Cooling

Many researchers have found innovative ways to increase film-cooling effectiveness by altering the strength and formation of CRVP, associated with the crossflow emanating from cylindrical holes and the antecedent for jet lift-off and increased mixing. Haven et al [37] found substantial evidence that shaped film-cooling holes weaken the CRVP by forming anti-kidney vortices, that have an opposite sense of rotation compared to the CRVP. In the last 30 odd years [11], 2700+ manuscripts have been published, dealing with a gamut of parameters in the area of film-cooling; yet, the only advancement has been the advent of shaped holes, which have proven to be more effective compared to the easily manufacturable and more popular cylindrical holes. Shaped holes have an expanded exit area on the plane of the surface of the injection jet, which result in two major occurrences: reducing

the blowing ratio at the exit of the hole leading to decreased penetration of the jet into the mainstream flow and the other being the Coanda Effect, causing the jet to hug the surface. Other research in the area of shaped holes includes Sen et al [24], Schmidt et al [23], Taslim and Khanicheh [4], etc. Researchers are being more innovative by experimenting with innovative hole shapes as manufacturing through electron-discharge machining becomes more common place. Okita and Nishiura [38] reported higher effectiveness values achieved from an arrowhead-shaped hole, while Lu et al [39] performed tests on crescent shaped holes and other novel hole shapes.

Numerical simulations were conducted by Reddy and Zaman [40] to study the implications of placing triangular tabs on the exit of cylindrical hole, as a mean to limit the disadvantageous effects of CRVP. They reported decreased vorticity in the flowfield of the tabbed case when compared to the no-tab case. Holes with horizontal tabs, studied by Ekkad et al [41] had shown an increase of nearly 200% in film-cooling effectiveness, which is credited to the vorticity generated by the tabs that counteract the CRVP of the coolant jets. As an extension of the above study, angled tabs were tested [42]; but the reports had mixed results. Although the tabs increased the effectiveness (200-300%), they also enhanced the heat transfer coefficients (40-50%). The authors admitted that the application of tabs would not be a practical solution in real engines.

In a bid to decrease the penalty imposed by CRVP, Ely and Jubran [43] presented numerical simulations that increased cooling effectiveness by a factor of 1.35 by utilizing sister holes. This study was preceded by Javadi et al [44], the first to introduce this concept. Sister holes is a new scheme of film-cooling geometry that makes use of three cylindrical holes: one primary injection hole bounded by two supplementary or sister holes. A similar study based on the sister hole concept was also presented by Dhungel et al [45].

2.5.1 Upstream Ramp

Na and Shih [2] modified the upstream geometry of film-cooling holes by inserting a ramp, modifying the hot-gas boundary layer and the cooling jet interaction, to improve cooling effectiveness. They numerically simulated three ramp designs each having a different angle, α (8.53°, 10° and 14°) with respect to the flat plate, with a constant length of $2D$, placed upstream of the short hole ($L/D = 3.5$) at varying

locations, $\beta = 0.5D$ and D (Figure 2.4). The design employs a large low speed reservoir type plenum ($H/D = 10$). They observed that the mainstream flow, deflected by the ramp, creates a circulation region between the backward-facing ramp and the upstream region of the hole, allowing the coolant to flow through the hole easily. The upstream ramp prevents the deflection of the coolant jet until further above the surface, thus increasing lateral spreading. The study concluded that all of the ramp configurations significantly improve film-cooling effectiveness.

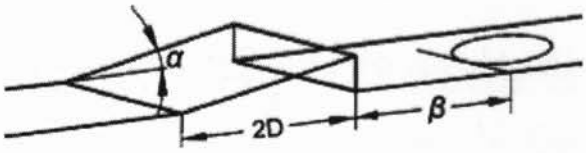

FIGURE 2.4: Schematic of the upstream ramp studied by Na & Shih [2]

Barigozzi et al [46] performed surface measurement experiments based on the above study but used a longer hole ($L/D = 7.0$) and an injection angle of 30° compared to 35° used by Na and Shih [2]. They tested a ramp case of $\alpha = 14°$ and $\beta = 0.5D$. They also observed trends of reduced mixing and better lateral distribution of coolant when compared to the baseline case. This advantage was prominent only in the near hole region and diminished downstream due to high turbulence. As an extension of the above study, Barigozzi et al [47] performed flowfield measurements and assessed that the aerodynamic losses incurred due to the upstream ramp were very high.

2.6 Two Rows of Film-Cooling Holes

Although, the majority of open literature data on film-cooling is based on single row holes; research done by Kruse [48] showed that double row of holes performed better. Le Brocq et al [49] concluded that a staggered pattern of holes provided better cooling than in-line holes, when investigating behavior of multiple rows of film-cooling arrangements. Jubran and Brown [50], Maiteh and Jubran [51] and more recently, Yuen and Martinez-Botas [52] had used a staggered row hole pattern to conduct their research, when investigating multi-row arrangements. All of the above studies had used long injection holes ($L/D > 4$), except Yuen and

Martinez-Botas [52] who had used an L/D ratio of 4. They also found that two rows were advantageous for all blowing ratios, compared to single row cases, as the upstream flow may redirect the downstream jets and increase the temperature gradient in the vertical direction at a given streamwise location, plus cool the surface between rows. They were also of the opinion that the spanwise variation in effectiveness diminished and better effectiveness values were achieved for P/D of 3. Similar findings were reported by Jubran and Brown [50].

2.7 Contributions of the Present Study

The literature available on short film-cooling holes is very limited and almost no studies have been conducted to study the effects of two rows of angled film-cooling holes with a narrow plenum. This study presents the effect of a narrow plenum coupled with the shortest angled film-cooling hole ($L/D = 0.87$), available in the open literature. The effects of adding an extra row of staggered holes in the upstream region are also studied. In lieu of increasing the adiabatic effectiveness, an upstream ramp is added to the single and double row configurations. The upstream ramp, in itself is a very new concept in film-cooling and the two studies that have been published use large L/D ratios. To this end, adiabatic effectiveness data is collected to asses the viability of the various configurations and report any significant improvements afforded by a second row or an upstream ramp.

Chapter 3

Experimental Apparatus and Procedures

This chapter describes the current experimental set-up utilized to perform the film-cooling research, including: measurement techniques, different instrumentations, calibrations and procedures that were followed. The experimental conditions as well as the post-processing of raw data accrued from various devices will also be considered in this section

3.1 Wind Tunnel

The wind-tunnel is constructed of $\frac{1}{8}$ inch sheet metal and lacked windows on all its original three sections, each measuring 4 feet. These sections, along with the bell, formed the wind-tunnel. The innards of the wind-tunnel were sanded and painted so as to form a smooth continuous surface, fit for film-cooling research. The exterior was also given a fresh coat of anti-rust paint. The basic platform, on which the test sections of the wind-tunnel rests, consists of a rail bar that connected all the sections of the wind tunnel together and allowed it to rest on the three legs or support bars, which were designed and constructed by Mr. Sandro Leoni [53] as part of a final-year undergraduate thesis.

In order to use the wind tunnel for film cooling research we needed to design a set-up where the film-cooling plate, along with the test plate, where the thermocouples would be embedded, could be fitted flush with the base or the floor.

Although there are multiple sections of the wind-tunnel that are joined together, the term test-section will be used for that particular segment of the wind-tunnel where the film-cooling research was carried out. Additionally, we also wanted to create windows on at least two sides of the test-section to allow for observation as well as retain the option to measure temperature change on the test-plate using optical devices such as laser or liquid crystal. To satisfy the above two requirements using the metal test section, we would have to cut out portions of the wind tunnel to allow for the film-cooling plates and the viewing windows. It was later discovered that the metal sections were warped and it was deemed unfit for further work. Thus, a new wooden test section was built and incorporated with the old metal ones; making sure that the joints of the wind-tunnel were flawless, aesthetically as well as aerodynamically. The wooden test section was designed and built to accommodate the film-cooling test plates, plenum and the thermocouple plate, the details of which will be discussed later. Figure 3.1 is an illustration of the wooden test section, with the injection and thermocouple attached and Figure 3.2 is a picture of the wind-tunnel facility where the film-cooling study was conducted.

3.2 Test-Section Trolley

Since the design of the wind tunnel was altered, our ambitions changed with it. The foresight for future research compelled us to design a portable test section that could be mounted on a trolley rather than the rail bars, to avoid fixing it and thus making it immobile. Having the test-section rest on a trolley would make it possible to conduct more than one research activity at a time, if multiple test sections were available. It would also give researchers the alternative to update or repair the current test section by conveniently rolling it out to the workshop or even allowing other faculties or students to conduct their own research by simply building their custom test-section.

A variety of options were considered for the trolley design: having a height adjustable pulley or winch jack, similar to ones used to raise cars, that could be removed once the test section was attached to the rest of the wind tunnel; a simple detachable push cart to attach the test section; or, a push cart fixed to the test section with storage underneath for the secondary supply loop. All of the above would have had rugged castors to allow for transportation. The last design was

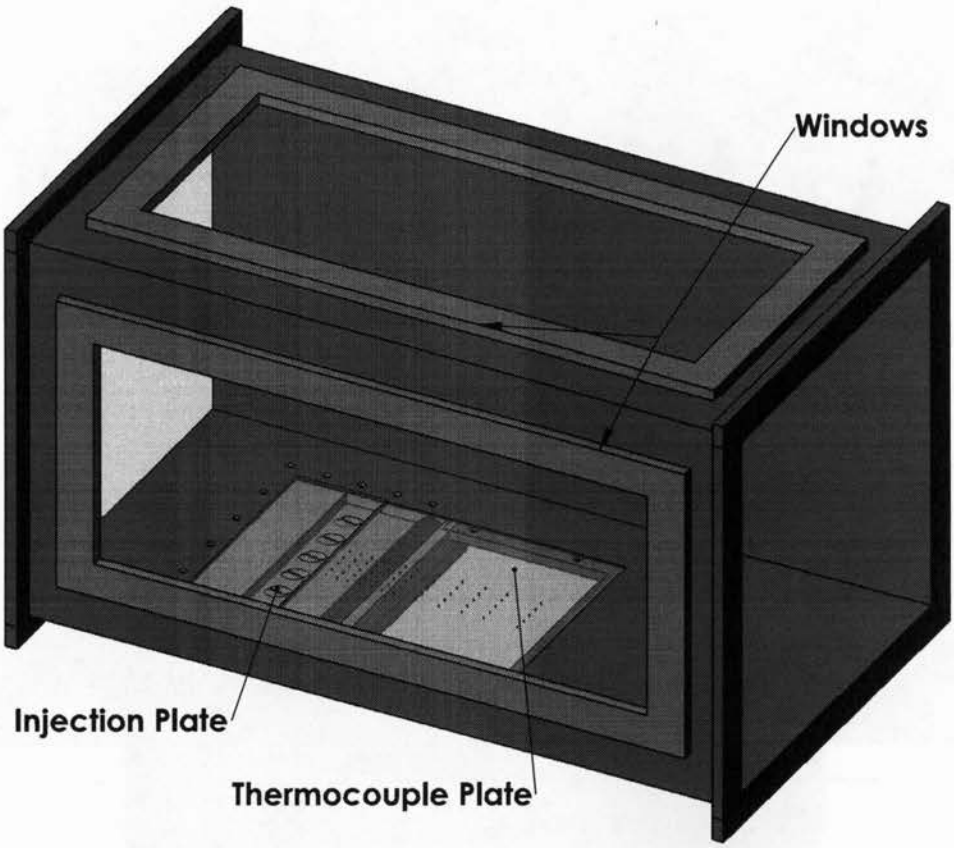

FIGURE 3.1: Wooden test-section built for conducting film-cooling experiments

selected as there was a trolley available to us, which could be just right for our set-up, with a few minor alterations, and save us time and money. To accommodate the cart, the rail bars which held the wind tunnel together were severed and an additional two supports, one for the bell and another for the section downstream of the test section, were built, to have the wind tunnel exist as a self supporting fixture, if and when the test section were removed. Figure 3.3 is an image of the trolley with the test section attached to it.

3.3 Fan Mount

The wind-tunnel was acquired by the ATML along with a Twin City Vane Axial 24B6 fan, but did not include a mount to hold and attach it to the tunnel. Thus, a mount had to be designed and built for the ~700 lb fan that would not only

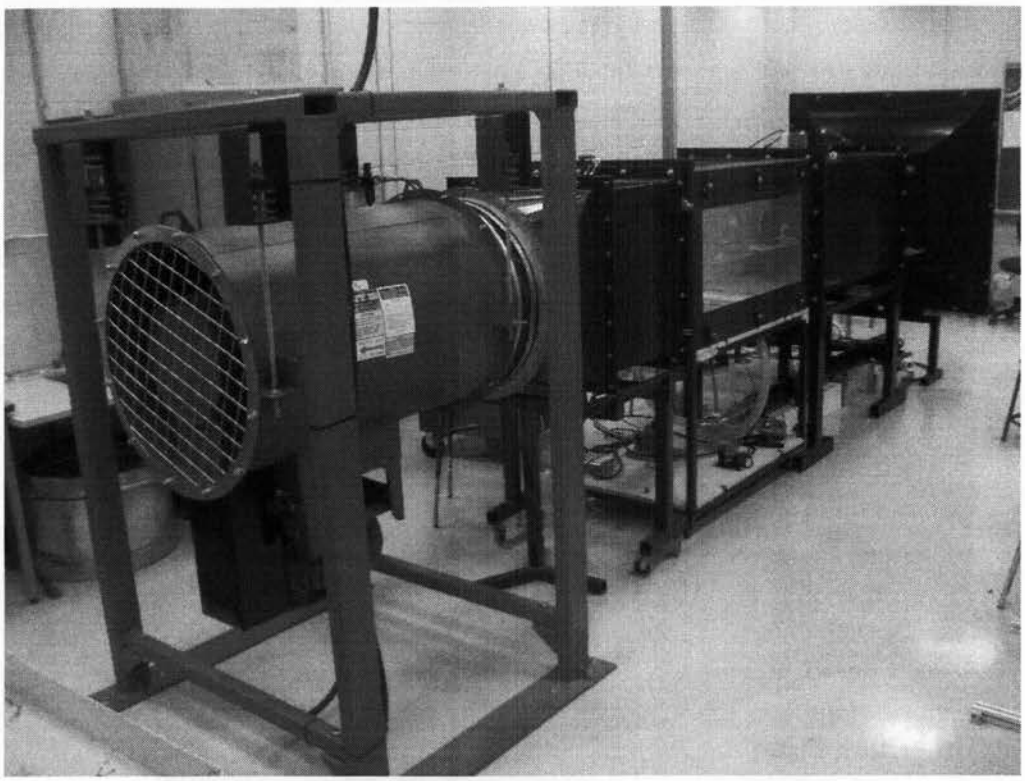

FIGURE 3.2: Wind-tunnel facility at ATML

support the weight but also sustain vibrations from the continuous operation of the wind-tunnel during experimentation. Various design options were considered, among which was the use of a cradle-type structure to hold the engine; but later turned down due to the fear of resonance and its adverse effect on the structural integrity of the mount.

On closer inspection of the fan and its accompanying user's manual, it was found that the fan was designed to be mounted from the ceiling, which was confirmed with the manufacturer of the fan. It would have been impractical to mount it from the ceiling, since it measures 15 feet at the present facility, as well as create a lot of formalities to be drawn out as special permissions would be required from the university and building management. The mount which was finally built simulated hanging from the ceiling through four steel rods, which were attached to rugged springs after making sure that they would hold the weight of the fan without being compressed and prevent it from going into resonance. These springs were housed in steel enclosures that were attached to the main frame of the mount

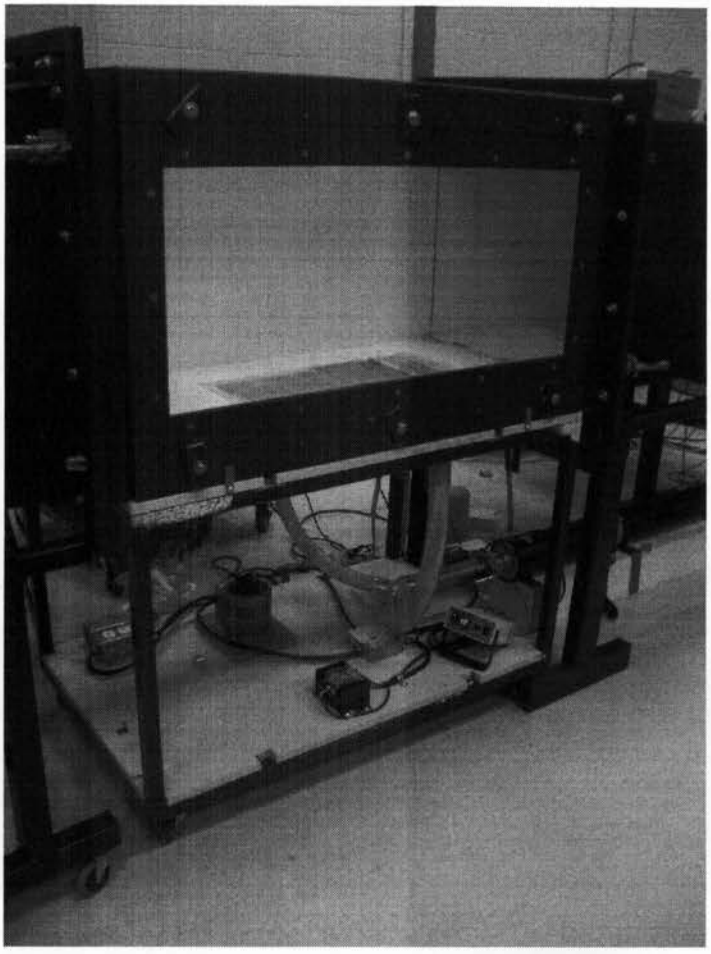

FIGURE 3.3: Trolley with the test section mounted

by heavy duty bolts. The frame consisted of hollow 2 × 4 inches and 2 × 2 inches of steel tubes, that were a $\frac{1}{4}$ inch in thickness; the sizing of the steel tubes were ratified by conducting a buckling analysis. Gussets were used on all edges of the frame to provide extra support to the weldment joints. Two horizontal steel bars were placed towards the bottom of the frame to prevent the fan and the mount from swinging. The whole frame was then attached to two $\frac{1}{4}$ inch steel plates at its base, which were ultimately bolted to the floor for stability. Figure 3.4 shows the fan mount that was finally built, with the fan attached. Though, some of the above features might sound like design overkill, they were carried out to ensure that the mount would not fail under any circumstances, as it would not only cause financial damage but also put students in the way of harm.

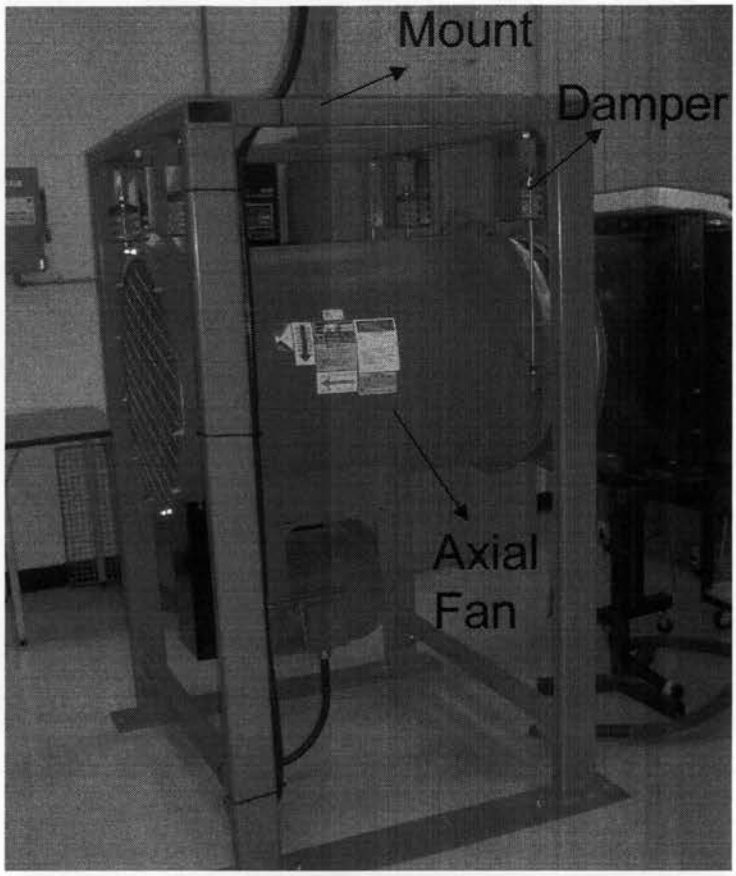

FIGURE 3.4: Fan mount with the engine attached

As expected, the frame supported the fan and prevented any vibrations. Testing of the fan showed that it could provide a maximum air velocity of 10.5 m/s, when operated through a variable speed AC motor controller, which came along with the wind-tunnel set up.

3.4 Secondary Injection Flow Apparatus

The secondary injection flow apparatus was situated under the test-section: with the plenum attached to the floor of the test section; the heater and its controller situated on the base of the trolley, while the supply line for the coolant flow extending till the bell section. To accommodate the requirements of the experiment a secondary loop was custom designed and built.

3.4.1 Secondary or Coolant Air Supply

To alleviate our budget for the experimental set-up, it was decided to use the compressed air supplied by the university, which is supplied in almost all laboratories by a central compressor. The compressed air was connected to a regulator to monitor as well as control the air that would be supplied to the plenum through a rubber hose. Although, the air from the university compressor was supplied at relatively high pressure of 65 psi, it only totaled up to 30 CFM at its maximum, which was later found out to be insufficient to carry tests higher than a blowing ratio of 0.5. Later calculations done by the author showed that to conduct tests at a blowing ratio of 1.5 would require at least 120 CFM of coolant air from the secondary supply loop. It was a common consensus to buy a supply source that would provide heated air to lessen the burden on the heater, but not compromising on the volume of air.

A ShopVac was used as an air blower, instead of its more conventional use as a vacuum. A ShopVac from the laboratory was tested and provided the right amount of pressurized air that was able to traverse the plenum. A hot air blower was used to pre-heat the air, by placing it in on the air inlet of the ShopVac, as the inline heater was unable to efficiently heat up the air to the required temperature of 55 °C.

3.4.2 Supply Loop

A secondary loop system with wider diameter fittings starting from the air inlet till the plenum, to facilitate free flow of air with the least amount of resistance as possible, was built. The new undertaking was planned to include a pitot tube and manometer as the measuring device to assess flow rate in the secondary loop. Literature [54] [55] on pitot tubes showed that for added accuracy measurement from a pitot tube should be conducted at least eight diameters downstream and two diameters upstream from any bends or curves. Additionally, the cross sectional area of the pipe or duct in which the flow is supposed to be measured should be 30× larger than the diameter of the Pitot tube. The smallest Pitot tube that was available was $\frac{1}{8}$ inches in diameter, thus a PVC tubing, 4 inches in diameter was procured as it satisfied the guidelines.

The new secondary loop was constructed of a 4 inch diameter PVC tube that extended for 5 feet. The inlet has a slot for the ShopVac and a NPT fitting for the compressed air. Following the inlet is a y-connector with a ball release valve to give the operator the option to regulate the flow of air: this was provided as there was no other way to adjust the air flow from the ShopVac, which had just one, on and off, setting. To maximize the flow and ease the static pressure, after the inline heater, $2\frac{1}{4}$ inch flexible fiber braided drainage pipes were fitted that were given a generous curvature to prevent any sharp turns. These pipes, one going on either side of the plenum, were connected to the inline heater with a custom designed connector that was built in a Rapid Prototyping Machine (RPM) recently acquired by the Aerospace Department. Care was taken to design the connecter so that it evenly distributes the airflow and that the flow does not impinge on a blunt surface, thus easing the static pressure inside the loop. The pipes were then attached to the plenum by another set of couplers that were custom designed and built in the RPM. The above connectors were custom built since we did not want to go through a series of couplers, attachments and diffusers that were available off the shelf in hardware stores, as it would decrease the flow area and incur an additional penalty of static pressure.

3.4.3 Velocity and Flow Measurement of Coolant

A hole, for the velocity measurement, was drilled 40 inches downstream from the y-connecter and 18 inches upstream of the inline heater, exceeding the guidelines provided by the manufacturer to measure air velocity. A thermo anemometer from TSI Model 9515 was ordered in the interest of long term research and the original plan of using a Pitot tube for velocity measurement was abandoned in lieu of added accuracy offered by a digital velocity meter. This anemometer or velocity meter could be used to measure air velocity ranging 0-4000 fpm and since it is portable, it could be used for other applications as well. The accuracy of this velocity meter as stated by the manufacturer was $\pm 5\%$ [56]. The ideal and most accurate way of measuring velocity in a pipe flow would be to take 16 measurements at various points in the cross sectional area of the pipe and then average it, but the design of our apparatus as well as the shortage of time prevented us from doing so. The velocity readings were taken in the centre of the PVC pipe, which is equable to 90% of the average velocity flowing in the pipe [54]. For example, to obtain an

average velocity of 100 fpm for a particular blowing rate; the flow rate was adjusted to read 111 fpm on the velocity meter.

3.4.4 Secondary Heater

It might be a little confusing for the novice film-cooling researcher to grasp the concept of heating the 'coolant' air, thus, this section will deal with explaining the decision to heat the coolant air as opposed to cooling it. In a conventional film-cooling scenario, the coolant air, being ejected from the film-cooling holes would be atleast 1.5× cooler than the mainstream flow and to measure the effectiveness in that case would be to see its effect on the adiabatic plate. If the adiabatic plate is at the temperature of the coolant ($\eta = 1$): it means that it is completely isolated from the temperature gradient of the hot mainstream flow. On the other hand, if it is at the temperature of the mainstream flow ($\eta = 0$) implies that the coolant is having absolutely no effect on lowering the heat load on the adiabatic test plate. In most cases, the temperature of the adiabatic plate would be some where between the temperature of the coolant and the mainstream flow ($\eta \simeq 0.5$). In essence, what is really of interest is to observe the temperature change on the adiabatic plate, before and after the introduction of the 'coolant', which would be at a different temperature from the mainstream flow. For the present study, the 'coolant' air is heated to a temperature of around 55 °C while the mainstream flow is the at room temperature. The goal of this, or any other film-cooling research, is to maintain the integrity of the coolant film to restrict heat-transfer to the adiabatic test plate and keeping it as close to the coolant temperature as possible. The absolute temperature of the coolant does not matter as much as the its relative temperature to mainstream flow. Additionally, the volume of air in the mainstream flow is astronomically higher than the secondary or coolant flow, as such, it is easier to change the temperature of the coolant air with a lot more ease than it would be to manipulate the temperature of the mainstream flow. Another option would have been to cool the the secondary or coolant air and keep the temperature of the mainstream flow at room temperature. But this process would require the facility to acquire a nitrogen tank which would incur a lot more time and funds. Thus, heating the coolant air with the aid of an in-line air heater was found to be the most convenient way of achieving the goal of conducting a film-cooling study to measure the cooling effectiveness. A thermocouple placed in the plenum right before the coolant exit was attached to the controller and responsible

for regulating its temperature. The temperature of the coolant flow was decided to be kept as high as possible to decrease the sensitivity of the effectiveness values. The lower the temperature difference between the coolant and mainstream flow, the more sensitive were the effectiveness values.

3.5 Plenum

The purpose of this study was to measure the influence of a counter-flow narrow plenum on short holes, similar to the study conducted by Hale [1]. It was imperative that the study be conducted on a plenum that corresponded with the hole length, as a large, reservoir-type plenum used previously in various studies would undermine the results by over-predicting the adiabatic effectiveness, as the flow would be well settled when ejected from the film cooling holes. The design of the plenum was loosely based on the drawing illustrated in Hale's thesis.

The counter-flow plenum used by Hale, closely resembles turbine blade patterns currently being investigated by industry. The plenum, designed and built for the current research, was constructed of wood, owing to its low thermal resistivity and building cost. The plenum was designed longer than the required length as two hole arrangments: single and double row were to be tested. The height of the plenum was 1D ($H/D = 1$), while the the endwall distance was also maintained at 1D for both single and double row cases by placing the appropriate length of thick (0.75 inch or 1D) Plexiglas, upstream of the hole entrance. Figure 3.5 shows an illustration of the plenum with a single row injection plate attached to it as well a spacer plate, which was used to manipulate endwall distance (E/D).

3.5.1 In-Plenum Flow Conditioner

Almost all of the studies reviewed on film-cooling have used some kind of flow straightening device inside the plenum to make the air flow more uniform and well settled, before being ejected. The flow straighteners used by other researchers are by themselves or a combination of honeycomb meshes, egg crate grids, gauze, sieves, nets, etc. Honeycomb meshes are the most commonly used flow straighteners employed for in-plenum conditioning of coolant, but due to the height constraint of the current plenum, an off the shelf, coarse grid, honeycomb mesh was

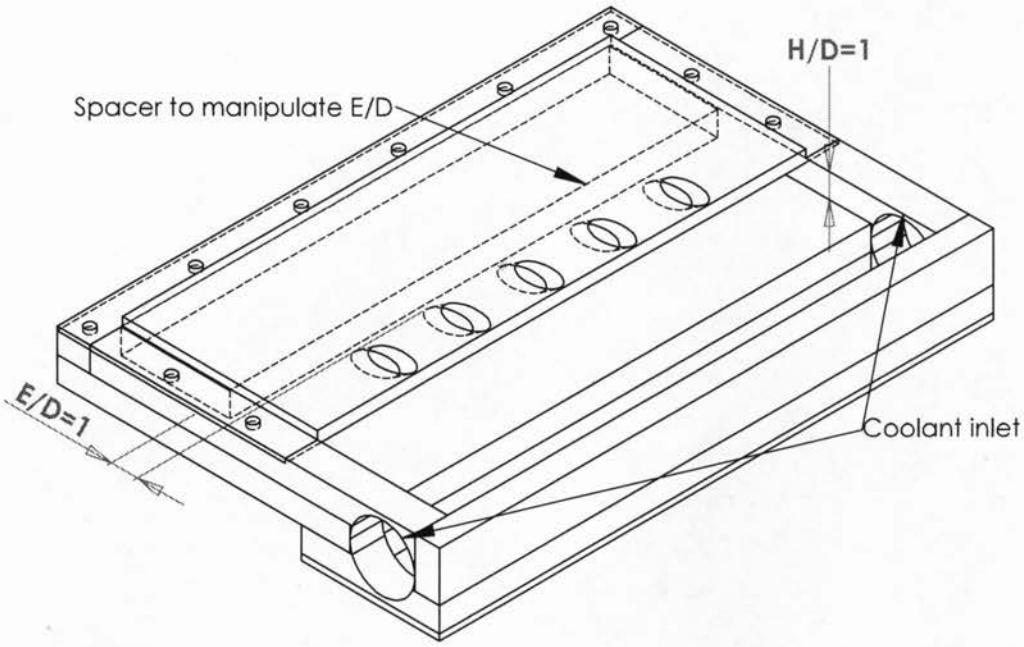

FIGURE 3.5: Plenum Configuration

deemed unsuitable. A finer grid could have been custom designed, but that would have resulted in flow impedance and a pressure drop, which was unacceptable.

A perforated bar, riddled with systematically placed holes, was considered as a potential flow conditioner. Similar systems are utilized by the HVAC industry in large ducts to evenly distribute a steady stream of mist to humidify re-conditioned air. Four rows of staggered $\frac{1}{4}$ inch holes were drilled in a 1.5 inch PVC pipe and placed in the lower step of the plenum (Figure 3.6). The perforated bar extended through the entire width of the plenum and was supplied with air from both sides. Tests done without any flow conditioning had the majority of the air coming from the centre film-cooling holes. This scenario was slightly improved by placing a coarse honeycomb mesh, but the majority of air flow was still ejected through the centre holes, while the holes on the ends barely had any air flow. The perforated bar performed exceptionally well: the flow was evenly distributed through all the film-cooling holes. This was expected to result in a uniform film over the test plate and better spanwise cooling. The uniformity of the flow was checked by sticking a small tuft of light fiber on the exit of the hole and observing the flutter produced by the flow of air emanating from the holes.

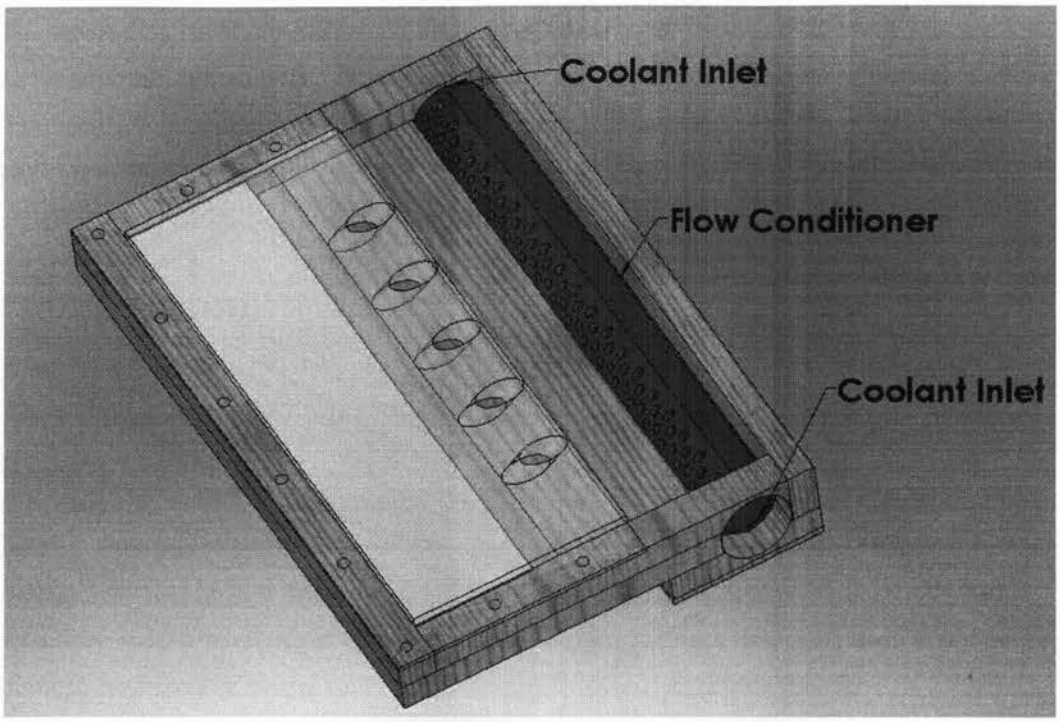

FIGURE 3.6: In-plenum flow conditioner: perforated bar

The perforated flow conditioner bar could serve a dual purpose in future studies of gas turbine cooling by providing internal impingement cooling to hot spots, while conditioning the flow at the same time. Although, such research is beyond the scope of the current thesis, its implication would be worth investigating.

3.6 Injection Plates and Adiabatic Test Floors

The injection plates were designed to fit perfectly flush with the floor of the wooden test section of the wind-tunnel. The tolerances of the the plate were vital for a good fit and a perfectly aligned floor so as to keep the approaching boundary layer undisturbed. The injection plates were constructed of $\frac{3}{8}$ inch Plexiglas and the holes were inclined at a 35° angle in the streamwise direction. Six injection plates were manufactured: three each of single row and double row configurations. To make the manufacturing process of the injection plate more consistent, a jig was built to attach and drill the Plexiglas work piece. The diameter of the holes is identical to Hale's [1] study: 0.75 inch (19.05 mm). The L/D ratio of 0.87 and

P/D ratio of 3, were kept constant for both the plate configurations.Although, Na and Shih [2] had used the term, β to represent the placement of the upstream ramp in their study, this present study will refrain from using it since it might be confused with an angle; the more conventional use of the symbol. A new term, R/D, is introduced here and will be used in the rest of this thesis to depict the non-dimensional distance of the ramp from the upstream edge of the injection holes. The single and two row injection plates were used for three cases each: baseline case (without ramp), ramp at $R/D = 0.5$ and $R/D = 1$. The single row plate had 5 holes. Figure 3.7(a) shows the baseline case for the single row configuration while, Figure 3.7(b) and Figure 3.7(c) depict the single row ramp cases. The double row plates have 9 injection holes: 4 upstream and 5 downstream holes having an S/D ratio of 3. The baseline case for the double row configuration is shown in Figure 3.7(d), while Figure 3.7(e) and Figure 3.7(f) are illustrations of double row ramp configurations.

The adiabatic test plate or thermocouple plate had a total of 60 thermocouples embedded in a $\frac{1}{8}$ inch thick Plexiglas plate, measuring 15 $\times$ 16 inch. In order to keep the test plate smooth; $\frac{1}{16}$ inch diameter, through holes were drilled and the thermocouples were inserted from the bottom of the plate, keeping the welded bead flushed with the surface to record the temperature of the coolant film. The thermocouples were glued to the bottom by an Epoxy adhesive and were then covered with aluminum tape for further reinforcement. The thermocouples were distributed over 12 rows, where the x/D locations were measured from the downstream edge of the film-cooling holes (Figure 3.8). Each row had 5 thermocouples, with the middle being at location $z/D = 0$. To keep the thermocouple plate isolated from the surrounding, it was layered with fiber-glass insulation and expanded polystyrene, from the base; but a large chunk of it was still in very close proximity to the plenum and injection plates, incurring a lot of heat conduction. Thus, the thermocouple plate was adiabatic only in name and the temperature data had to be corrected for the conduction effect, details of which have been explained in Appendix C.

3.6.1 Upstream Ramp

The upstream ramp used in the present study is similar to the one of the ramps utilized by Na and Shih [2]. The ramps angled at, $\alpha = 8.5°$ were placed at two R/D locations: 1 and 0.5. The ramp was manufactured in the RPM. Unlike Shih

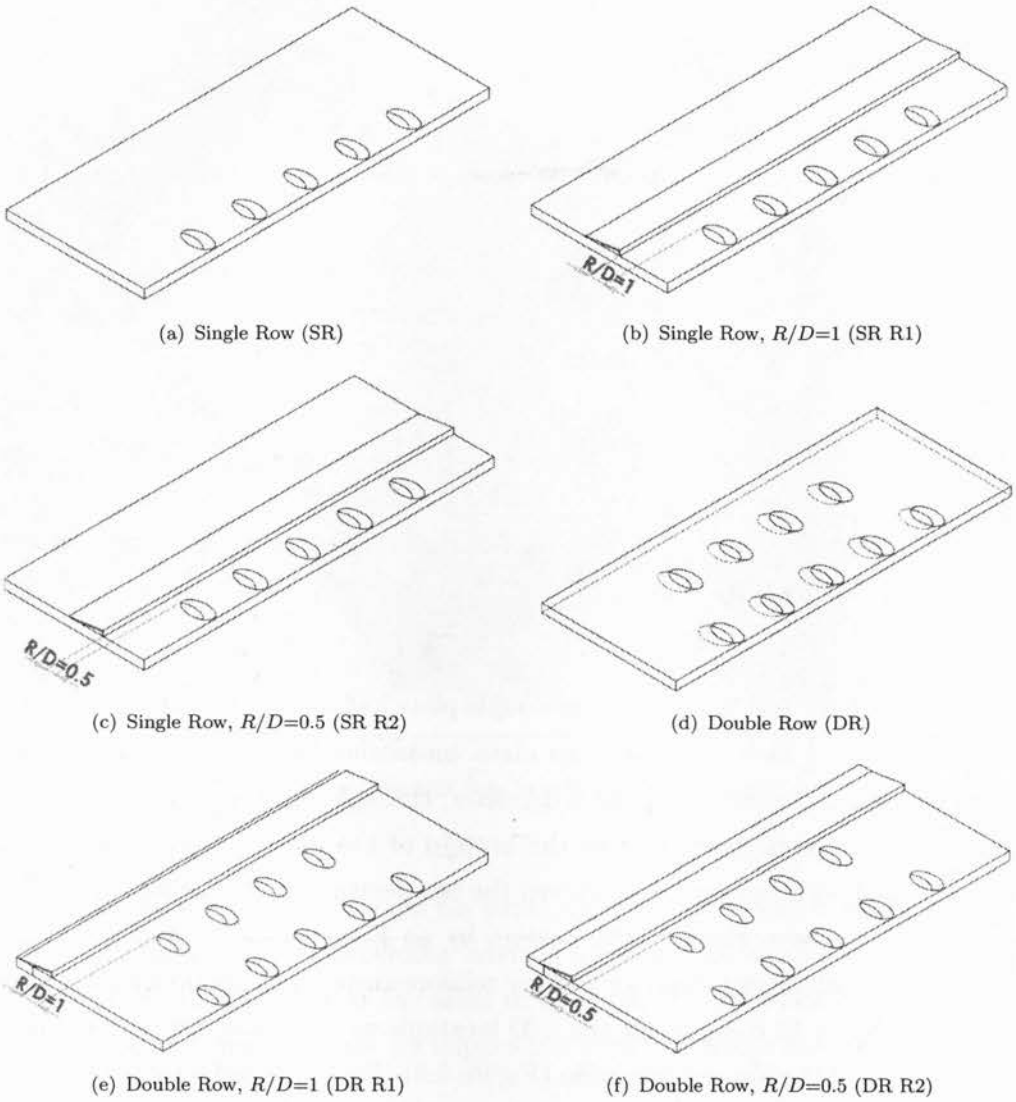

(a) Single Row (SR)

(b) Single Row, R/D=1 (SR R1)

(c) Single Row, R/D=0.5 (SR R2)

(d) Double Row (DR)

(e) Double Row, R/D=1 (DR R1)

(f) Double Row, R/D=0.5 (DR R2)

FIGURE 3.7: Injection plates used for experimentation

and Na's numerical study, the ramp does not span the entire width of the wind-tunnel, but is constricted by the dimensions of the injection plate to present the results in an engine-like scenario. Figure 3.9 shows an illustration of the ramp and displaying the nomenclature associated with it.

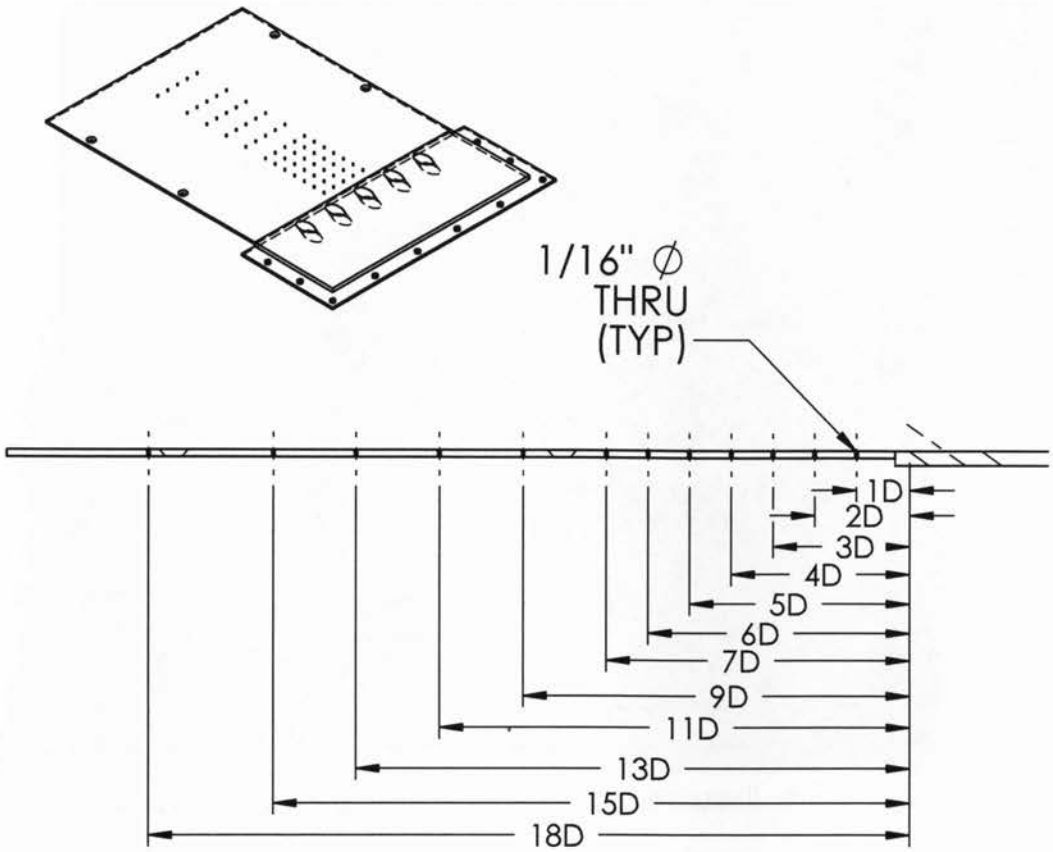

FIGURE 3.8: Thermocouple row location on adiabatic plate in x/D direction

3.7 Assembling the Test Equipment

The floor of the $\frac{3}{4}$ inch wooden test section had a 1 inch wide slot ($\frac{1}{4}$ inch deep) at the periphery of the rectangular cut-out, where the plate was supposed to be positioned. The $\frac{3}{8}$ inch thick injection plates have a complementing raised section to fit into the rectangular cut-out and slot – so as to remain flushed with the floor of the wind-tunnel. The plate rests on the plenum and is installed as one unit. Ten one inch screws, tightened from the top surface of the floor, hold the injection plate and plenum in place.

A lip and groove arrangement has been employed at the downstream edge of the injection plate and the adiabatic plate to eliminate any protruding edges and maintain a smooth uniform boundary layer (Figure 3.10).

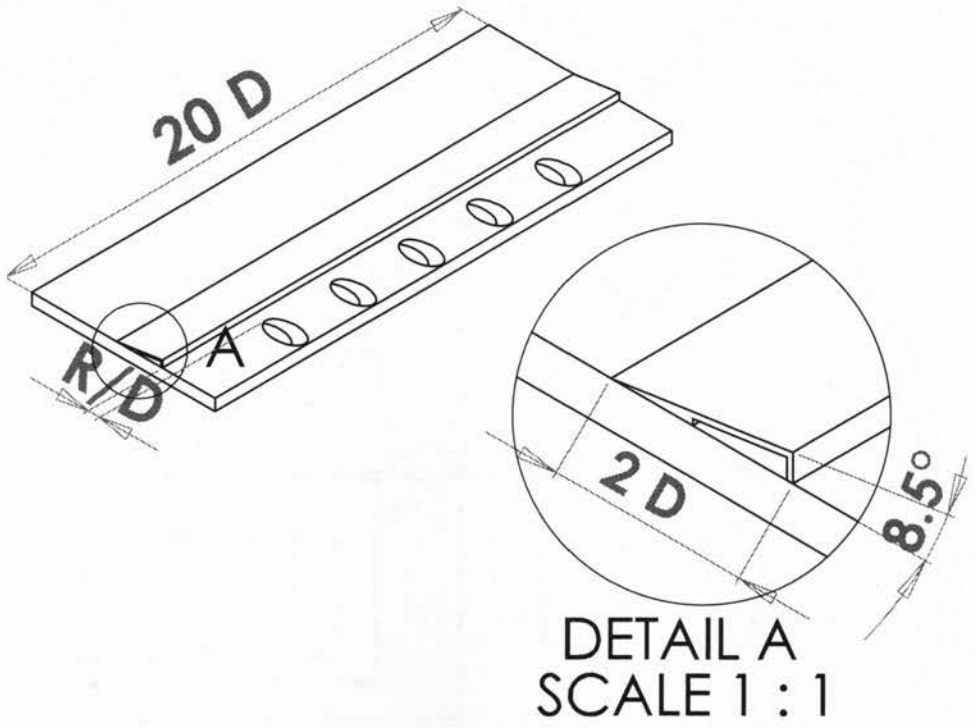

FIGURE 3.9: Illustration of the upstream ramp used in the present study

The adiabatic test plate is installed from the top of the test-section and is held in place by 8 screws.

Further, the screws are driven in counter-sunk holes to prevent any potential boundary layer disturbances.

3.8 Boundary Layer Characterization

The freestream velocity was kept constant at 8 m/s throughout all of the experimental cases by adjusting the fan controller and reading the velocity on the manometer. The boundary layer was triggered by the trip (a $\frac{1}{8}$ inch thick and and $\frac{1}{2}$ inch wide strip of wood that was glued to the floor of the wind tunnel), placed: 0.66 m or 26 inches before the upstream edge of the film cooling holes. This trip acts as the leading edge of a flat plate. As a result of this, the $Re_x = 3.52 \times 10^5$ at the cross-flow, which is representative of engine conditions. The turbulent boundary layer profile just before the injection holes is presented in Figure 3.11 and all of

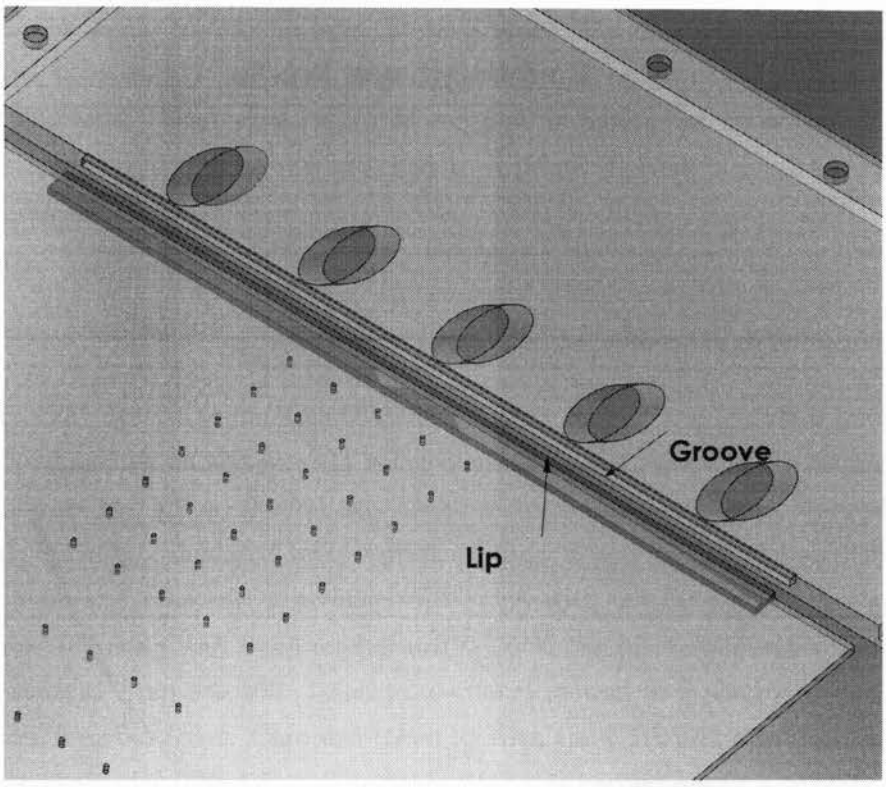

FIGURE 3.10: Lip and groove arrangement between injection and adiabatic plate

the relevant boundary layer characteristics at the location of injection are summarized in Table 3.8. Boundary layer calculations made by the power law agree very well with quantitative measurements performed by Jubran [57] and Jovanović [58] who used sophisticated instruments like constant temperature anemometer (CTA) to measure boundary layer flows, proving to be a valid substitution in the absence of in-situ measurements.

3.9 Data Acquisition

3.9.1 Constant Temperature Anemometer

A high-precision Streamline Research CTA system was utilised to obtain velocity measurements for the mainstream flow as well as its turbulence intensity (Tu). The general system consists of a frame, where only one of the six available modules

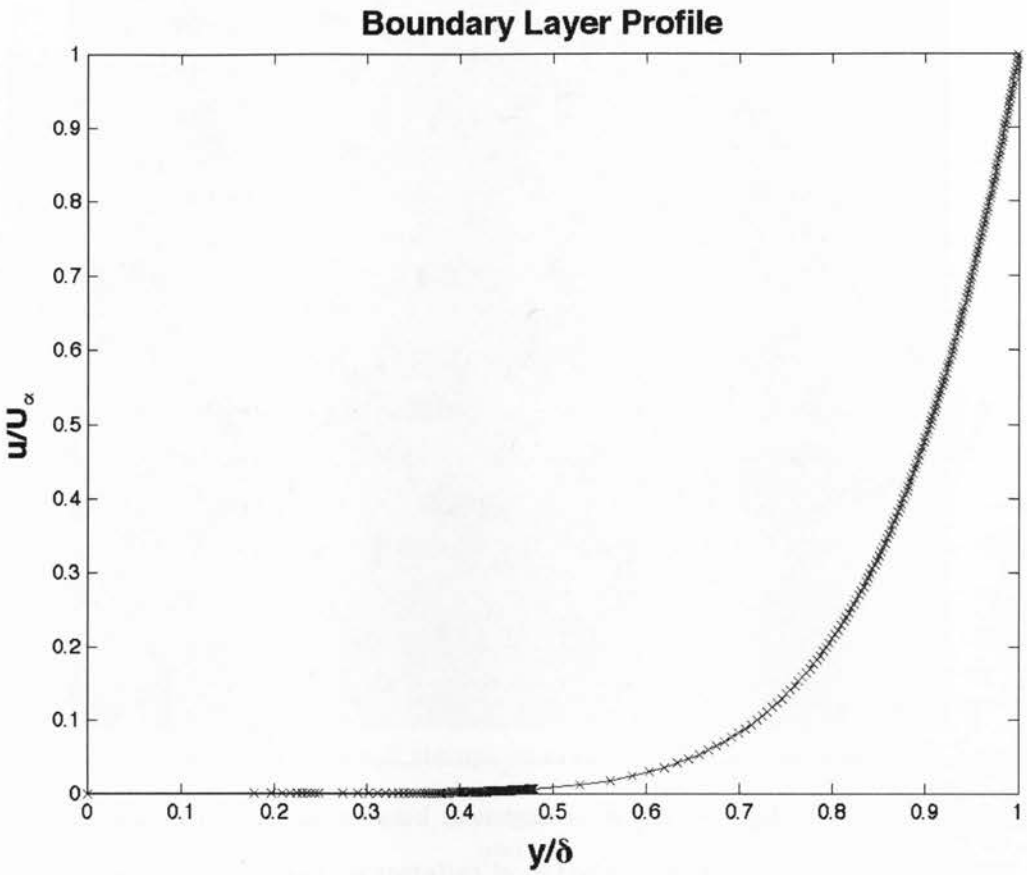

FIGURE 3.11: Boundary layer profile created right before the injection hole exit

TABLE 3.1: Boundary layer characteristics for $U_\infty = 8\ m/s$, immediately upstream of the injection hole exit

Trip wire location	0.66 m
Reynolds Number (Re_x)	3.52×10^5
Displacement Thickness (δ^*/D)	0.11
Momentum Thickness (θ/D)	0.087
Boundary Layer Thickness (δ)	17 mm

is active; a signal conditioner and an A/D board that converts analogue signals received from the CTA module into digital data, to be displayed on the PC for data reduction. The temperature of the flow is monitored by a probe, while a one-dimensional wire probe attached to a probe support is used for velocity measurement.

3.9.1.1 Calibration

For the CTA system to function effectively for our current application it had to be calibrated against an independent velocity measurement device, like a manometer. To calibrate the probe, the voltage, obtained from the anemometer were plotted against velocity, calculated by the pressure drop introduced by the air flow in a Pitot tube and manometer arrangement along with the air density, barometric pressure, humidity and room temperature. Both, the pitot tube and CTA probe were inserted from the top of the wind-tunnel section and placed on the same location, 8 inches apart. Care was taken to align the CTA probe so that the wire was perpendicular to the flow. The calibration was carried out in a velocity range of 2 –12 m/s, so as to operate the wind-tunnel at 8 m/s as per the manufacturers advice. For each of the 15 different velocities, the voltage response from the CTA probe and the pressure drop across the manometer was noted. This data was fed into the Streamware software to produce the calibration curve, which was stored as a reference for future tests. Figure 3.12 shows one such calibration curve. If the probes were not operational for more than week, they were re-calibrated using the above methodology.

3.9.1.2 Turbulence Intensity

Although the CTA was not used as the standard velocity measurement device during experimentation, it was essential to ascertain the Tu of the mainstream flow. The Tu was calculated by the Streamware software by examining the instantaneous velocity and the mean or average velocity and was determined to be 3.3% for a mainstream velocity of 8 m/s (Equation 3.1).

$$Tu = \frac{u_{rms}}{U_{mean}} \tag{3.1}$$

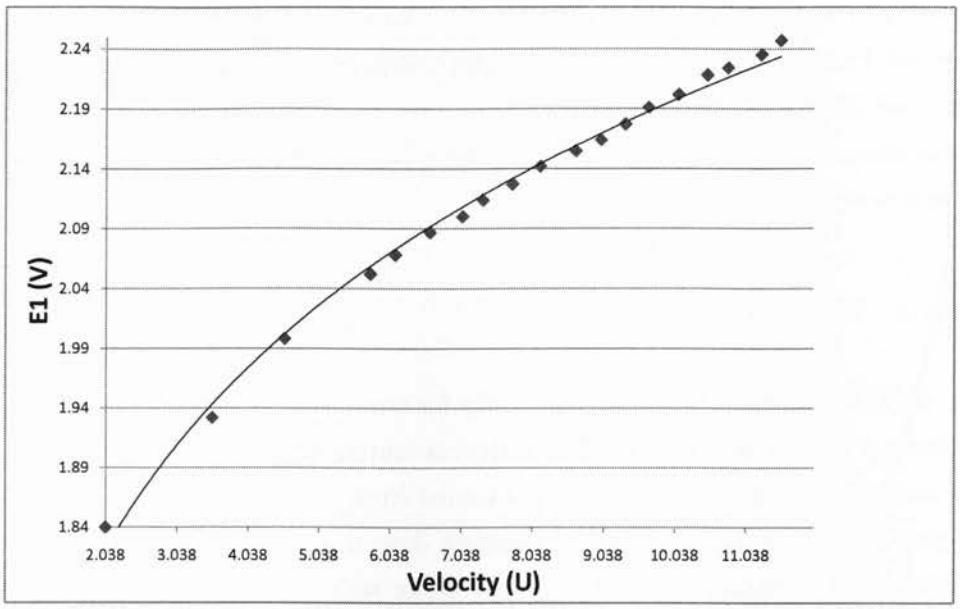

FIGURE 3.12: CTA Calibration Curve

3.9.2 Temperature Acquisition

The 60 thermocouples used on the test-plate were connect to 24 channel A/D converter, out of which only 16 were functional. The A/D data acquisition board would convert the analog signal received from the T-type 30 gauge thermocouples and display it in degrees Fahrenheit. To acquire results for a particular experiment, the temperature would be recorded 3 rows or 15 thermocouples at a time. The temperature was displayed and recorded by a propreitory software supplied by the manufacturer, Orchestrator.

3.10 Experimental Procedure

Following is a typical procedure that was followed to run any one of the 21 experimental cases tested for this study.

1. The internal edges of the plenum were lined with a thin bead of silicone to prevent any air leaks.

2. A thick bead of silicone was applied on the outer edge of the plenum, where the injection plate was placed. This was done to make the plenum air-tight.

3. The plenum along with the plate was secured on the bottom of the wind-tunnel with screws. At this point, fiber braided pipes were connected on either side of the plenum and air supply was turned on.

4. A soap water test was conducted to check for leaks on all sides of the plenum and wherever else there might be a connection or a joint. The air supply was then turned off.

5. The adiabatic test floor was connected on the injection-plate utilizing the lip and groove arrangement and then bolted to the floor of the test section on the remaining three sides.

6. After making sure everything was secured inside the wind-tunnel, it is shut-off with $\frac{3}{4}$ inch Plexiglas window.

7. The axial fan was now switched on and adjusted till the free-stream velocity was at 8 m/s.

8. The first three thermocouple rows of the adiabatic test plate were connected to the temperature DAQ system and monitored to match the temperature of the mainstream flow, which was proctored with a T-type thermocouple placed on the roof of the wind-tunnel.

9. Once the first three rows of thermocouple were all at uniform temperature; the secondary supply was turned on.

10. The secondary supply air was adjusted via the regulator and the ball valve to achieve the desired velocity, which was supervised by the aid of the thermo-anemometer in the secondary loop.

11. The heater was turned on and temperature was recorded on the adiabatic plate every 30 seconds, to determine when steady state was achieved, which usually took 15-20 minutes. Appendix B provides a detailed explanation of how steady state was determined.

12. Once steady state was reached; the temperature of the first three rows were recorded at a frequency of 1 reading/second over a time-period of one minute.

13. Then the next three (Rows: 3-6) thermocouple rows were connected in the DAQ, replacing the first three rows and the above step was repeated. The same steps were repeated for the next six rows.

14. After all the temperature recordings are finished, the secondary heater is turned off with the secondary air on, to cool the plenum back to ambient temperature. The axial fan in the wind-tunnel is also left on to normalize the adiabatic test plate back to room-temperature before the next experiment could be started.

15. If the following experiment was the same case, with just a different blowing ratio then the first 5 steps were skipped.

3.11 Errors, Uncertainties and Repeatability

A detailed approach and calculation of the errors and uncertainties of the experimental results is given in Appendix A. The methodology to arrive at the estimation of errors is adapted from Kline and Mclintock [59]. The error associated with results for cooling effectiveness is at worst 0.5% for $\eta > 0.45$ and at least 4% for $\eta < 0.05$. The error in determining the secondary flow rate was 7%.

The reproducibility of the present study was quantified by repeating a randomly chosen experimental case and comparing the data obtained from both the cases. Figure 3.13 gives the laterally averaged adiabatic effectiveness obtained from the two runs, performed for the baseline configuration for $M = 1$. The average difference between the two runs is 12%.

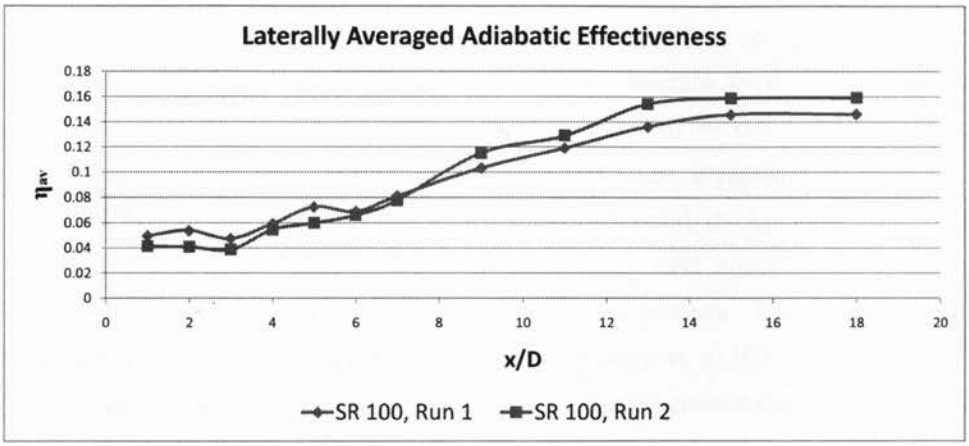

FIGURE 3.13: Repeatability Analysis

Chapter 4

Results and Discussion

In this chapter, the influence of two rows of short holes and an upstream ramp on adiabatic film-cooling effectiveness will be discussed and compared to a single row of holes. Experiments were conducted in the suction type, low-speed wind tunnel at a variety of blowing rations, ranging from $M = 0.5 - 1.5$. Since, the thermocouple plate is not completely adiabatic in nature, Equation 1.1 is used with some reservation. The conduction correction, discussed in Appendix C, details the procedure used to correct the measured values and compensate it for the conduction accrued from the injection plate and the plenum. The procedure used for conduction correction was developed by Etheridge et al [60] and explained in great detail by Colban [61]. All the experiments were conducted at a freestream velocity of 8 m/s, which generated $Tu = 3.3\%$.

The first part of this chapter will present results for the effect of different blowing ratios on film-cooling effectiveness. The second part shows the effect of two rows of holes and the last section delves into the improvement of film-cooling by implementing an upstream ramp. All of the sections are divided into smaller sub-sections to present the results; followed by a summary.

The results presented in this section are for laterally averaged film-cooling effectiveness, η_{av} and centerline effectiveness, η_{cl}. For the laterally averaged film-cooling effectiveness, η_{av}, the data is averaged for the five thermocouples in each row and plotted against a non-dimensional distance, x/D – the downstream distance divided by the inlet hole diameter.

Table 4 lists the case nomenclature which will be used from now on to refer to the 21 cases tested.

TABLE 4.1: Case Nomenclature

Case Name	**Parameters**
SR 50	Single Row, M=0.5
SR 75	Single Row, M=0.75
SR 100	Single Row, M=1.0
SR 150	Single Row, M=1.5
SR R1 50	Single Row, M=0.5, R/D=1.0
SR R1 75	Single Row, M=0.75, R/D=1.0
SR R1 100	Single Row, M=1.0, R/D=1.0
SR R1 150	Single Row, M=1.5, R/D=1.0
SR R2 50	Single Row, M=0.5, R/D=0.5
SR R2 75	Single Row, M=0.75, R/D=0.5
SR R2 100	Single Row, M=1.0, R/D=0.5
SR R2 150	Single Row, M=1.5, R/D=0.5
DR 50	Double Row, M=0.5
DR 75	Double Row, M=0.75
DR 100	Double Row, M=1.0
DR R1 50	Double Row, M=0.5, R/D=1.0
DR R1 75	Double Row, M=0.75, R/D=1.0
DR R1 100	Double Row, M=1.0, R/D=1.0
DR R2 50	Double Row, M=0.5, R/D=0.5
DR R2 75	Double Row, M=0.75, R/D=0.5
DR R2 100	Double Row, M=1.0, R/D=0.5

4.1 Effect of Blowing Ratio on Film-Cooling Effectiveness

4.1.1 Single Row Cases

Four blowing ratios were tested for the single row case. The most significant effect of blowing ratio is seen near the near hole region for $x/d < 7$ (Figure 4.1). Highest effectiveness is seen for $M = 0.5$. As the exit speed of the coolant increases, so is its tendency towards jetting. A steady decrease in efficiency can be noticed with increasing blowing ratio, where there is little to no protection offered for $M = 1.5$. For $M = 0.5$, the adiabatic efficiency decreases till $x/D = 6$ and then stabilizes till the downstream region. The opposite trend is noticed for $0.75 \leqslant M \leqslant 1.5$, where the cooling effectiveness increases downstream of the hole relative to the upstream effectiveness. This phenomenon is called jet re-attachment: at higher blowing ratios the jet lifts-off from the surface due to excessive momentum [1], but as it loses momentum downstream of the hole, it re-attaches itself. Similar, trends of blowing ratios have been reported by Jubran and Brown [50] and Hale et al [34], where a decrease in cooling efficiency is noted for $M > 0.5$.

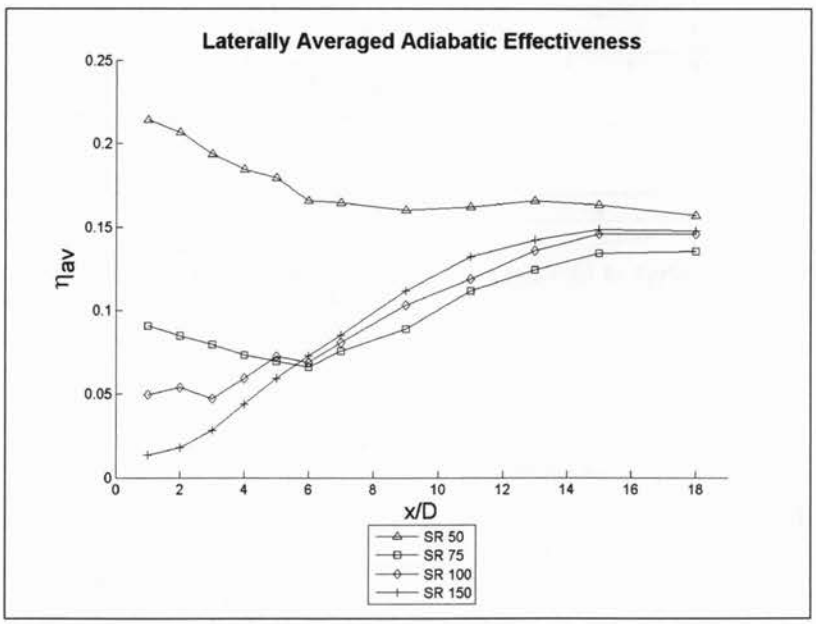

FIGURE 4.1: Effect of blowing ratio on single row (SR) case

The results for single row, $R/D = 1.0$ (SR R1) show decrease in effectiveness with higher blowing ratio, where $M = 0.5$ offers the best protection (Figure 4.2). The near hole region, for $0.75 \leqslant M \leqslant 1.5$, shows an instantaneous drop in efficiency after $x/D = 1$, but manages to re-attach between $2 \leqslant x/D \leqslant 8$, then remaining more or less constant till the downstream region. Similar trends are noticed for the single row, $R/D = 0.5$ (SR R2) (Figure 4.3). Another important feature that exists for both scenarios involving the upstream ramp is that the increase in blowing ratios between, $0.75 \leqslant M \leqslant 1.5$, does not show much depreciation in cooling effectiveness after $x/D > 6$. The centerline effectiveness data for the above three cases have been presented in Figures 4.4 – 4.6.

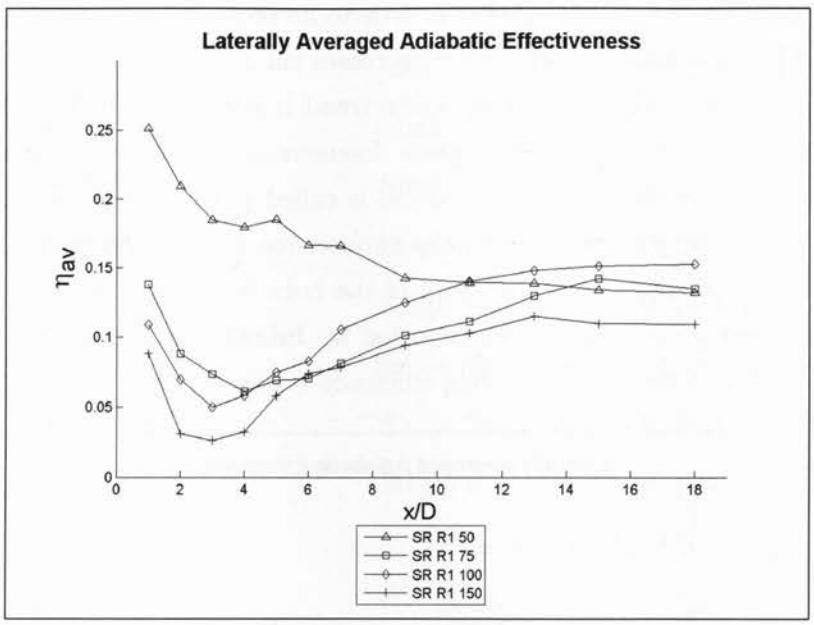

FIGURE 4.2: Effect of blowing ratio on single row case with upstream ramp at $R/D = 1$ (SR R1)

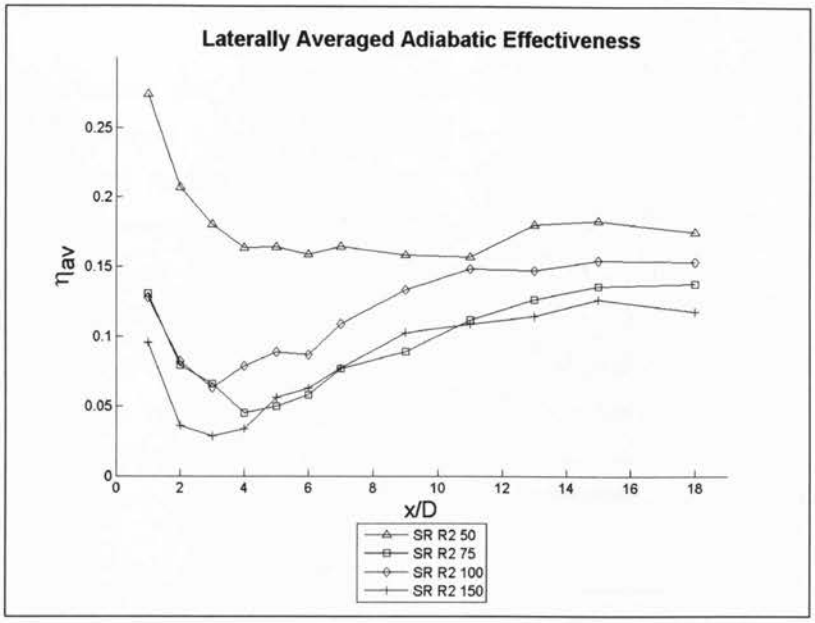

FIGURE 4.3: Effect of blowing ratio on single row case with upstream ramp at $R/D = 0.5$ (SR R2)

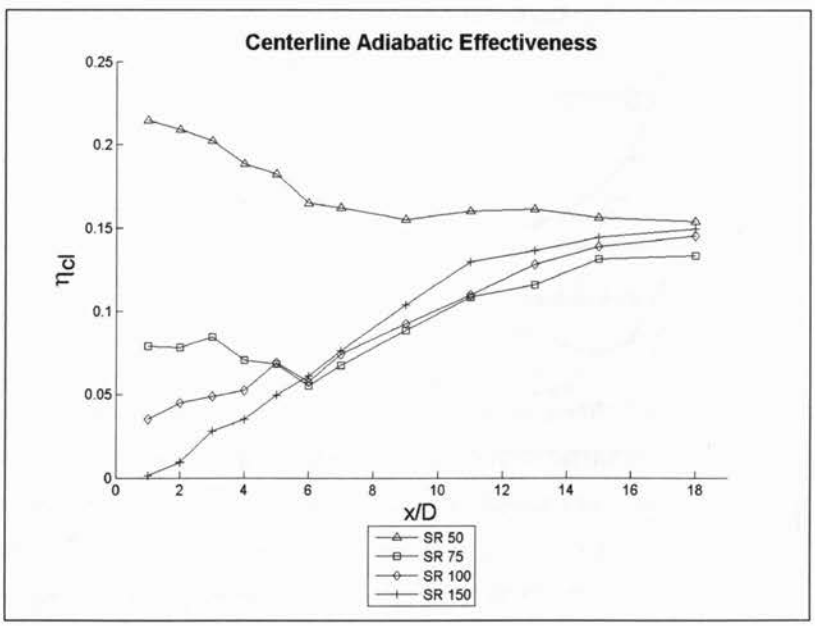

FIGURE 4.4: Centerline data for the effect of blowing ratio on single row (SR) case

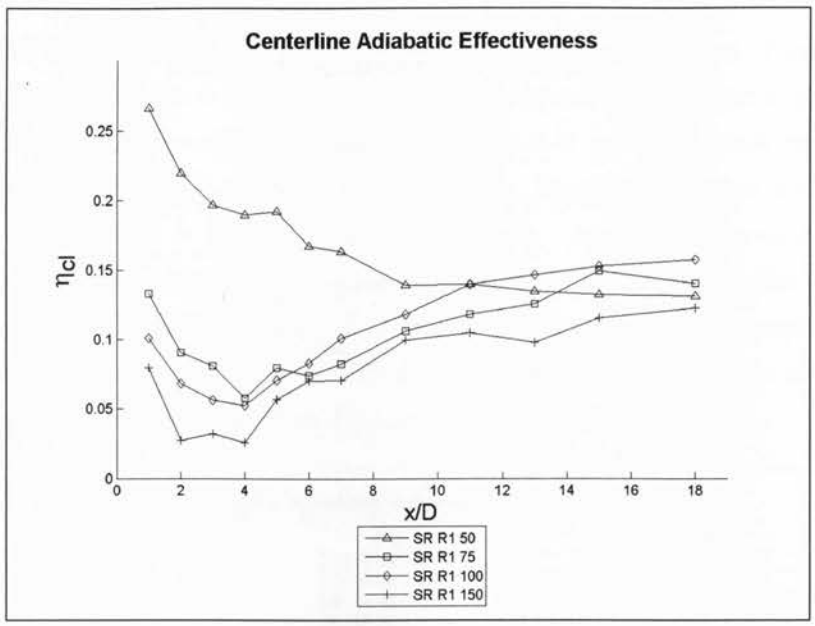

FIGURE 4.5: Centerline data for the effect of blowing ratio on single row case with upstream ramp at $R/D = 1$ (SR R1)

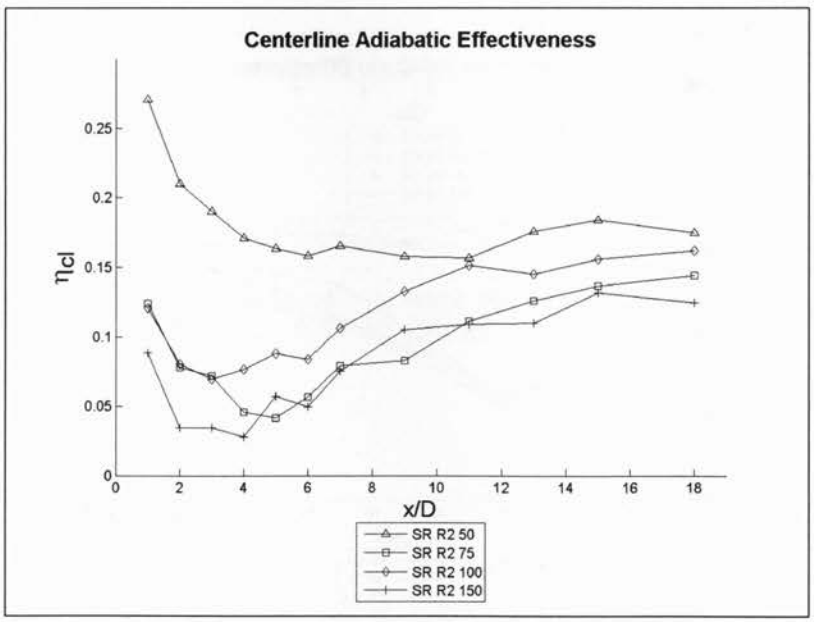

FIGURE 4.6: Centerline data for the effect of blowing ratio on single row case with upstream ramp at $R/D = 0.5$ (SR R2)

4.1.2 Double Row Cases

The baseline double row configuration (DR) results for varying blowing ratios is presented in Figure 4.7. The trend seen in this set of results is very similar to the one noticed in the single row cases, where the film cooling effectiveness decreases with increasing blowing ratio. The coolant flow for higher blowing ratios, $M > 0.5$, is lifting off – resulting in low effectiveness immediately downstream of the injection holes but re-attaches itself, achieving its peak effectiveness value at exactly the same location of $x/D = 6$. The peak effectiveness value for M =0.5 is achieved $x/D = 4$, where-after a monotonic decrease is noticed.

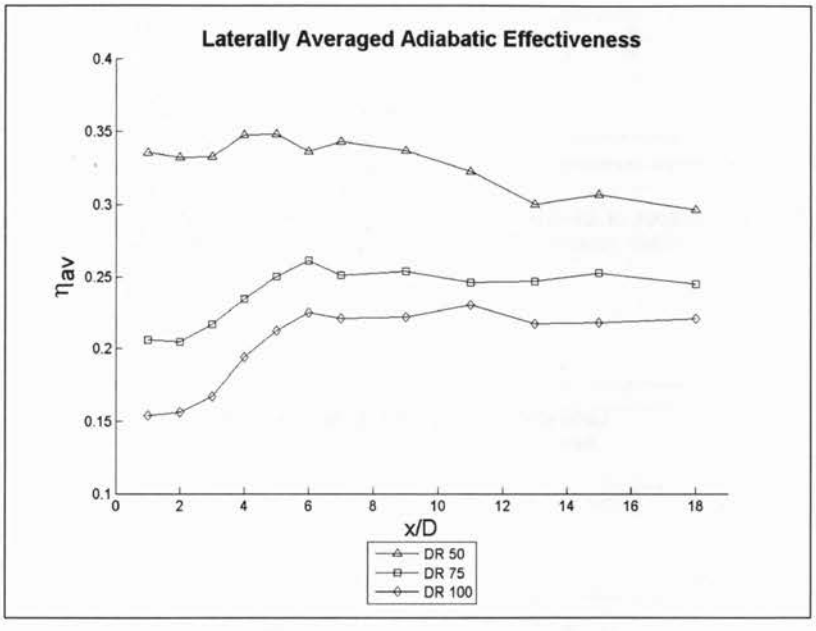

FIGURE 4.7: Effect of blowing ratio on double row (DR) case

The laterally averaged film-cooling effectiveness results for the two ramp cases (Figure 4.8 & Figure 4.9) show nothing different in terms of patterns, when compared to the above cases. The only difference being that the peak value for film-cooling effectiveness is achieved at $x/D = 4$ for $M > 0.5$. The presence of the upstream ramp has improved the uniformity of the coolant jet coverage downstream of the hole, especially for higher blowing ratios, but the performance is still lackluster when compared to $M = 0.5$. The centerline effectiveness data for the above three cases have been presented in Figures 4.10 – 4.12.

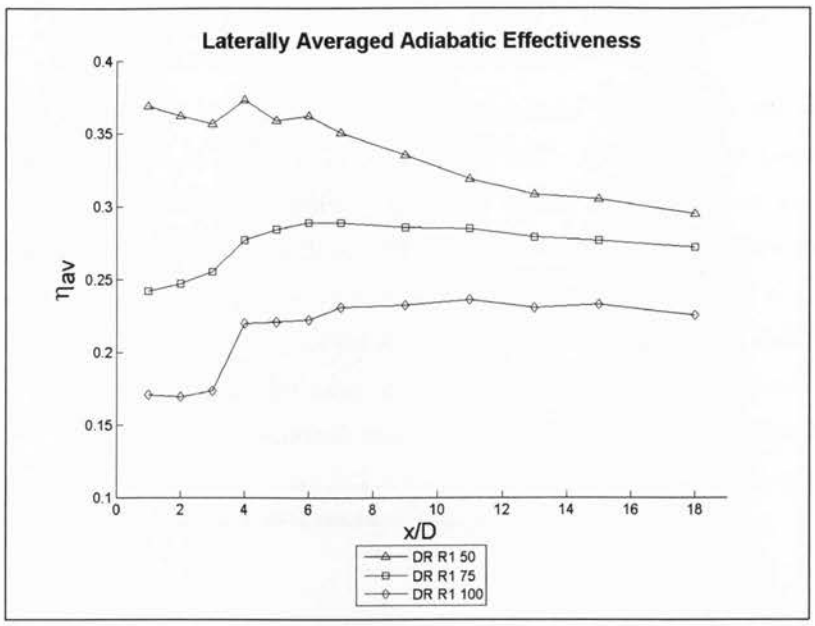

FIGURE 4.8: Effect of blowing ratio on double row case with upstream ramp at $R/D = 1$ (DR R1)

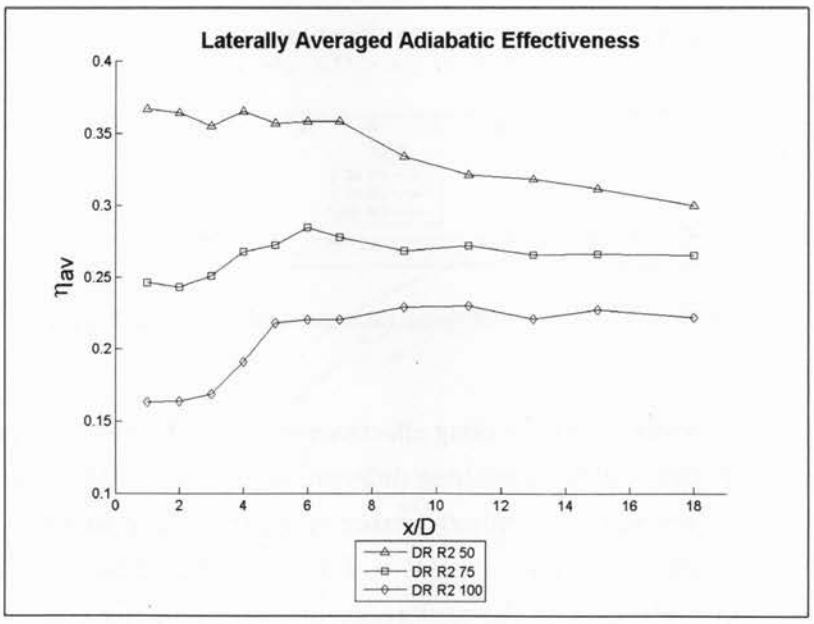

FIGURE 4.9: Effect of blowing ratio on double row case with upstream ramp at $R/D = 0.5$ (DR R2)

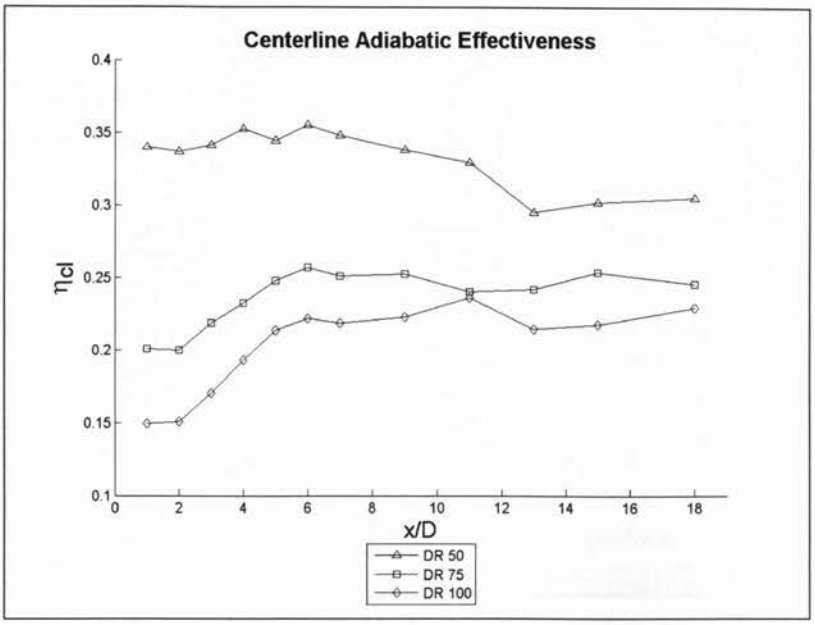

FIGURE 4.10: Centerline data for the effect of blowing ratio on double row (DR) case

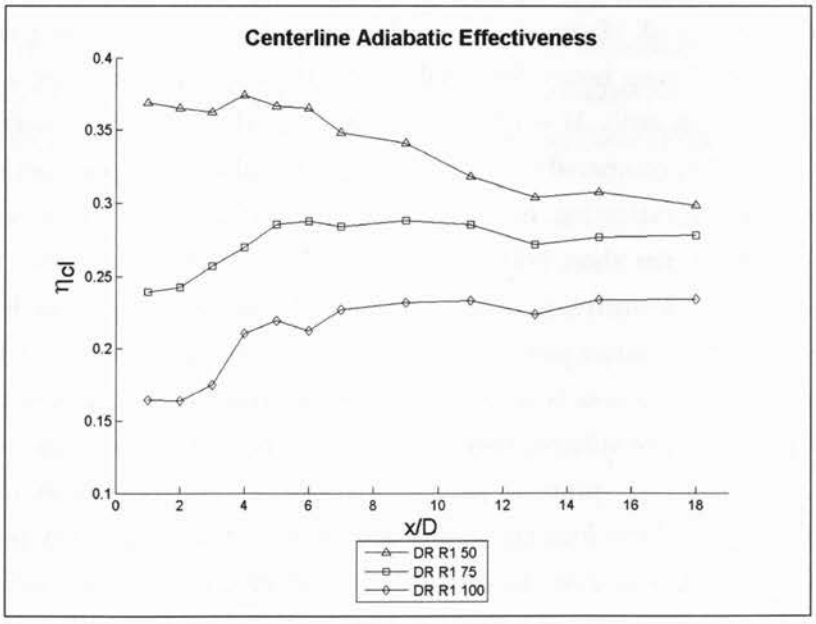

FIGURE 4.11: Centerline data for the effect of blowing ratio on double row case with upstream ramp at $R/D = 1$ (DR R1)

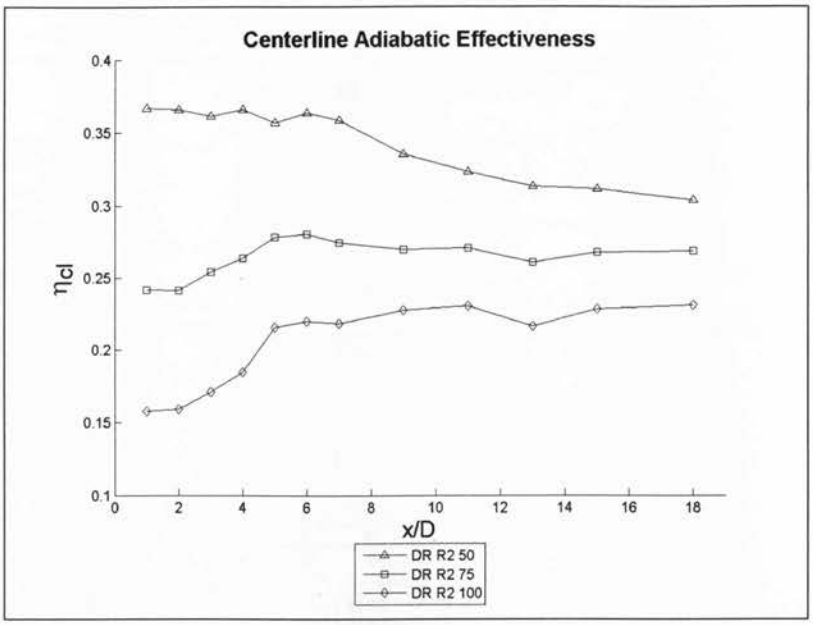

FIGURE 4.12: Centerline data for the effect of blowing ratio on double row case with upstream ramp at $R/D = 0.5$ (DR R2)

4.1.3 Summary

The trends seen in all of the above results, prove that higher blowing ratios are ineffective at providing better film-cooling effectiveness for short injection holes. The lowest blowing ratio, $M = 0.5$, has so far provided far superior coverage in all the six cases, when compared to the higher blowing ratios. The poor performance of higher blowing ratios has been documented by Hale et al [34] as well, who had conducted similar short hole studies ($L/D = 1.16$) and commented that the separation region downstream of the coolant holes could be responsible for low effectiveness. The intuitive perception that more coolant, in theory, should provide better cooling effectiveness is refuted by the above results. Higher blowing ratios not only provide more volume, they also increase the average exit velocity of the coolant: making it more prone to jetting. The jetting in turn causes an increment in mixing of the coolant with the mainstream flow; defeating the very purpose of film-cooling, which is to have the coolant act as an insulator for the blade. At low values of blowing rate, the injectant jet has low momentum, so the momentum of the mainstream flow in capable of deflecting it to the surface; providing better cooling [57].

4.2 Effect of Second Row of Holes

Three blowing ratios, $M = 0.5$, 0.75 and 1, were tested for double row configurations as opposed to four blowing ratios, $M = 0.5$, 0.75, 1 and 1.5, which were tested for the single row configuration; hence results pertaining to only the three blowing ratios tested for the double row cases will be presented in the following section. The maximum blowing ratio for the double row configuration was decided upon by the limitations imposed by the secondary or coolant supply source.

4.2.1 Blowing Ratio, $M = 0.5$

Figures 4.13 – 4.15 show the results comparing the performance of single and double row injection holes for $M = 0.5$ by presenting laterally averaged adiabatic effectiveness values downstream of the film-cooling plates; while Figures 4.16 – 4.18 present the centerline effectiveness data for the same cases. As can be seen, double row configurations increase the adiabatic cooling effectiveness by at least 1.5× for all the three scenarios. Due to ejection of coolant from an upstream row of holes, a significant increase in adiabatic effectiveness downstream of the second row of holes has been reported by Jubran and Brown [50], Maiteh and Jubran [51] and Saumweber and Schulz [62]. Another advantage of using a double row configuration is that the monotonic decline in effectiveness values is reduced considerably between $1 \leqslant x/D \leqslant 4$ for both the ramp cases (Figures 4.14 & 4.15).

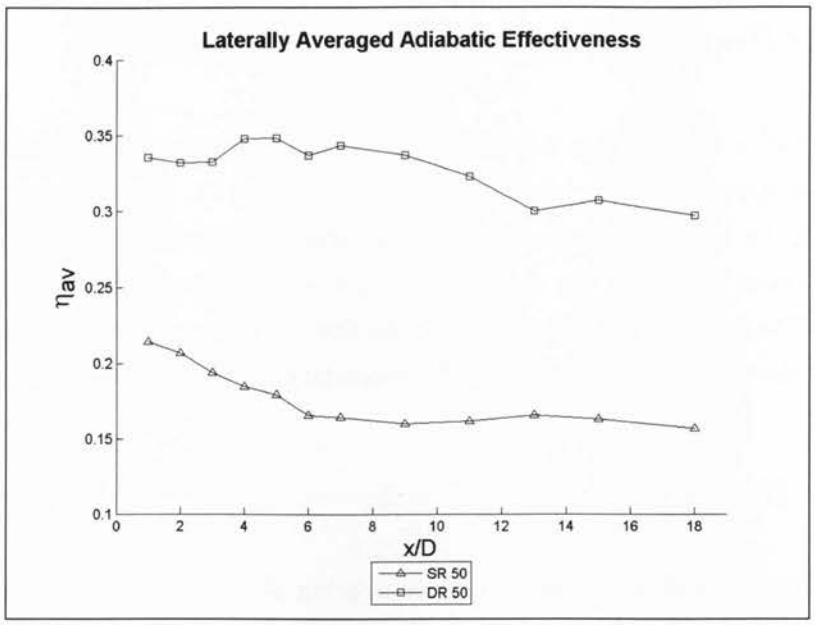

FIGURE 4.13: Effect of two rows of holes for baseline cases (SR & DR) at $M = 0.5$

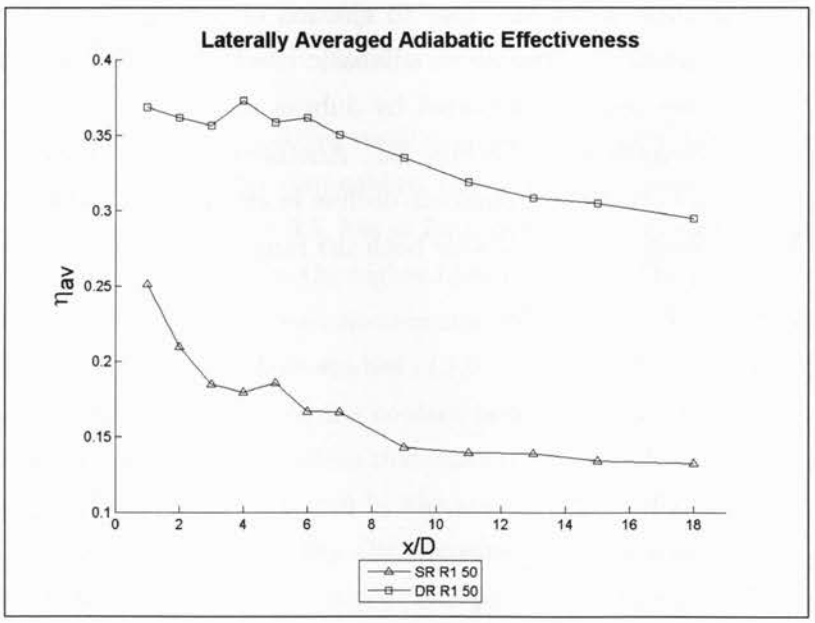

FIGURE 4.14: Effect of two rows of holes for $R/D = 1$ cases (SR R1 & DR R1) at $M = 0.5$

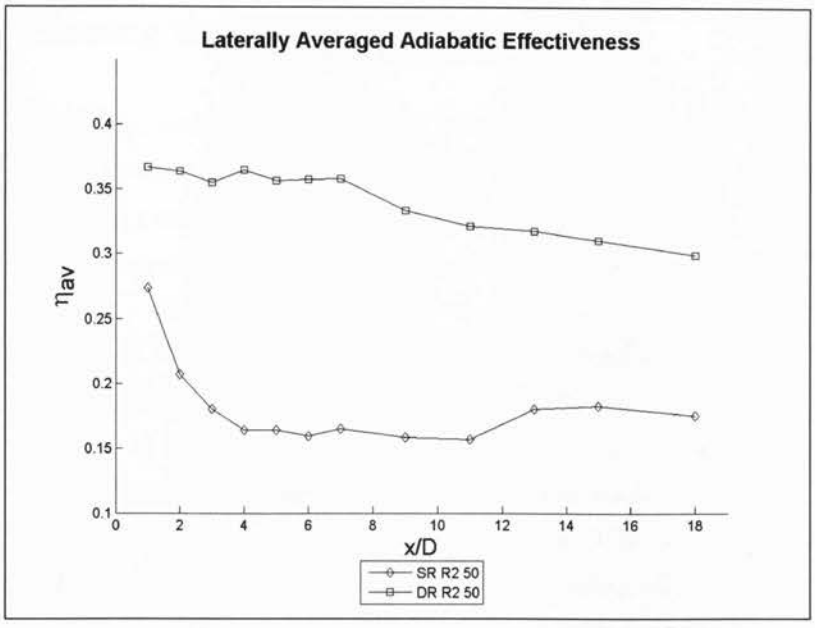

FIGURE 4.15: Effect of two rows of holes for $R/D = 0.5$ cases (SR R2 & DR R2) at $M = 0.5$

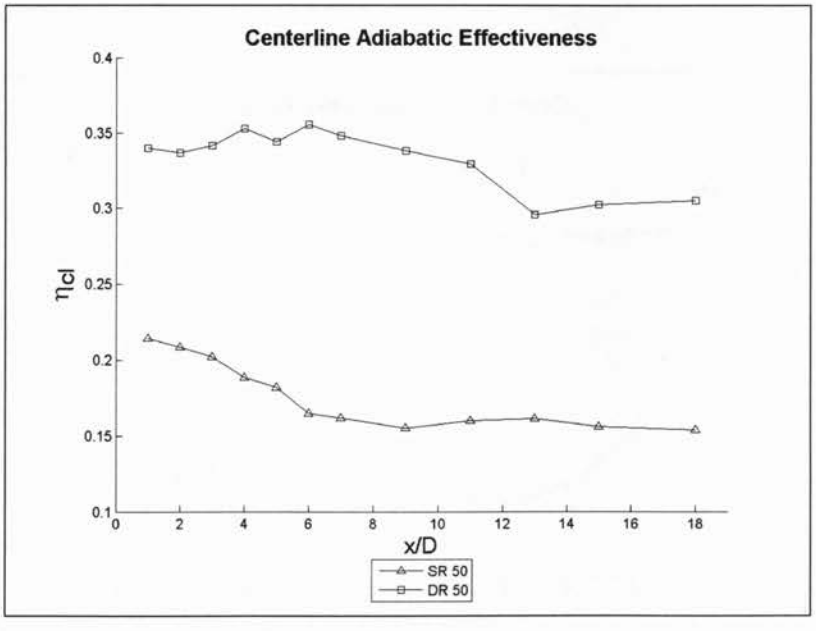

FIGURE 4.16: Centerline data for the effect of two rows of holes for baseline cases (SR & DR) at $M = 0.5$

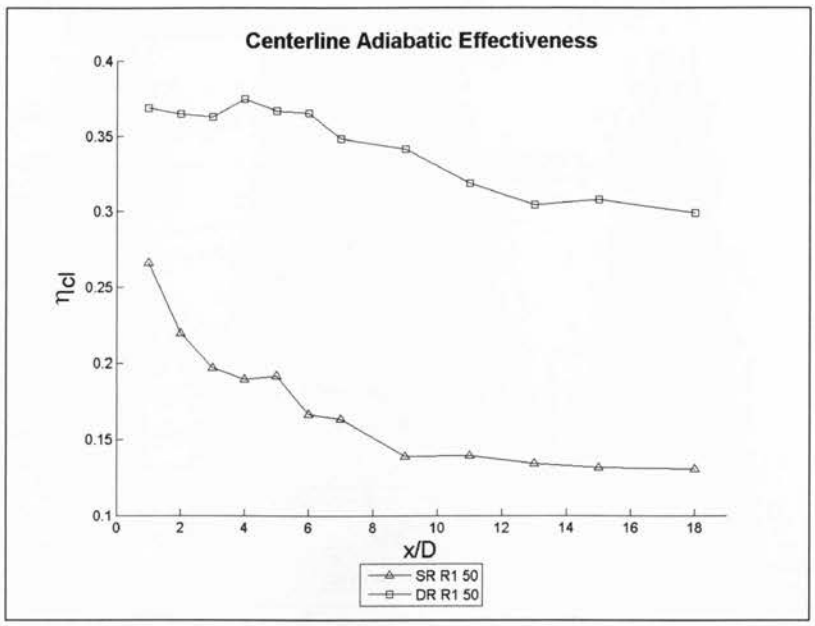

FIGURE 4.17: Centerline data for the effect of two rows of holes for $R/D = 1$ cases (SR R1 & DR R1) at $M = 0.5$

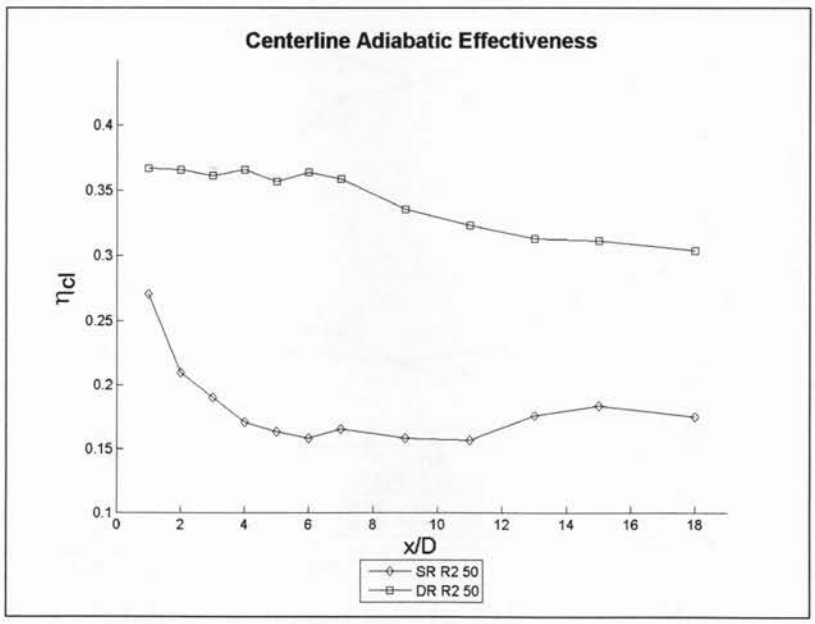

FIGURE 4.18: Centerline data for the effect of two rows of holes for $R/D = 0.5$ cases (SR R2 & DR R2) at $M = 0.5$

4.2.2 Blowing Ratio, $M = 0.75$

Figures 4.19 – 4.21 compare the laterally averaged effectiveness values obtained from single and double row configurations for a $M = 0.75$; while Figures 4.22 – 4.24 contrasts the centerline effectiveness data for the same cases. The increase in cooling effectiveness from two rows is even more apparent at higher blowing ratios ($M > 0.5$), where an improvement of more than 100% is noticed; when compared to single row cases. The increased mixing downstream of a single row of holes with the freestream flow is partly responsible for low effectiveness, but an upstream row of holes changes the flow pattern of the coolant ejecting from the downstream row, by interaction; regenerating the coolant film [62]. The jet lift-off seen in the baseline case, for $x/D \leqslant 7$ (Figure 4.19) is almost eliminated completely with the double row ramp cases. The cooling effectiveness increases by an astronomical 400% for the double row ramp cases between $2 \leqslant x/D \leqslant 8$; where jet detachment is noticed for the single row cases (Figures 4.20 & 4.21). The double row cases with the ramp provide almost uniform cooling throughout the surface of the plate; and the decrease in effectiveness values, in the downstream region, from its peak at $x/D = 6$ is marginal, at worst.

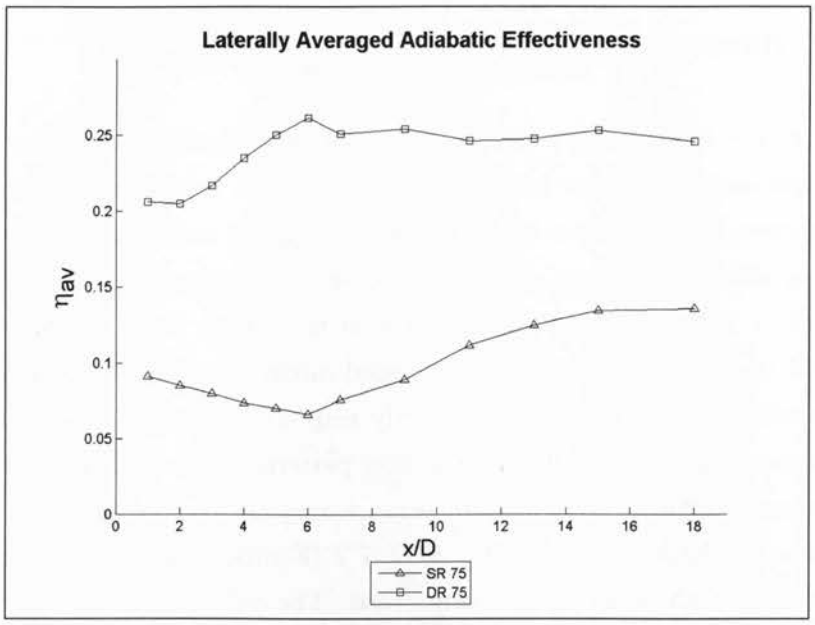

FIGURE 4.19: Effect of two rows of holes for baseline cases (SR & DR) at $M = 0.75$

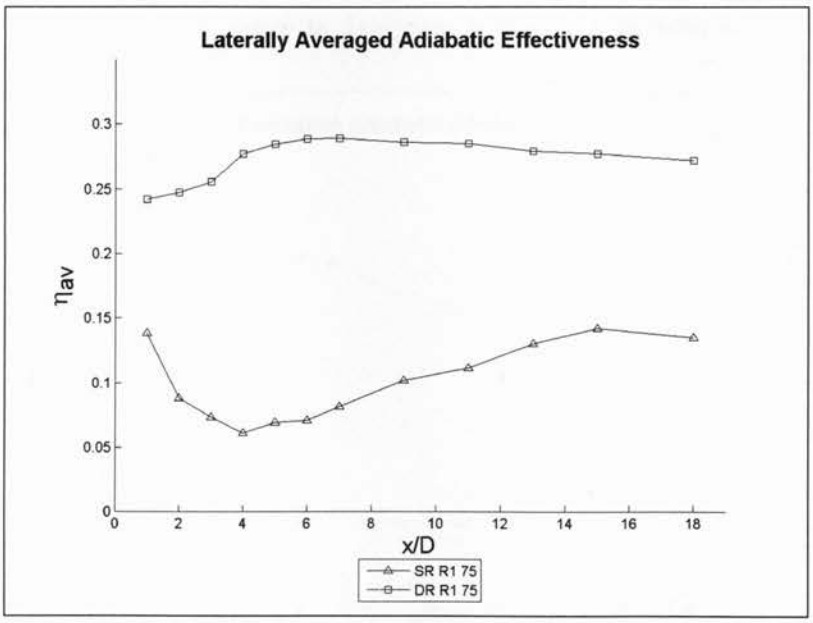

FIGURE 4.20: Effect of two rows of holes for $R/D = 1$ cases (SR R1 & DR R1) at $M = 0.75$

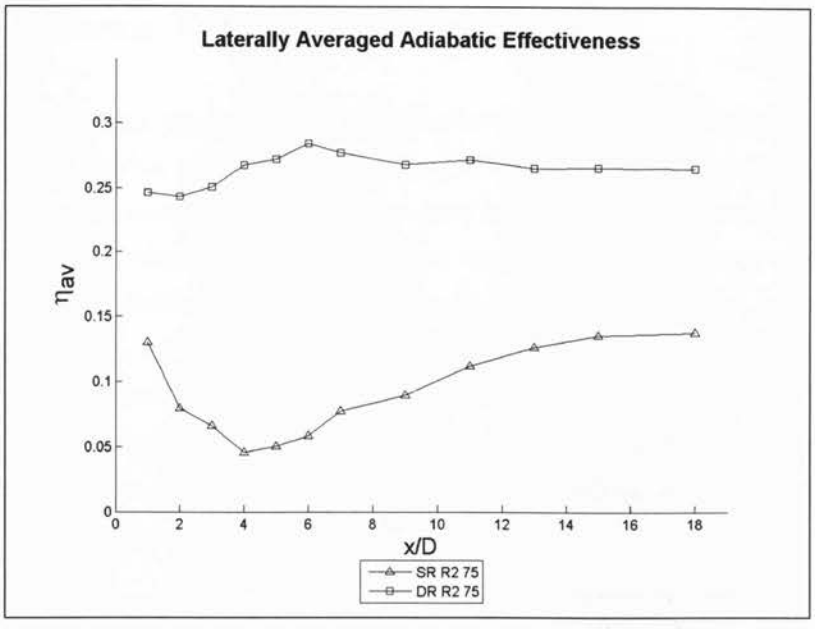

FIGURE 4.21: Effect of two rows of holes for $R/D = 0.5$ cases (SR R2 & DR R2) at $M = 0.75$

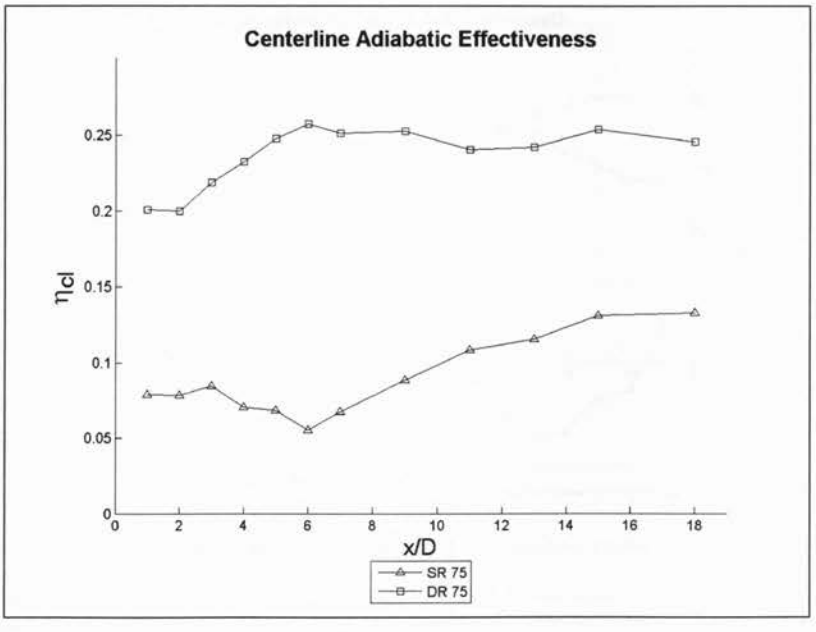

FIGURE 4.22: Centerline data for the effect of two rows of holes for baseline cases (SR & DR) at $M = 0.75$

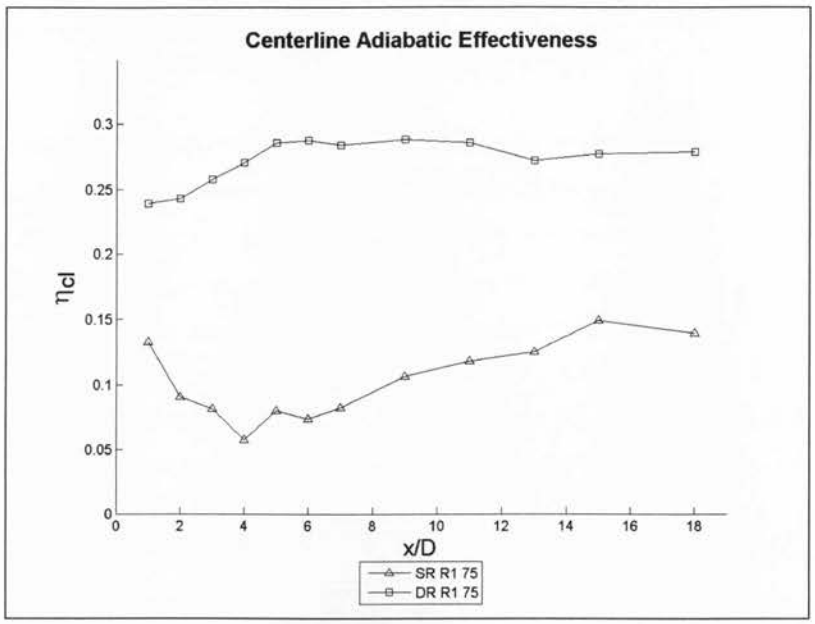

FIGURE 4.23: Centerline data for the effect of two rows of holes for $R/D = 1$ cases (SR R1 & DR R1) at $M = 0.75$

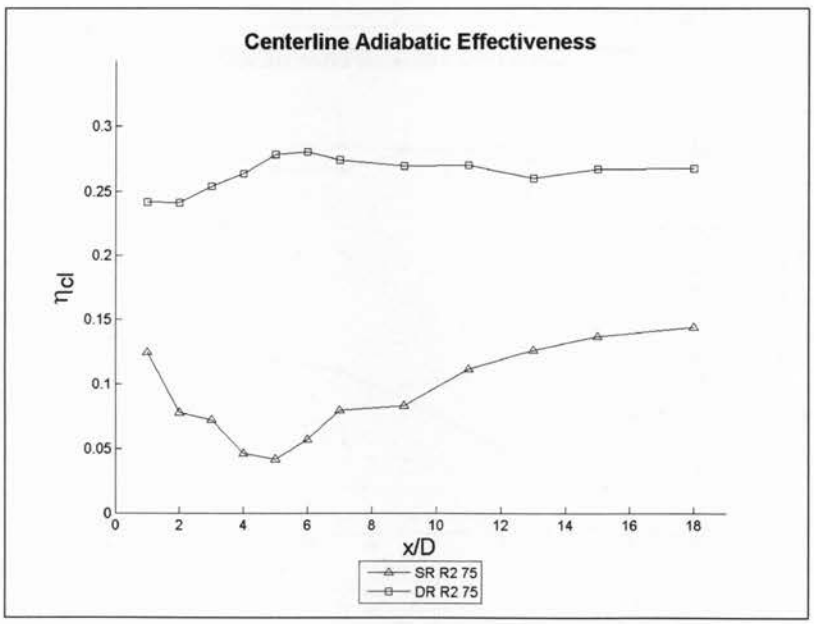

FIGURE 4.24: Centerline data for the effect of two rows of holes for $R/D = 0.5$ cases (SR R2 & DR R2) at $M = 0.75$

4.2.3 Blowing Ratio, $M = 1$

Comparsion data for the laterally averaged effectiveness values obtained from testing single and double row configurations at $M = 1$ are presented in Figures 4.25 – 4.27; while the centerline effectiveness data for the cases are shown in Figures 4.28 – 4.30 . The results in this section are very similar to the ones seen above, where the double row configuration transcends the cooling provided by the single row configuration. At higher blowing ratios the detachment of the jet is more noticeable for the double row cases (Figure 4.25); alleviated to a large extent by the presence of the upstream ramp (Figures 4.26 & 4.27). The increase in effectiveness values as compared to the single row cases is not as high as it was for $M = 0.75$; but is still significant – over 200% for $M = 1$.

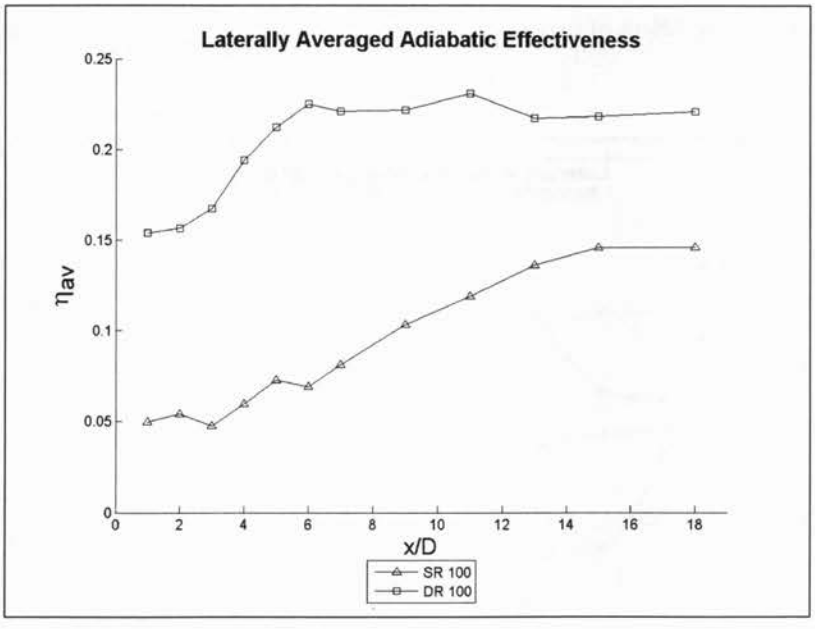

FIGURE 4.25: Effect of two rows of holes for baseline cases (SR & DR) at $M = 1$

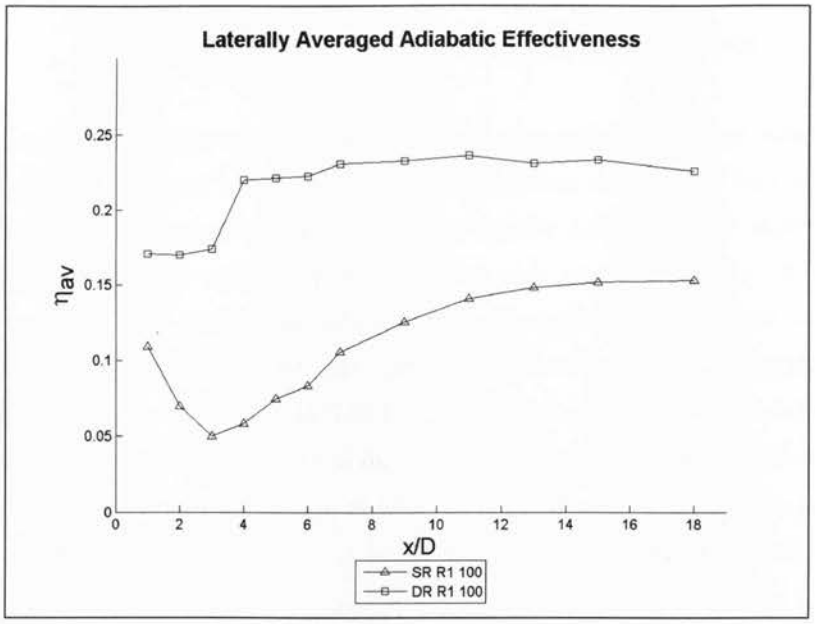

FIGURE 4.26: Effect of two rows of holes for $R/D = 1$ cases (SR R1 & DR R1) at $M = 1$

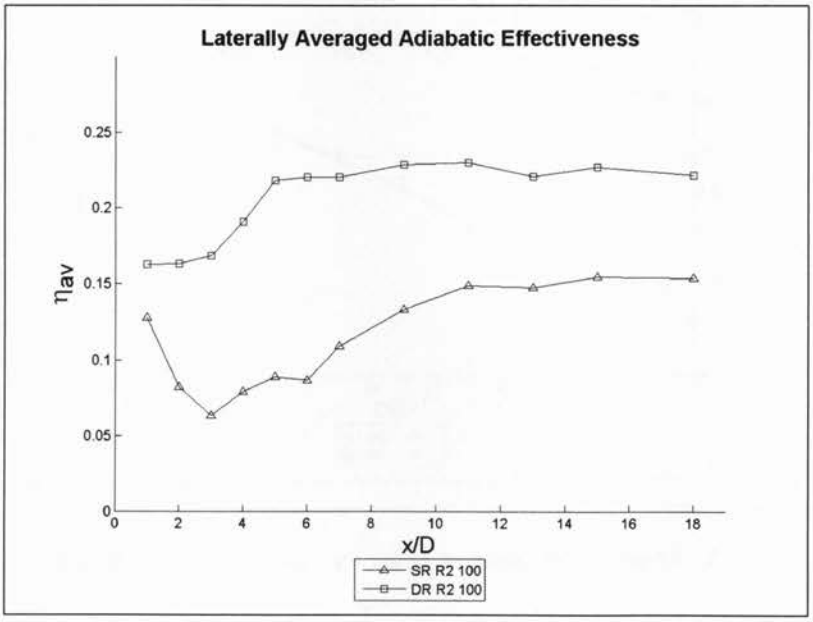

FIGURE 4.27: Effect of two rows of holes for $R/D = 0.5$ cases (SR R2 & DR R2) at $M = 1$

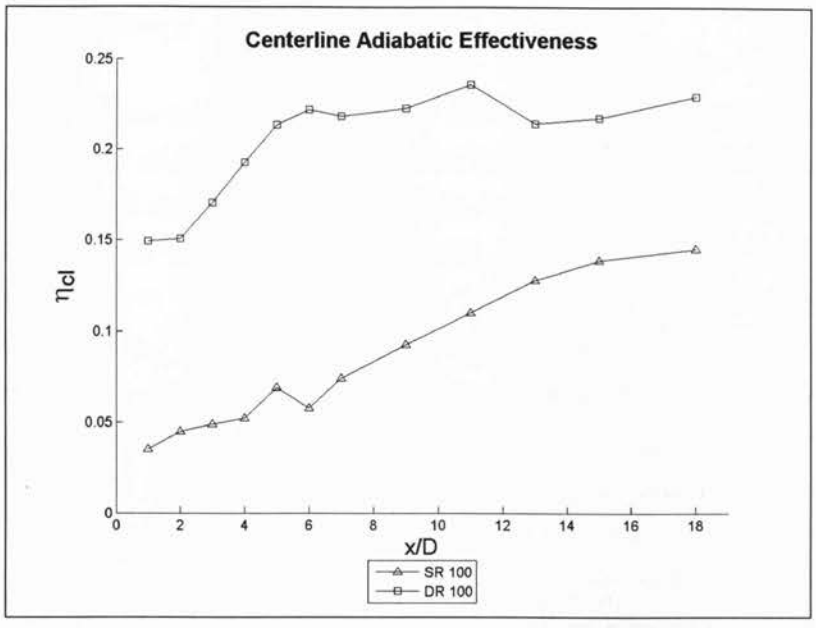

FIGURE 4.28: Centerline data for the effect of two rows of holes for baseline cases (SR & DR) at $M = 1$

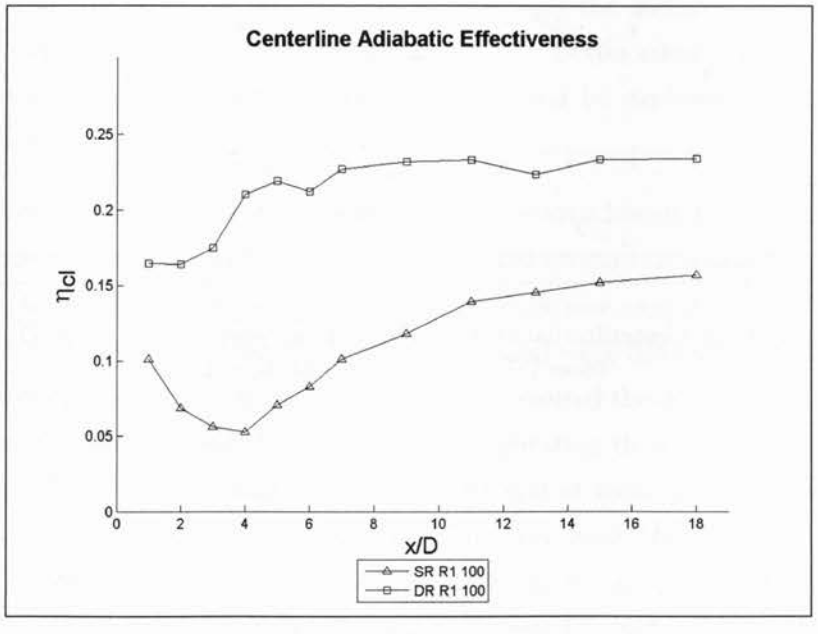

FIGURE 4.29: Centerline data for the effect of two rows of holes for $R/D = 1$ cases (SR R1 & DR R1) at $M = 1$

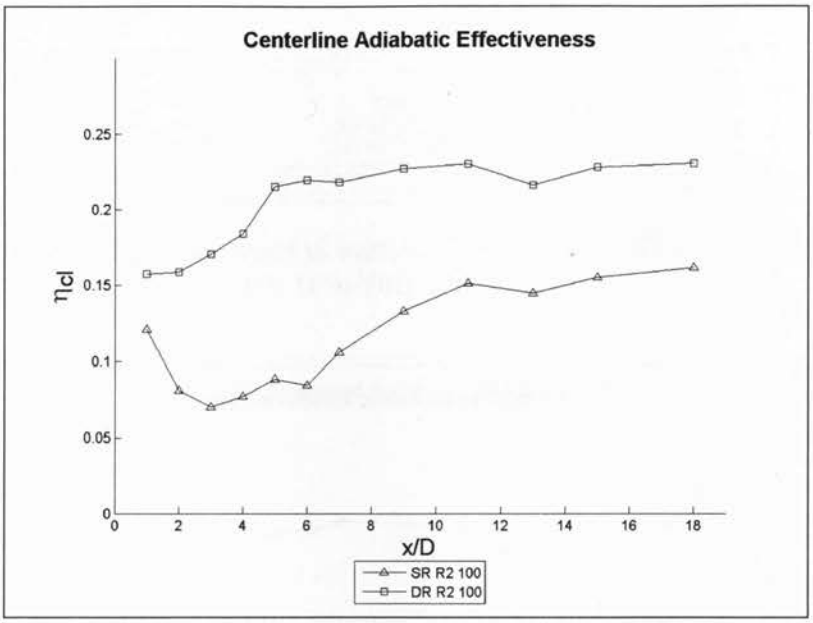

FIGURE 4.30: Centerline data for the effect of two rows of holes for $R/D = 0.5$ cases (SR R2 & DR R2) at $M = 1$

4.2.4 Summary

Certain trends have been repeating in the above three section: two rows of holes increase adiabatic effectiveness by at least 200% when compared to the same blowing ratio for single row cases. A very obvious explanation for that could be that since there are 80% more holes in the double row case (9 holes as opposed to 5 holes for single row) there is more coolant; hence more coolant would obviously mean better cooling. This simple explanation, although true, is invalid in certain other cases where more coolant does not necessarily provide more protection as we had seen in the previous section (Chapter 4.1); where higher blowing ratio had a detrimental effect on the cooling effectiveness. A possible explanation for the superior performance of the two rows of injections could be the interaction between the coolant flows emanating from the upstream and downstream rows. Jubran and Brown [50] observed that the film-cooling effectiveness downstream of the second row of holes is largely dependent on the state of development of the film formed from the first row of holes. Additionally, CRVPs generated from the upstream row generate a secondary flow which is oriented towards the wall; pushing the flow from the downstream row towards the surface. This phenomena decreases the likelihood of jet detachment [62]. Better effectiveness value and lesser jet detachment of higher blowing ratios could be explained by the above occurrence.

Figures 4.26 & 4.27 explicitly show the jet re-attachment for the single row case happening at $x/D > 3$. The non-dimensional distance is measured from the downstream edge of the film-cooling holes in a single row case (Figure 3.8); this is the exact datum used for the double row case as well – the downstream edge of the second row of holes is assumed $x/D = 0$. If we measured the downstream distance from the upstream row for the double row configuration then we can come to the conclusion, looking at the single row case, that right at location of the second row of holes, the jet emanating from the upstream row would be re-attaching; thus thrusting down the coolant flow emanating from the second row. This could very well be another reason for reduced jet detachment for higher blowing ratios in double row cases.

4.3 Effect of Upstream Ramp

An upstream ramp was placed at two distances, $R/D = 0.5$ & 0.1,on both: single row and double row configurations. The results obtained from conducting the above tests have been compared against the baseline cases with no ramps attached. The results have been presented below in two main sections depending on the type of configuration and analyzed against each other on the basis of the blowing ratio.

4.3.1 Single Row Cases

Figures 4.31 – 4.34 present the laterally averaged effectiveness results obtained for the single row injection plates at different blowing ratios; contrasting the values of cases with and without an upstream ramp. Figures 4.35 – 4.38 show the centerline results for the same cases. The most significant improvement for the use of an upstream ramp has been noticed in the near hole region, $x/D < 3$, irrespective of the blowing ratio. For the two cases of ramps tested, $R/D = 0.5$ performs slightly better than than $R/D = 1$. The improvement in cooling effectiveness in the downstream region is only noticed for the case of $M = 0.5$, where SR R2 50 outperforms the other configurations (Figure 4.31). Apart from increment in cooling effectiveness offered by the upstream ramps for higher blowing ratios ($M > 0.5$) in the near hole region; there is no added advantage in the downstream region of using the ramps. The baseline case performed better than the upstream ramp for $M = 1.5$ (Figure 4.34).

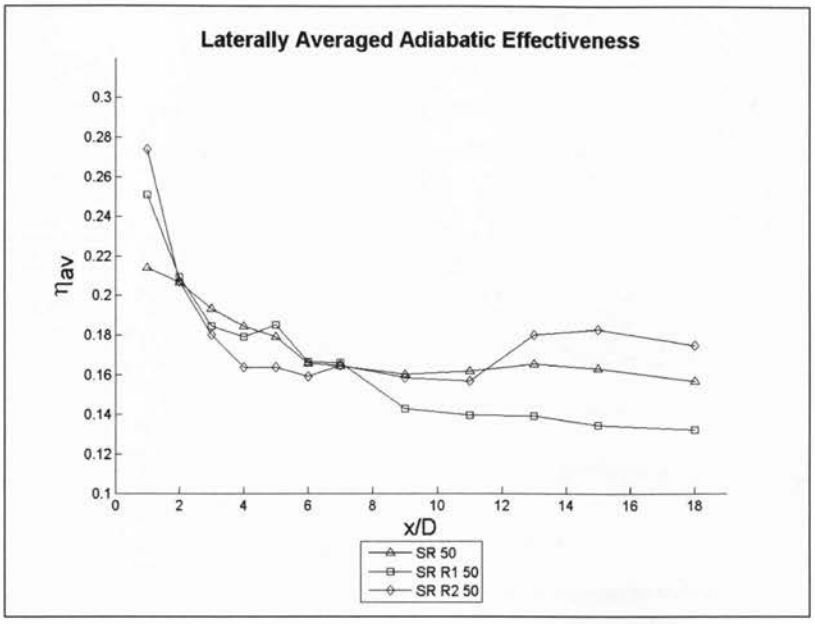

FIGURE 4.31: Effect of ramp on single row cases at $M = 0.5$

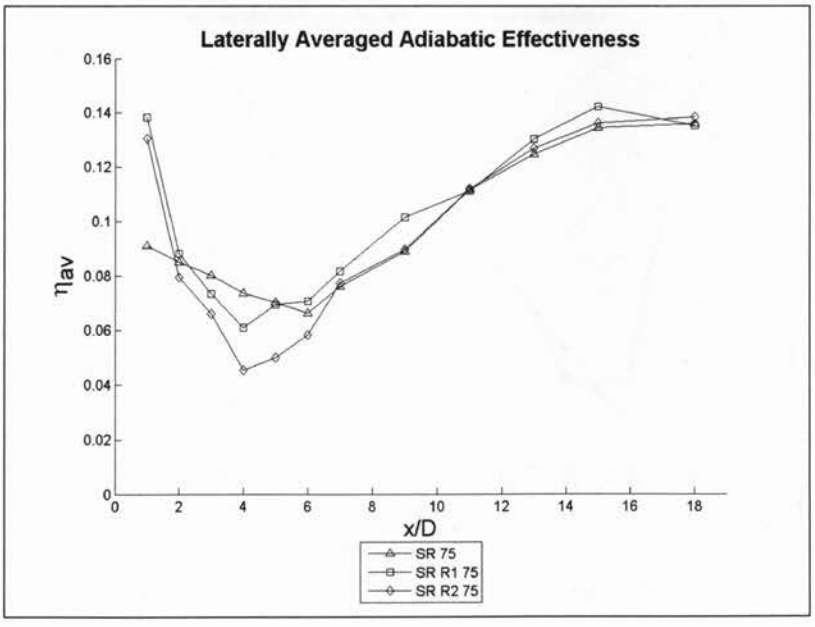

FIGURE 4.32: Effect of ramp on single row cases at M =0.75

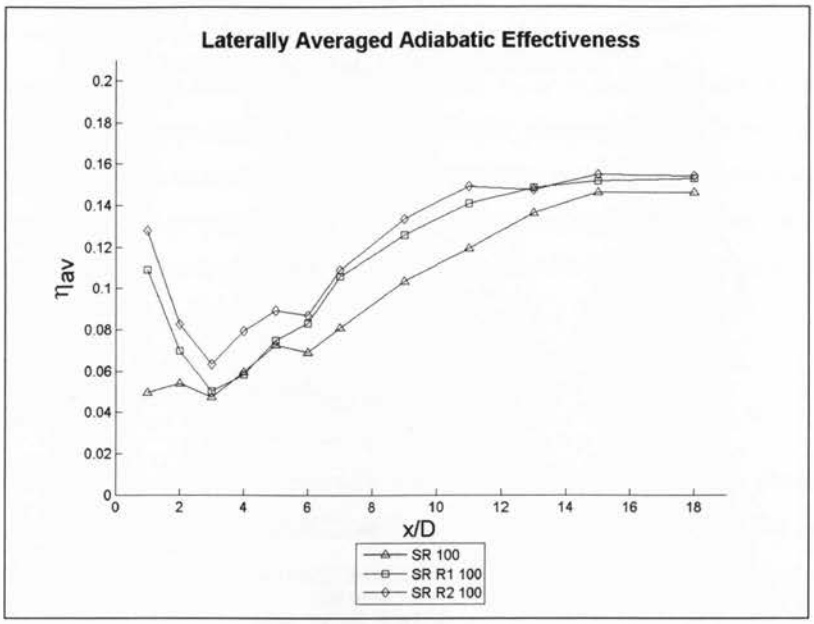

FIGURE 4.33: Effect of ramp on single row cases at $M = 1$

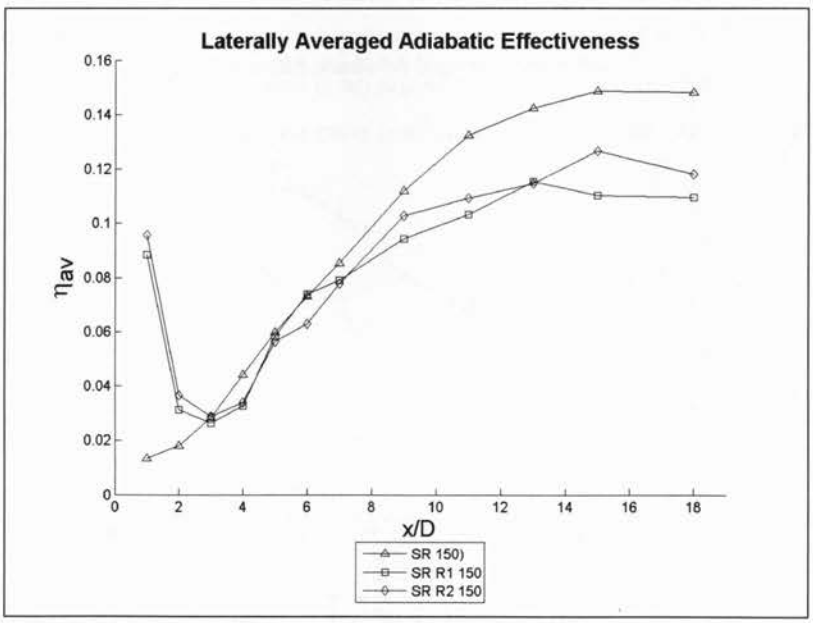

FIGURE 4.34: Effect of ramp on single row cases at M =1.5

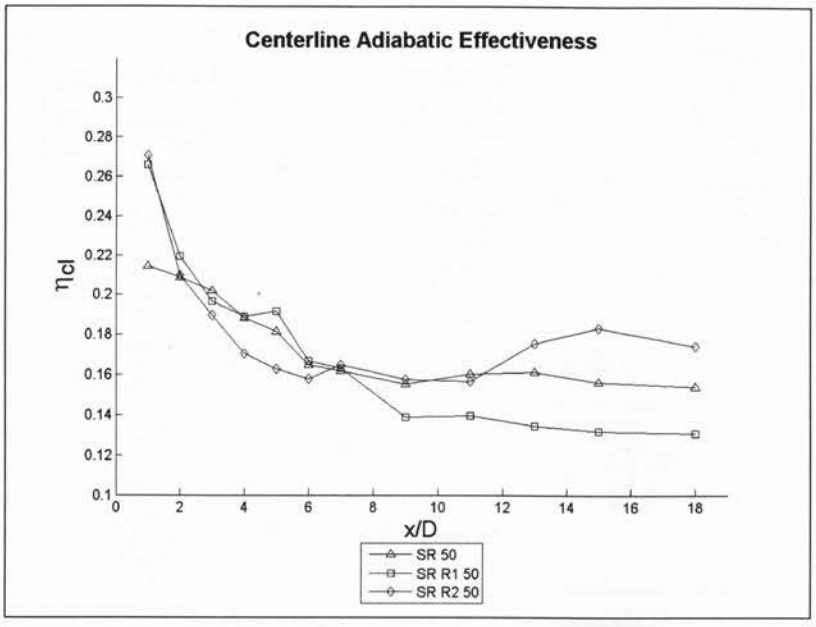

FIGURE 4.35: Centerline data for the effect of ramp on single row cases at M = 0.5

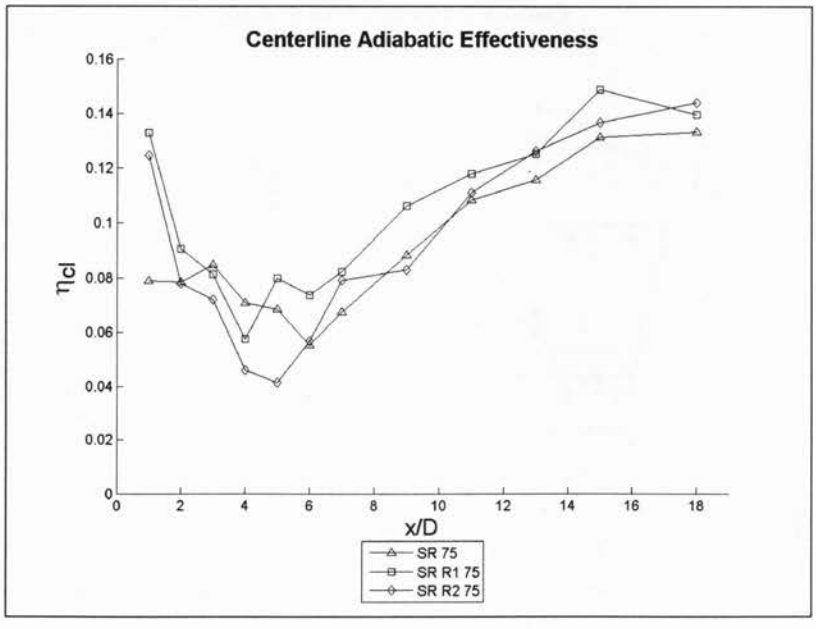

FIGURE 4.36: Centerline data for the effect of ramp on single row cases at M =0.75

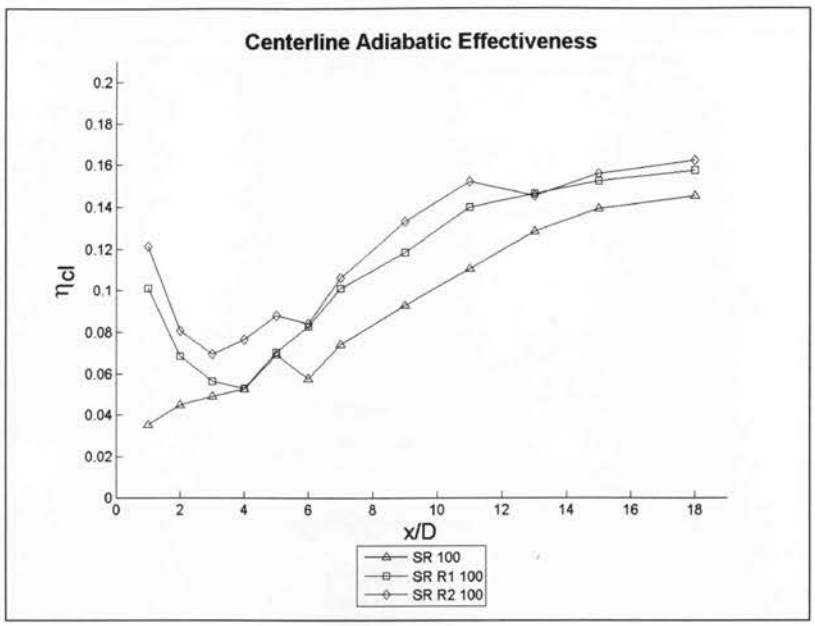

FIGURE 4.37: Centerline data for the effect of ramp on single row cases at M = 1

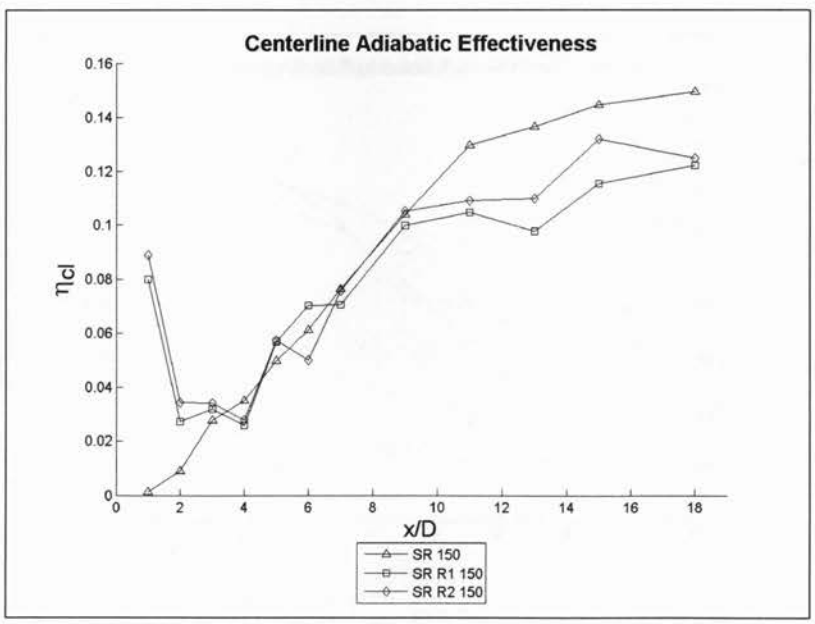

FIGURE 4.38: Centerline data for the effect of ramp on single row cases at M =1.5

4.3.2 Double Row Cases

The results obtained for the double row injection plates at different blowing ratios; contrasting the values of cases with and without an upstream ramp have been presented in Figures 4.39 - 4.41. The corresponding centerline effectiveness data is shown in Figures 4.42 - 4.44. The significant improvement in cooling effectiveness noticed for single row cases in the near hole region is not apparent for the double row cases; where the increment in cooling effectiveness is barely noticeable for $M = 1$ (4.41). Results for $M = 0.5$, show a 10% improvement for an upstream ramp in the near hole region ($x/D < 9$), with little or no effect in the downstream region. The most improvement after using an upstream ramp is noticed for $M = 0.75$; where an increase of 20% is seen throughout the test domain.

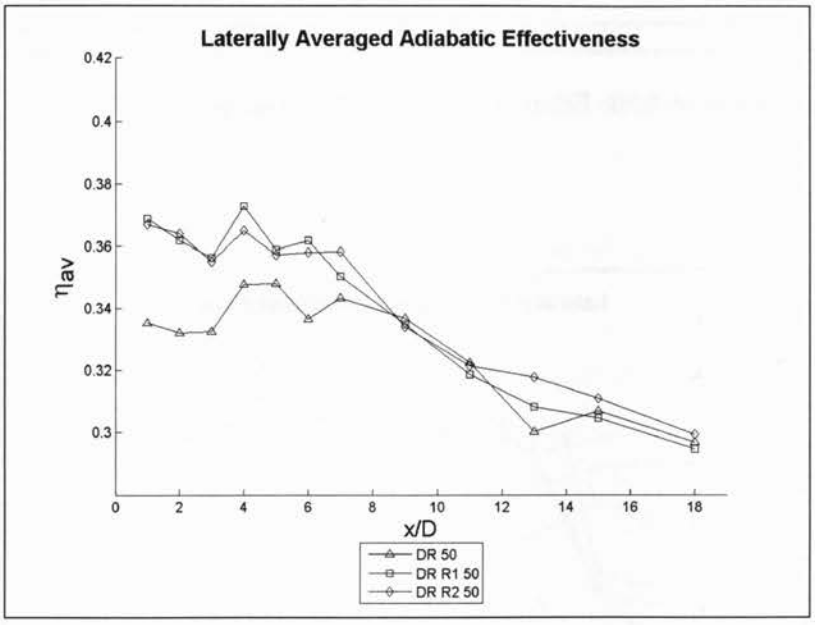

FIGURE 4.39: Effect of ramp on double row cases at $M = 0.5$

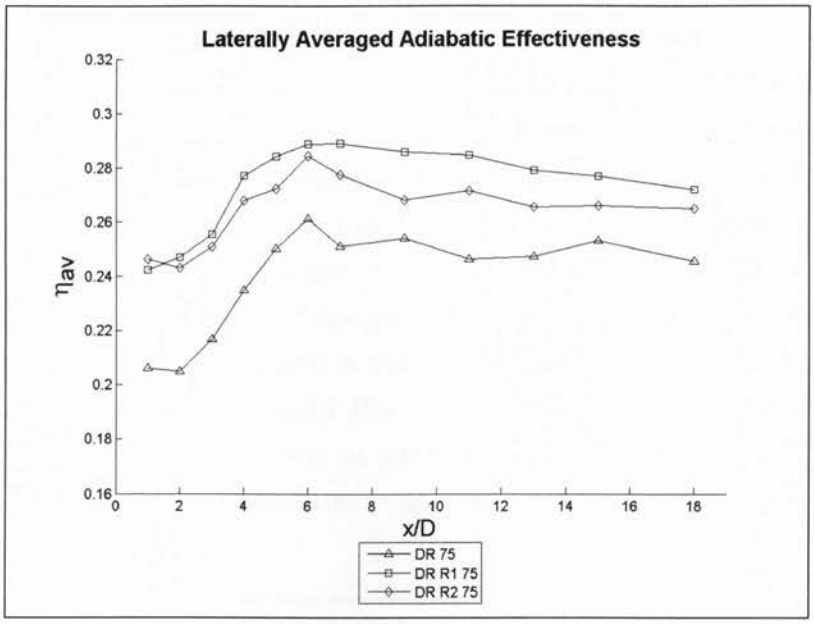

FIGURE 4.40: Effect of ramp on double row cases at M =0.75

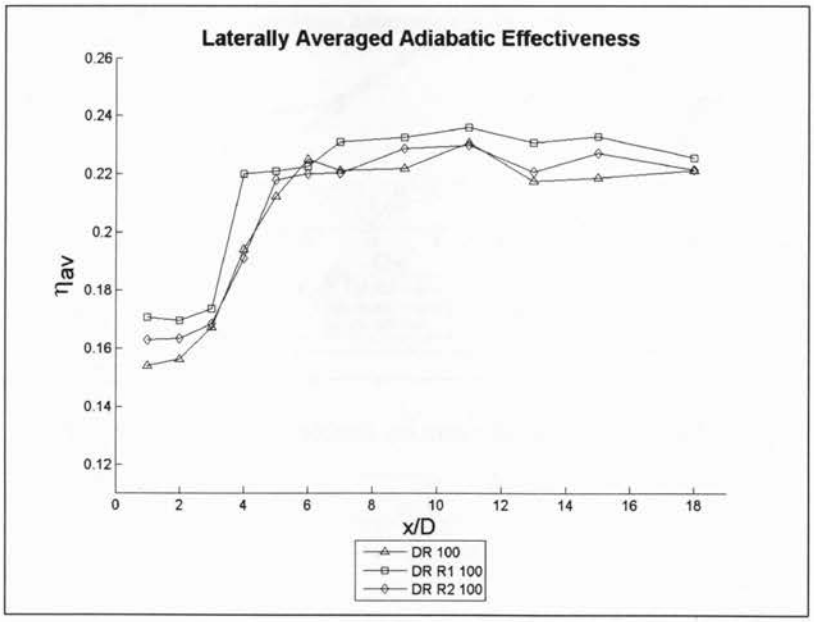

FIGURE 4.41: Effect of ramp on double row cases at $M = 1$

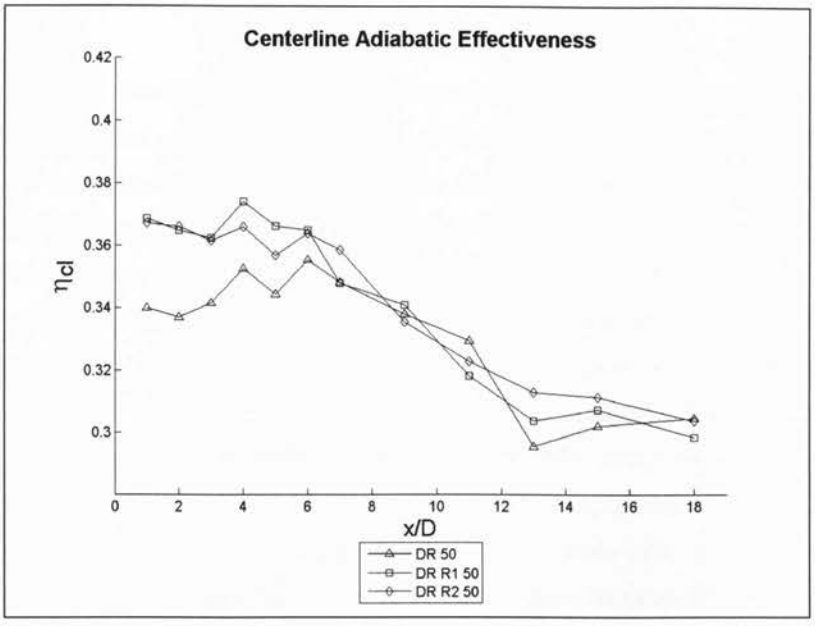

FIGURE 4.42: Centerline data for the effect of ramp on double row cases at M = 0.5

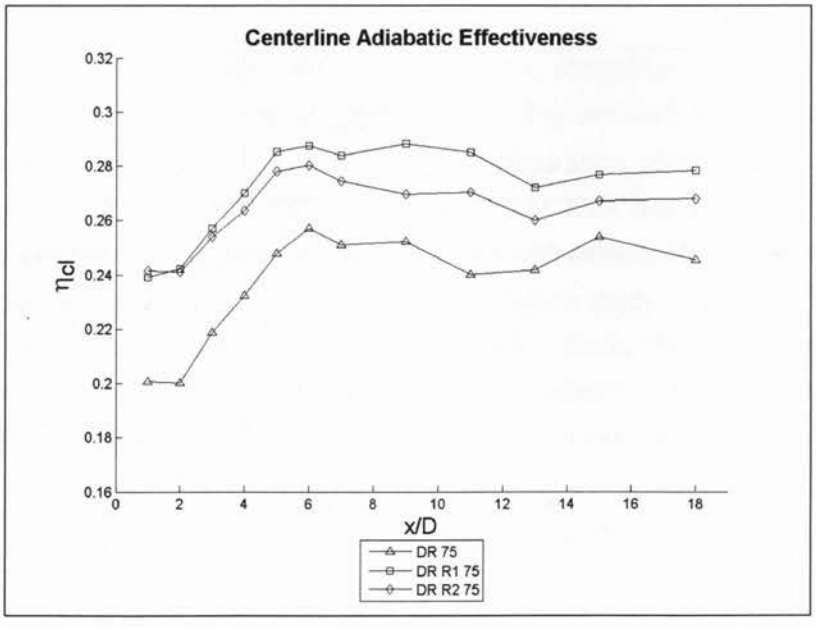

FIGURE 4.43: Centerline data for the effect of ramp on double row cases at M =0.75

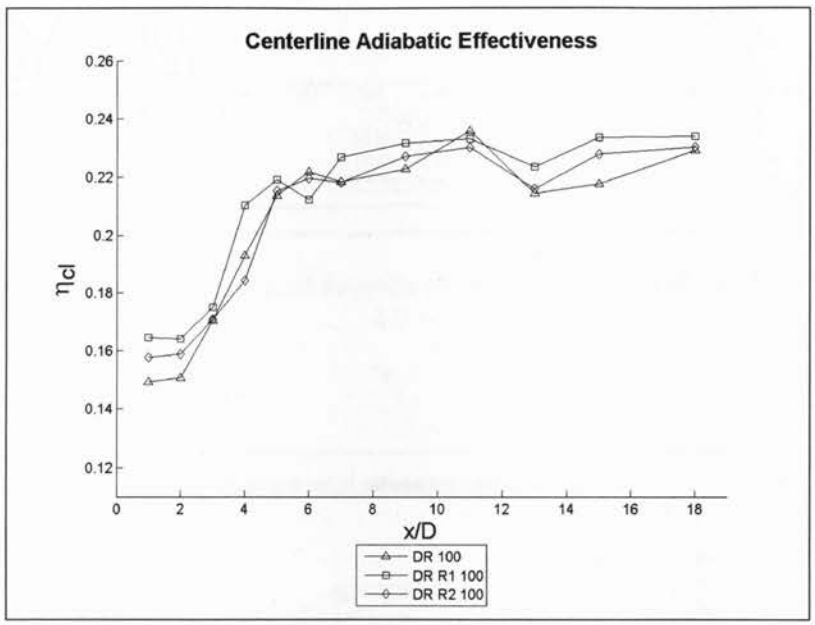

FIGURE 4.44: Centerline data for the effect of ramp on double row cases at $M = 1$

4.3.3 Summary

Na and Shih [2] concluded from their numerical studies on upstream ramps that the boundary layer of the approaching mainstream flow is diverted due to the presence of a bump; causing the coolant jet to interact with the mainstream flow at a distance above the surface. According to their results, there is a wake region created in between the ramp and the upstream edge of the hole that entrains the coolant flow. This could be the reason for increased lateral spreading of the coolant, resulting in more cooling in the near hole region of the injection holes, seen especially in the single row cases (Figures 4.31 – 4.34). The sudden loss of effectiveness between $2 \leqslant x/D \leqslant 8$, for single row cases, could be attributed to the delayed interaction of the coolant with the mainstream, which causes mixing and entrainment of the coolant jet farther away from the hole exit. At higher blowing ratios, the upstream ramp may cause the effectiveness to drop below the baseline case as the coolant jet has a large momentum causing it to lift-off; overpowering the protective wake region [47].

4.4 Comparison with Previous Studies

To comprehend the accuracy of the above results, comparisons have been made with previous studies with similar parameters. Figures 4.45 and 4.46 compare the results obtained for SR 50 and SR 100 configuration with data from Hale's [1] study. The important thing to be noted is that Hale had used a longer hole length, $L/D = 1.16$, compared to $L/D = 0.87$ of the current study. Secondly, the turbulence intensity of the mainstream flow for Hale's study was much lower (Tu = 0.2-0.5%) than the present study (Tu = 3.3%). Since, the parameters of the present study are not exactly the same as Hale's research, there are bound to be discrepancies; but still the effectiveness values are in close agreement.

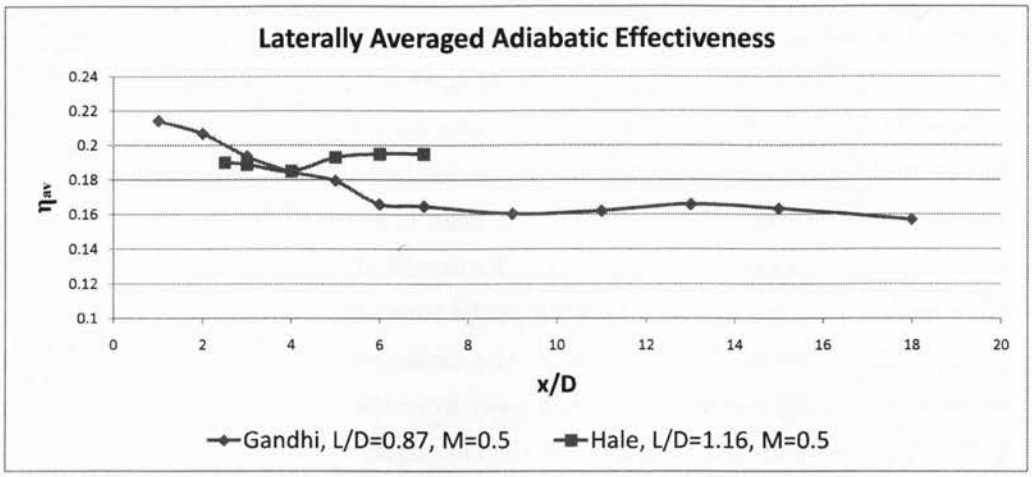

FIGURE 4.45: Comparison of SR 50 with Hale [1] for M=0.5

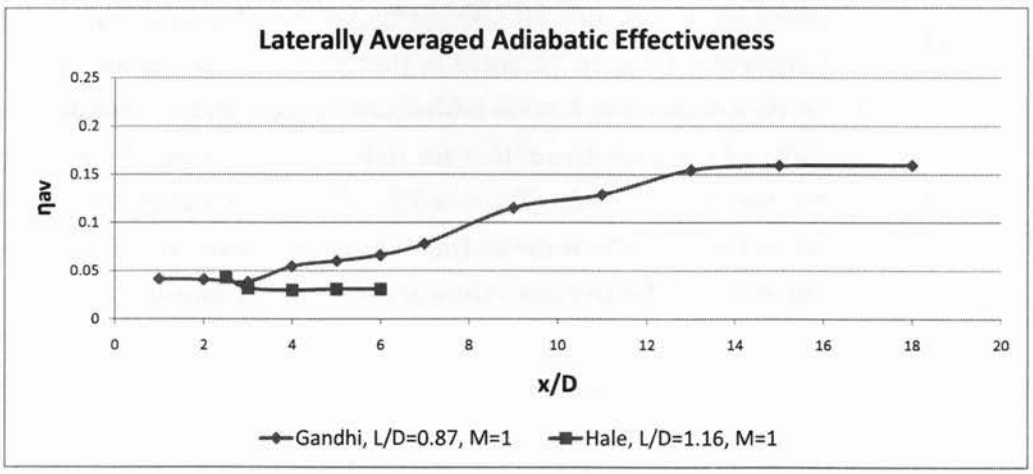

FIGURE 4.46: Comparison of SR 100 with Hale [1] for M=1

The ramp cases, SR R1 50 and SR R1 100, are compared with Na & Shih [2] in Figures 4.47 and 4.48. The trends are in very good agreement; but the lower values of this present research can be explained by the fact that Shih & Na had used a longer hole length of $L/D = 3.5$ and Tu $= 0\%$. Both, the longer hole length and low level of turbulence, result in higher effectiveness values [12] [30]. Additionally, overestimation arising from the numerical approach as well as different geometrical parameters may account for the differences in effectiveness values.

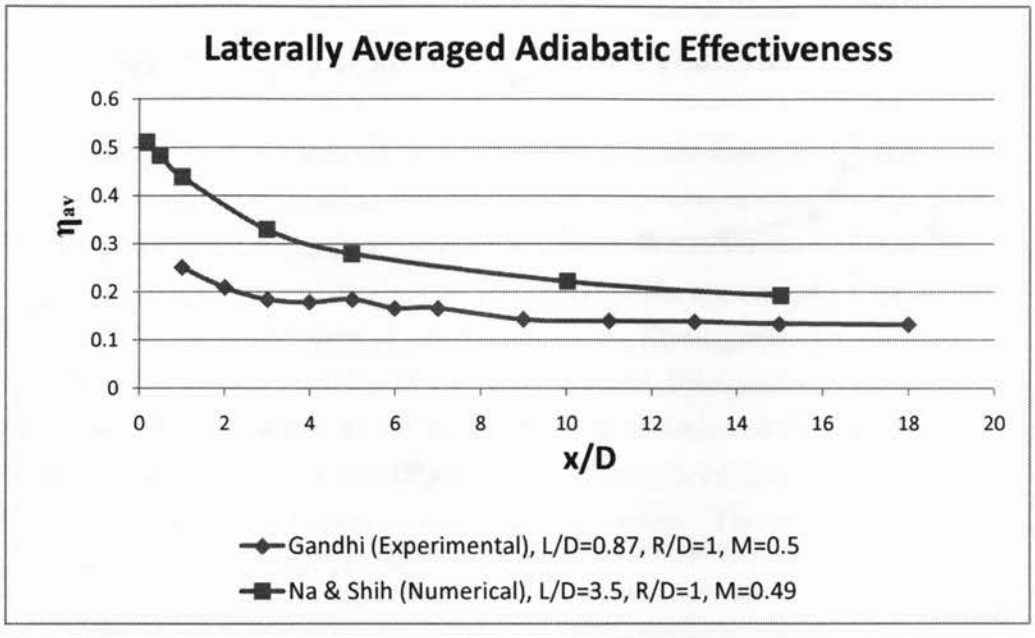

FIGURE 4.47: Comparison of SR R1 50 with Na & Shih [2] for M=0.5

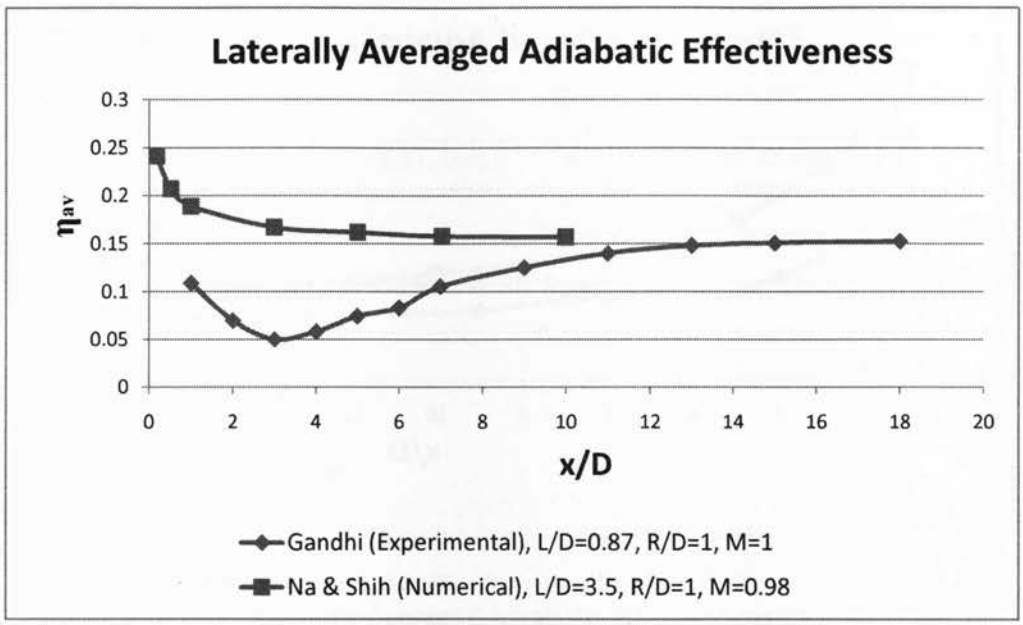

FIGURE 4.48: Comparison of SR R1 100 with Na & Shih [2] for M=1

Chapter 5

Conclusions

An experimental study was conducted to investigate the film cooling effectiveness of a few configurations of short injection holes: single row, double row and both of the preceding cases with an upstream ramp placed at two different locations. In order to perform the above study, a wind-tunnel facility was assembled to facilitate in the successful culmination of the experiments. The focus of the study was to determine the cooling provided by the short injection holes at a variety of blowing ratios and whether adding an extra row of holes, upstream of the first row would make a difference. For the second part, a ramp was placed upstream of the single and double row configuration to help improve cooling. The key findings of this study will be summarized in this chapter.

The second part of this chapter will give a few recommendations for future work to continue and expand the current study on experimental short hole film-cooling.

5.1 Concluding Remarks

Higher blowing ratios failed to provide better effectiveness for short injection holes; going against the common notion that more coolant would result in better cooling. The poor performance of higher blowing ratios ($M > 0.5$) was attributed to to the jet lift-off which increased the mixing of the coolant flow with the mainstream flow resulting in poor effectiveness values. The lowest blowing ratio, $M = 0.5$, has so far provided far superior coverage in all the six cases, when compared to the higher blowing ratios. The above findings have been consistent with other studies of short injection holes [34] [1].

Two rows of staggered holes increased adiabatic effectiveness by at least 200% when compared to the same blowing ratio for single row cases. CRVPs generated from the upstream row generate a secondary flow which is oriented towards the wall; pushing the flow from the downstream row towards the surface. This phenomena decreases the likelihood of jet detachment [62]. Better effectiveness value and lesser jet detachment of higher blowing ratios could be explained by the above occurrence. Similar observations of superior performance of two rows of film-cooling holes have also been reported by previous studies [50] [51] [62].

The results for the presence of an upstream ramp were indifferent. Significant improvement in film-cooling effectiveness was observed mostly in the near hole region for the single row cases for moderately high blowing ratios. The sudden loss of effectiveness between $2 \leqslant x/D \leqslant 8$, for single row cases, could be attributed to the delayed interaction of the coolant with the mainstream, which causes mixing and entrainment of the coolant jet farther away from the hole exit. An upstream ramp had barely any effect on double row effectiveness. The trends produced by the current investigation were similar to previous research [2] [47].

5.2 Recommendations for Future Work

- Temperature visualization techniques like thermographic liquid crystals (transient and/or steady state), pressure sensitive paints and infrared thermography should be used to gain a better understanding of the temperature contours formed by the introduction of film-cooling. The current experimental set-up is designed to accommodate different measurement techniques with minimal structural change.

- The current research should also be extended to include flowfield measurements for the aerodynamic effects of an upstream ramp as well as the structural properties of the coolant jet emanating from short injection holes.

- A numerical study would also be advised to complement the experimental data that has been accrued by the present study. Simulations conducted in computational fluid dynamic (CFD) programs would save a lot of time and funds as well as give researchers the flexibility of studying a host of different parameters.

- Heat transfer measurements conducted on the present experimental set-up of short hole film-cooling would be another way of expanding the current work.

- Important film-cooling parameters like higher density ratio and elevated free-stream turbulence could also be introduced to make the present work resemble engine like conditions.

Appendix A

Errors and Uncertainties

A.1 Approach

The uncertainty analysis performed for the experimental data presented in this study has been derived from Kline and McClintock [59]. This method takes into account the contribution of all experimentally measured value and shows its accrued effect on the reported result. If the value of a parameter Y is calculated from and thus, is a linear functions on n independent variables: $X_1, X_2, ..., X_n$, then it can be represented by Equation A.1.

$$Y = f(X_1, X_2, ..., X_n) \tag{A.1}$$

The total uncertainty in reporting parameter Y can be estimated by Equation A.2.

$$\triangle Y = \sqrt{\left\{\frac{\partial Y}{\partial X_1} \cdot \triangle X_1\right\}^2 + \left\{\frac{\partial Y}{\partial X_2} \cdot \triangle X_2\right\}^2 + \cdots + \left\{\frac{\partial Y}{\partial X_n} \cdot \triangle X_n\right\}^2} \tag{A.2}$$

The variables $\triangle X_1$, $\triangle X_2$, ... , $\triangle X_3$ are the uncertainties associated with the measured variables: $X_1, X_2, ..., X_n$; which were derived from the root-sum-square of the bias uncertainty and the precision uncertainty. The difference between the true and expected value, displayed or read by an instrument, is called a bias uncertainty and is generally related to the measuring device. The precision uncertainty

arises from the ability of a measuring device to to repeat the same measurement of a variable that is expected to remain unchanged. In the absence of a predefined precision uncertainty value, the standard deviation, of a sample of measurements of a single unchanging quantity, was used.

A.2 Adiabatic Effectiveness

The adiabatic effectiveness of the test surface, downstream of the film-cooling plate was calculated by using Equation A.3.

$$\eta_{meas} = \frac{T_\infty - T_{aw}}{T_\infty - T_c} \tag{A.3}$$

All of the temperatures recorded for the purpose of this experiment were measured using T-type thermocouples. The freestream temperature, T_∞ was measured upstream of the test-section; the coolant temperature, T_c was monitored inside the plenum, just before ejection; while the temperature of the the adiabatic wall was recorded on the the thermocouple test plate downstream of the injection holes. The bias (supplied by the manufacturer) and precision (standard deviation of measured values) uncertainties associated with each of the the three temperatures is given in Table A.1.

TABLE A.1: Uncertainties associated with measured variables for calculating adiabatic effectiveness

	Bias Uncertainty (°F)	Precision Uncertainty (°F)	Total Uncertainty (△)
T_∞	± 2	± 0.1	2.0
T_{aw}	± 2	± 0.02	2.0
T_c	± 2	± 4	4.47

The total uncertainty of the measured adiabatic effectiveness was calculated by the Equation A.4 , which was derived from Equation A.2.

$$\triangle\eta = \sqrt{\left\{\frac{\partial\eta}{\partial T_\infty}\cdot\triangle T_\infty\right\}^2 + \left\{\frac{\partial\eta}{\partial T_{aw}}\cdot\triangle T_{aw}\right\}^2 + \left\{\frac{\partial\eta}{\partial T_c}\cdot\triangle T_c\right\}^2} \tag{A.4}$$

Further substitution of partial derivatives in Equation A.4, resulted in Equation A.5.

$$\triangle\eta = \sqrt{\left\{\frac{T_{aw}-T_c}{(T_\infty-T_c)^2}\cdot\triangle T_\infty\right\}^2+\left\{\frac{1}{T_c-T_\infty}\cdot\triangle T_{aw}\right\}^2+\left\{\frac{T_\infty-T_{aw}}{(T_\infty-T_c)^2}\cdot\triangle T_c\right\}^2} \tag{A.5}$$

The percentage error was simply achieved by dividing the uncertainty calculated from Equation A.5 by the actual measured value of η. The percentage error associated with results for cooling effectiveness is at worst 0.5% for $\eta > 0.45$ and at least 4% for $\eta < 0.05$.

A similar analysis was performed to determine the error in measuring the secondary or coolant flow rate, which was calculated to be 7%.

Appendix B

Determination of Steady State

A number of theses and papers, written on the topic of film-cooling, reviewed by the author; stated in their experimentation and procedures section that they recorded the temperature of the adiabatic test wall after a certain period of time when steady state was achieved. The period of waiting time before the commencement of temperature recording ranged from 15 minutes to upwards of 2 hours. This waiting period was perceived as being very vague, since it differed from study to study and gave no definite indicator of the apparent steady state. The need to find some concrete way of establishing when it was appropriate to start recording the temperature of the adiabatic wall was the driving source of formulating this method for determining steady state. For the benefit of fellow dilettante researchers, who might find themselves in the same quandary; this method is explained in detail.

For a typical experimental run, steps 1-10 stated in Chapter 3.10 were followed. The first three rows of the thermocouple plate were attached to the temperature DAQ and as soon as the heater in the secondary loop was started: so was the temperature logger. The temperature was measured and logged every 30 seconds by the DAQ. After around 20 measurements or ten minutes; the logged values were transported into an MS Excel file, where the temperature values were plotted against time. If the temperature, recorded by the thermocouples, did not fluctuate with time, then steady state was established; if not, then additional measurements were recorded. The current experimental apparatus, allowed steady state to be achieved no later than 25 minutes after commencement. Monitoring the change in temperature by calculating the percentage difference of successive readings was another method employed by the author, if the temperature fluctuation, or the

lack of it. was not very apparent from the graphed values. A percentage difference of less than 1%, between successive temperature readings, was deemed as enough proof for the attainment of steady state. The rest of the steps, in the experimental procedure were followed diligently to conclude the test. Figure B.1 is an example of a typical graph that was produced for a steady state analysis. At Time = 0 sec, the temperature of all the thermocouples start out to be the same i.e. temperature of the mainstream flow, but as soon as the heater is turned on and the coolant starts spewing hot-air; temperature begins to rise steadily until a certain point in the graph, where it becomes more or less invariant or reaches steady-state.

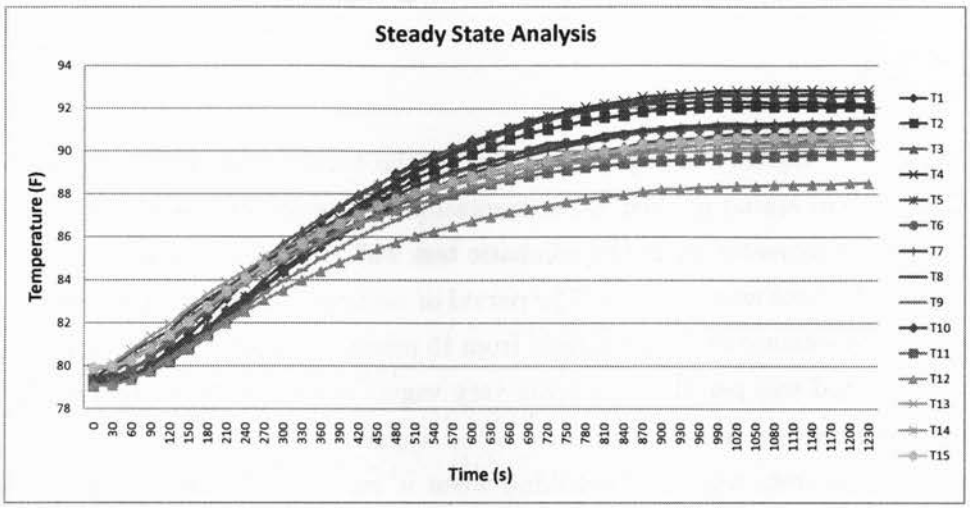

FIGURE B.1: Typical steady state analysis

Although, the time saved in following the above methodology was beneficial in itself; another advantage was that the experimental data was polluted to a lesser extent by conduction heat transfer to the adiabatic test plate. In an ideal case scenario, when the test plate is truly adiabatic, the temperature of the test plate should in theory remain the same once steady state is achieved; which is hardly the case in any film-cooling study, especially the current one. The conduction, from the the injection plate and and due to the close proximity of the plenum to the adiabatic wall drove the temperature higher by at least 10 °F, when test cases were kept running for the duration of 2 hours, which was the time suggested to achieve steady state in a number of studies. Therefore, conducting a steady state analysis was more of a necessity than a mere convenience.

Appendix C

Conduction Correction

Although, the following method of conduction correction was developed by Dr. Bogard's Research Group and discussed briefly in a paper by Ethridge et al [60]; it has been very well explained by Colban [61].

Correcting the obtained experimental data was necessary to negate the effects of the true non-adiabatic nature of the Plexiglas plate embedded with the thermocouples. The conduction correction method calls for the temperature to be measured on the surface at experimental conditions with no coolant flow. In essence, the mainstream flow is operative at the normal freestream velocity of 8 m/s, while the plenum has a flow of 55 °C running through it; exiting through a vent pipe instead of the injection holes, which were plugged. Doing this would measure the temperature change on the 'adiabatic plate' due to the conduction effect of the injection plate as well as the plenum. If the plate is completely adiabatic in nature then there should be absolutely no change in temperature on the surface of the plate: which is not the case. The surface temperature, acquired through the thermocouples, is measured for all the 12 rows on the adiabatic plate.

The measurement obtained without any coolant flow, yields an effectiveness value that is a function of x/D: the distance of the row of thermocouples from the downstream edge of the, now plugged, injection holes. The surface effectiveness without the coolant flow was calculated by Equation C.1, where $T_{surf,o}$ is the temperature of the uncooled surface or adiabatic plate.

$$\eta_o = \frac{T_\infty - T_{surf,o}}{T_\infty - T_c} \tag{C.1}$$

The normal film-cooling effectiveness, which is measured when the injection holes are unplugged and the coolant ejecting from within the plenum is calculated by Equation C.2, where T_{surf} is the temperature of the cooled surface. An important thing to note is that the correction factor will be applied to the following equation.

$$\eta_{meas} = \frac{T_\infty - T_{surf}}{T_\infty - T_c} \tag{C.2}$$

The true, conduction corrected adiabatic film-cooling effectiveness is then calculated by Equation C.3 using the effectiveness values obtained from Equation C.1 and Equation C.2.

$$\eta_{aw} = \frac{\eta_{meas} - \eta_o}{1 - \eta_o} \tag{C.3}$$

The values of η_o varied from 0.15 – 0.014 and were dependant on the proximity to the injection plate and the plenum; the highest value occurring close to injection hole at $x/D = 1$ and decreased almost to insignificant values at $x/D = 18$. Figure C.1 shows the difference of the laterally averaged film-cooling effectiveness with and without the application of conduction correction, for case SR 100. Similar order of magnitude for conduction correction was obtained by Ethridge et al [60], Colban [61] and Hale [1]: Hale being the only one, in the above list, who had used numerical simulations to account for conduction correction; while the rest had utilized experimental procedures, identical to the present study.

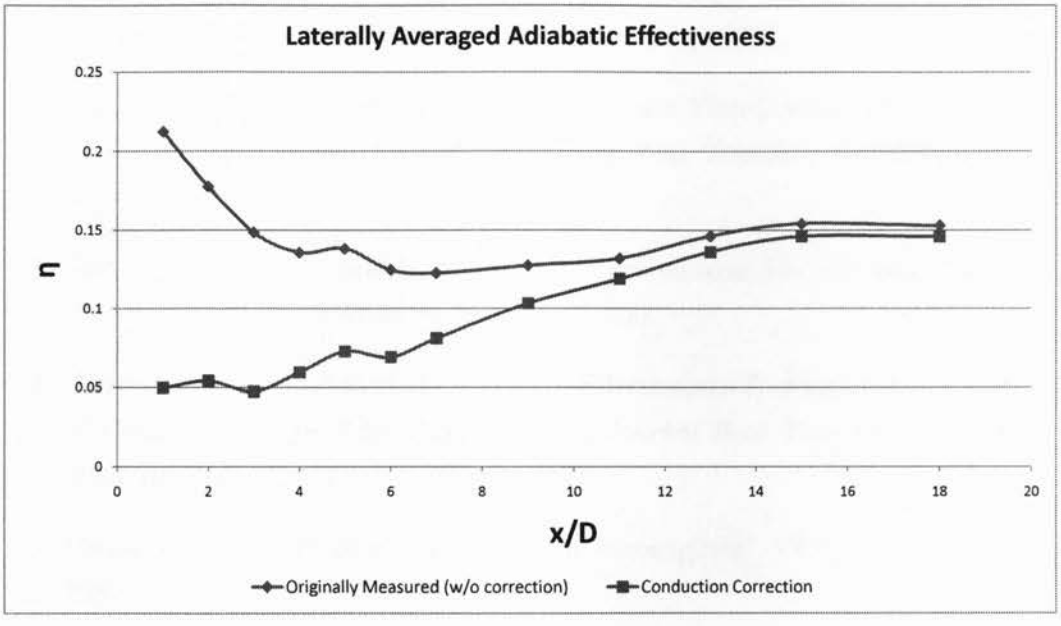

FIGURE C.1: Comparison of effectiveness data with and without the application of conduction correction

References

[1] Hale, C. A., *An Experimental and Numerical Study of the Hydrodynamics and Surface Heat Transfer Associated with Short Film Cooling Holes Fed by a Narrow Plenum*, Ph.D. thesis, Purdue University, 1999.

[2] Na, S. and Shih, T. I.-P., "Increasing Adiabatic Film-Cooling Effectiveness by Using an Upstream Ramp," *Journal of Heat Transfer*, Vol. 129, 2007, pp. 464–471.

[3] Han, J.-C., Dutta, S., and Ekkad, S., *Gas Turbine Heat Transfer and Cooling Technology*, Taylor & Francis, New York, 2000.

[4] Taslim, M. E. and Khanicheh, A., "Film Effectiveness Downstream of a Row of Compound Angle Film Holes," *ASME Journal Heat Transfer*, Vol. 127, 2005, pp. 434–439.

[5] Hennecke, K., "Turbine Blade Cooling in Aeroengines," VKI Lecture Series, 1982.

[6] Scrivener, C. T. J., "Heat Transfer in Aero Engine Gas Turbines - Part I," *Journal of the Gas Turbine Society of Japan*, 1990.

[7] Heidmann, J. D., *The Effect of Wake Passing on Turbine Blade Film Cooling*, Ph.D. thesis, Case Western Reserve University, 1997.

[8] Verhoeven, J. C. J., *Modelling Laser Percussion Drilling*, Ph.D. thesis, Eindhoven University of Technology, 2004.

[9] Han, J.-C. and Ekkad, S., "Recent Development in Turbine Blade Film Cooling," *International Journal of Rotating Machinery*, Vol. 7, No. 1, 2001, pp. 21–40.

[10] French, P. W., Naeem, M., and Watkins, K. G., "Laser Percussion Drilling of Aerospace Material using a 10kW Peak Power Laser using a 400 μm Fibre Delivery System," *ICALEO*, Vol. 95, Laser Institute of America, 2003.

[11] Bunker, R. S., "A Review of Shaped Hole Turbine Film-Cooling Technology," *Journal of Heat Transfer*, Vol. 127, 2005, pp. 441–453.

[12] Burd, S. W. and Simon, T. W., "The Influence of Coolant Supply Geometry on Film Coolant Exit Flow and Surface Adiabatic Effectiveness," *ASME Paper 97-GT-25*, 1997.

[13] Denton, J. D., "Loss Mechanisms in Turbomachines," *ASME Journal of Turbomachinery*, Vol. 115, 1993, pp. 621–656.

[14] Peterson, S. D. and Plesniak, M. W., "Evolution of Jets Emanating from Short Holes into Crossfow," *Journal of Fluid Mechanics*, Vol. 503, 2004, pp. 57–91.

[15] Ou, S. and Rivir, R. B., "Leading Edge Film Cooling Heat Transfer with High Freestream Turbulence Using a Transient Liquid Crystal Image Method," *International Journal of Heat and Fluid Flow*, Vol. 22, 2001, pp. 614–623.

[16] Brown, A. and Saluja, C. L., "Film Cooling from a Single Hole and a Row of Holes of Variable Pitch to Diameter Ratio," *International Journal of Heat and Mass Transfer*, Vol. 22, 1979, pp. 525–533.

[17] Ligrani, P. M., Joseph, S. L., Ortiz, A., and Evans, D. L., "Heat Transfer in Film-Cooled Turbulent Boundary Layers at Different Blowing Ratios as Affected by Longitudinal Vortices," *Experimental Thermal and Fluid Science*, Vol. 1, 1988, pp. 347–362.

[18] Sinha, A. K., Bogard, D. G., and Crawford, M. E., "Film-Cooling Effectiveness Downstream of a Single Row of Holes with Variable Density Ratio," *Journal of Turbomachinery*, Vol. 113, 1991, pp. 442–449.

[19] Pietrzyk, J. R., Bogard, D. G., and Crawford, M. E., "Effects of Density Ratio on the Hydrodynamics of Film Cooling," *Journal of Turbomachinery*, Vol. 112, 1990, pp. 437–443.

[20] Kohli, A. and Bogard, D. G., "Adiabatic Effectiveness, Thermal Fields, and Velocity Fields for Film Cooling with Large Angle Injection," *Journal of Turbomachinery*, Vol. 119, 1997, pp. 352–358.

[21] Lutum, E. and Johnson, B. V., "Influence of the Hole Length-to-Diameter Ratio on Film Cooling with Cylindrical Holes," *Journal of Turbomachinery*, Vol. 121, 1999, pp. 209–216.

[22] Bons, J. P., MacArthur, C. S., and Rivir, R. B., "The Effect of High Free-Stream Turbulence on Film Cooling Effectiveness," *Journal of Turbomachinery*, Vol. 118, No. 814–825, 1996.

[23] Schmidt, D. L., Sen, B., and Bogard, D. G., "Film Cooling with Compound Angle Holes: Adiabatic Effectiveness," *Journal of Turbomachinery*, Vol. 118, 1996, pp. 807–813.

[24] Sen, B., Schmidt, D. L., and Bogard, D. G., "Film Cooling with Compound Angle Holes: Heat Transfer," *Journal of Turbomachinery*, Vol. 118, 1996, pp. 800–806.

[25] Harrington, M., McWaters, M., Bogard, D. G., Lemmon, C., and Thole, K., "Full Coverage Film Cooling with Short Normal Injection Holes," *Journal of Turbomachinery*, Vol. 123, 2001, pp. 798–805.

[26] Sasaki, M., Takahara, K., Kumagai, T., and Hamano, M., "Film Cooling Effectiveness for Injection from Multirow Holes," *Journal Engines and Gas Turbines Power*, Vol. 101, 1979, pp. 101–108.

[27] Leylek, J. H. and Zerkle, R. D., "Discrete-Jet Film Cooling: A Comparison of Computational Results with Experiments," *Journal of Turbomachinery*, Vol. 116, 1994, pp. 358–368.

[28] Laroche, E., "Influence of Freestream Turbulence Intensity on Cooling Effectiveness," *46th ASME International Gas Turbine & Aeroengine Technical Congress*, 2001.

[29] Walters, D. K. and Leylek, J. H., "A Systematic Computational Methodology Applied to a Three-Dimensional Film-Cooling Flowfield," *Journal of Turbomachinery*, Vol. 119, No. 777-785, 1997.

[30] Burd, S. W., Kaszeta, R. W., and Simon, T. W., "Measurements in Film Cooling Flows: Hole L/D and Turbulence Intensity Effects," *Journal of Turbomachinery*, Vol. 120, 1998, pp. 791–798.

[31] Berhe, M. K. and Patankar, S. V., "Curvature Effects on Discrete-Hole Film Cooling," *Journal of Turbomachinery*, Vol. 121, 1999, pp. 781–791.

[32] Berhe, M. K. and Patankar, S. V., "Investigation of Discrete-Hole Film Cooling Parameters Using Curved-Plate Models," *Journal of Turbomachinery*, Vol. 121, 1999, pp. 792–803.

[33] Walters, D. K. and Leylek, J. H., "A Detailed Analysis of Film-Cooling Physics: Part I- Streamwise Injection with Cylindrical Holes," *Journal of Turbomachinery*, Vol. 122, 2000, pp. 102–112.

[34] Hale, C. A., Plesniak, M. W., and Ramadhyani, S., "Film Cooling Effectiveness for Short Film Cooling Holes Fed by a Narrow Plenum," *Journal of Turbomachinery*, Vol. 122, 2000, pp. 553–557.

[35] Peterson, S. D. and Plesniak, M. W., "Short-Hole Jet-In-Crossflow Velocity Field and its Relationship to Film-Cooling," *Experiments in Fluids*, Vol. 33, 2002, pp. 889–898.

[36] Hale, C. A., Plesniak, M. W., and Ramadhyani, S., "Structural Features and Surface Heat Transfer Associated with a Row of Short–Hole Jets in Crossflow," *International Journal of Heat and Fluid Flow*, Vol. 21, 2000, pp. 542–553.

[37] Haven, B. A., Yamagat, D. K., Kurosaka, M., Yamawaki, S., and Maya, T., "Anti-Kidney Pair of Vortices in Shaped Holes and their Inluence on Film Cooling Effectiveness," *IGTI Turbo Expo 97-GT-45*, 1997.

[38] Okita, Y. and Nishiura, M., "Film Effectiveness Performance of an Arrowhead-Shaped Film-Cooling Hole Geometry," *Journal of Turbomachinery*, Vol. 129, 2007, pp. 331–339.

[39] Lu, Y., Nasir, H., Faucheaux, D., and Ekkad, S., "Film Cooling Measurements for Novel Hole Configurations," *Journal of Heat Transfer (Visualization of Heat Transfer Phenomena)*, Vol. 128, 2006, pp. 737.

[40] Reddy, D. R. and Zaman, K. B. M. Q., "Computational Study of Effect of Tabs on a Jet in a Cross Flow," *Computer & Fluids*, Vol. 35, 2006, pp. 712–723.

[41] Ekkad, S., Nasir, H., and Acharya, S., "Film Cooling on a Flat Surface with a single Row of Cylindrical Angled Hole: Effect of Discrete Tabs," *2000 IMECE*, 2000.

[42] Nasir, H., Acharya, S., and Ekkad, S., "Improved Film Cooling from Cylindrical Angled Holes with Triangular Tabs: Effect of Tab Orientation," *International Journal of Heat and Fluid Flow*, Vol. 24, 2003, pp. 657–668.

[43] Ely, M. and Jubran, B. A., "A Numerical Study on Increasing Film Cooling Effectiveness Through the Use of Sister Holes," *ASME Turbo Expo*, 2008.

[44] Javadi, K., Taebi-Rahni, M., and Darbandi, M., "Jet into Cross Flow baoundary Layer Control-an Innovation in Gas Turbine Blade Cooling," *35th AIAA Fluid Dynamics Conference and Exhibit*, 2005.

[45] Dhungel, A., Lu, Y., Phillips, W. A., Ekkad, S., and Heidmann, J. D., "Measurements for Anti-Vortex Film Hole Design," *ASME IGTI Conference*, 2007.

[46] Barigozzi, G., Franchini, G., and Perdichizzi, A., "The Effect of an Upstream Ramp on Cylindrical and Fan Shaped Hole Film Cooling-Part II: Adiabatic Effectiveness Results," *ASME Turbo Expo*, 2007.

[47] Barigozzi, G., Franchini, G., and Perdichizzi, A., "The Effect of an Upstream Ramp on Cylindrical and Fan Shaped Hole Film Cooling-Part I: Aerodynamic Results," *ASME Turbo Expo*, 2007.

[48] Kruse, H., "Film Cooling Measurements," Tech. rep., DEVLR Report No. 35274/9, 1974.

[49] LeBrocq, P. V., Launder, B. E., and Priddin, C. H., "Experiments on Transpirational Film Cooling," *Proc. I MechE*, Vol. 187, 1973, pp. 149–157.

[50] Jubran, B. A. and Brown, A., "Film Cooling from Two Rows of Holes Inclined in the Streamwise and Spanwise Directions," *ASME Journal of Engineering for Gas Turbines and Power*, Vol. 107, 1985, pp. 84–91.

[51] Maiteh, B. Y. and Jubran, B. A., "Influence of Mainstream Flow History on Film Cooling and Heat Transfer from Two Rows of Simple and Compound Angle Holes in Combination," *International Journal of Heat and Fluid Flow*, Vol. 20, 1999, pp. 158–165.

[52] Yuen, C. H. N. and Martinez-Botas, R. F., "Film Cooling Charecteristics of Rows of Holes at Various Streamwise Angles in a Crossflow: Part I. Effectiveness," *International Journal of Heat and Mass Transfer*, Vol. 48, 2005, pp. 4995–5016.

[53] Leoni, S., "Wind Tunnel Design," Tech. rep., Ryerson University, 2005.

[54] TSI, *Traversing a Duct to Determine Average Air Velocity or Volume.*

[55] Klopfenstein Jr., R., "Air Velocity and Flow Measurement Using a Pitot Tube," *ISA Transactions*, Vol. 37, 1998, pp. 257–263.

[56] TSI, *User Manual: TSI Model 9515.*

[57] Jubran, B. A., *Film Coolin Effectiveness from two Rows of Holes*, Ph.D. thesis, University of Wales, 1982.

[58] Jovanović, M., *Film Cooling Through Imperfect Holes*, Ph.D. thesis, Eindhoven University of Technology, 2006.

[59] Kline, S. J. and McClintock, F. A., "Describing Uncertainties in a Single Sample Experiment," *Mechanical Engineering*, Vol. 75, 1953, pp. 3–8.

[60] Ethridge, M. I., Cutbirth, J. M., and Bogard, D. G., "Scaling of Performance for Varying Density Ratio Coolants on an Airfoil with Strong Curvature and Pressure Gradient Effects," *Journal of Turbomachinery*, Vol. 123, 2001, pp. 231–237.

[61] Colban, W. F., *A Detailed Study of Fan-Shaped Film-Cooling for a Nozzle Guide Vane for an Industrial Gas Turbine*, Ph.D. thesis, Virginia Polytechnic Institute and State University, 2005.

[62] Saumweber, C. and Schulz, A., "Interaction of Film Cooling Rows: Effects of Hole Geometry and Row Spacing on the Cooling Performance Downstream of the Second Row of Holes," *Journal of Turbomachinery*, Vol. 126, 2004, pp. 237–246.

"This problem, too, will look simple after it is solved."

Charles Francis Kettering